

Cranfield University

Renaud Sirdey

Image Fusion Using Wavelets

School of Mechanical Engineering

MSc Thesis

Cranfield University

School of Mechanical Engineering
Applied Mathematics and Computing Group

MSc Thesis

Academic Year 1997-98

Renaud Sirdey

Image Fusion Using Wavelets

Supervisor: D.A. Fish

September 1998

This thesis is submitted in partial fulfilment of the requirements for the degree of Master of Science

Abstract

This thesis deals with the problem of image fusion, with application to night vision systems for the car industry. Roughly speaking, an image fusion procedure intends to produce a single image from a set of images having different characteristics and providing complementary information. Because of the application, this work mainly focuses on multisensor image fusion, and most of the experimental results are provided on near and far infrared data. The main purpose of this thesis is to explore the relevancy of using wavelet-based algorithms for performing an image fusion task. In the first chapter, we deal with the registration problem, which is, most of the time, a required preprocessing task. In the second chapter, we briefly introduce the wavelet theory. The third and fourth chapters are then devoted to image fusion: the third chapter deals with the use of orthogonal wavelet decompositions for performing the fusion task and presents some experimental results, while the fourth one studies, on a theoretical point of view, the feasibility of a feature-based image fusion procedure using the wavelet maxima representation.

Cette page n'est plus blanche puisque ce texte y figure !

“I can remember when there wasn’t an automobile in the world with brains enough to find its own way home. I chauffeured dead lumps of machines that needed a man’s hand at their control every minutes. Every year machines like that used to kill tens of thousands of people. The automatics fixed that. A positronic brain can react much faster than a human one, of course, and it paid people to keep hands off the controls. You got in, punched your destination and let it go its own way.”

Isaac Asimov [1].

Contents

Acknowledgements	9
Introduction	11
1 Image registration in presence of non-linear distortion	13
1.1 A simple (distortion-free) camera model	14
1.2 Mathematical model of the lens distortion	14
1.2.1 Radial distortion	14
1.2.2 Decentering distortion	15
1.2.3 Thin-prism distortion	16
1.2.4 Complete model	17
1.3 Assumptions	17
1.3.1 Positions of the cameras	17
1.3.2 Imaged objects	18
1.3.3 Distortion of the NIR camera	18
1.4 Quadratic model	19
1.4.1 Model	19
1.4.2 LS/ML estimates of the parameters	19
1.5 Third order model	20
1.5.1 Model	20
1.5.2 LS/ML estimates of the parameters	20
1.6 Experimental results	20
1.6.1 Quadratic model	20
1.6.2 Third order model	21
1.7 Image registration	21
2 A partial overview of the wavelet theory	25
2.1 Preliminaries	26
2.2 The continuous wavelet transform	27
2.2.1 Definition and properties	27
2.2.2 The Weyl-Heisenberg undeterminacy relation	28
2.2.3 Inversion of the continuous wavelet transform	28
2.2.4 Reproducing kernel	29

2.2.5	Scaling function	29
2.2.6	Examples of wavelets	30
2.3	Dyadic wavelet transform	31
2.3.1	Definition and inversion formula	31
2.3.2	Reproducing kernel	32
2.3.3	Dyadic wavelets and <i>algorithme à trous</i>	32
2.3.4	Practical considerations	33
2.4	Multiresolution analysis of $L^2(R)$	34
2.4.1	Definition	34
2.4.2	Dilation equation and basic consequences	36
2.4.3	Complementary subspaces	37
2.5	Orthogonal multiresolution analysis	37
2.5.1	Definition and perfect reconstruction constraint	37
2.5.2	Relation between $\hat{h}(\xi)$ and $\hat{g}(\xi)$	39
2.5.3	Extension: biorthogonal multiresolution analysis	40
2.6	Orthogonal wavelets and fast algorithm	41
2.6.1	Fast orthogonal wavelet transform	41
2.6.2	Practical considerations	43
2.6.3	Examples of orthogonal wavelets	44
3	Image fusion in orthogonal wavelet basis	49
3.1	Previous work and litterature survey	50
3.2	Multifocus and multisensor data	51
3.2.1	The multifocus problem	51
3.2.2	The multisensor problem	51
3.3	Linear operators	53
3.4	Wavelet transform of some Hölder-0 singularities	53
3.4.1	Sharp Hölder-0 singularity	54
3.4.2	Smooth Hölder-0 singularity	54
3.5	Sharpest singularity selection	56
3.5.1	Piecewise regular functions	57
3.5.2	Windowed maximum operator	57
3.5.3	Limitations	58
3.6	Bi(multi)dimensional wavelet transform	58
3.6.1	Spaces: $L^2(R^2)$, $L^2(R^n)$ and $L^p(R^n)$	59
3.6.2	Continuous wavelet transform on $L^2(R^2)$	59
3.6.3	Multiresolution analysis of $L^2(R^2)$	60
3.7	Wavelet based image fusion	60
3.7.1	Extension of the results derived in §3.4	60
3.7.2	Area based maximum selection	63
3.7.3	Limitations	63
3.8	Experimental results	65
3.8.1	Multifocus image fusion	65

3.8.2	Multisensor image fusion	65
3.9	Denoising in the wavelet space	67
3.9.1	Denoising via wavelet shrinkage	71
3.9.2	Image fusion in a noisy environment	74
3.9.3	Other wavelet-based denoising methods	75
4	Feature-based image fusion	77
4.1	Multiscale edges	78
4.1.1	Quadratic spline wavelet	78
4.1.2	<i>Algorithme à trous</i> in two dimensions	79
4.1.3	Contours extraction	79
4.2	Reconstruction from local maxima	81
4.2.1	The alternate projection algorithm	81
4.2.2	Practical considerations	83
4.3	Image fusion	84
4.3.1	Estimation of K , α and σ	84
4.3.2	The wavelet maxima tree	86
4.3.3	Signal fusion	87
4.3.4	Extension to images	87
	Conclusion	89
	Bibliography	91
A	Registration: linear systems	103
A.1	Quadratic model: systems	103
A.2	Third order model: systems	103
B	Towards an automatic registration	107
B.1	Contours extraction	107
B.1.1	Optimal edge detectors	108
B.1.2	Local maxima and hysteresis thresholding	109
B.2	Corners extraction	112
B.2.1	Existing operators	113
B.2.2	A hybrid operator	113
B.3	Control points matching	113
C	Wavelet transform algorithms	117
D	Mathematical complement	123
D.1	Hilbert space and Riesz basis	123
D.2	Hölder (Lipschitz) regularity	124
D.2.1	Definition	124
D.2.2	A few remarks	124

D.3 Spaces: W^α , $B_{p,q}^\alpha$, C^α	125
D.3.1 Short presentation	125
D.3.2 Example: <i>l'algèbre des bosses</i>	127
List of figures	129
List of algorithms, programs and systems	131

Acknowledgements

I would like to thank Dave Fish for having supervised this thesis and given me the opportunity of working on this subject. I acknowledge Patrice Simard for his advices, the interesting discussions we had and for the interest he has shown for my work. I also thank Jean Charpin for having provided me Yves Meyer's book: "Ondelettes et Opérateurs" and for having tried to go through the tricky notion of Besov space with me. Finally, I acknowledge Delphine Delisse for having read this text entirely.

Introduction

This thesis deals with the problem of image fusion, with application to night vision systems for the car industry. Roughly speaking, an image fusion algorithm intends to produce a single image from a set of images having different characteristics and providing complementary information. Because of the application, this work concentrates mainly on multisensor image fusion, i.e. the images involved in the fusion process are coming from sensors observing at different wavelengths. Experimental tests are performed using a sequence of corresponding near-infrared (NIR: 0.8 to 1.2 μm) and far-infrared (FIR: 8 to 12 μm) images taken at night. These data have been provided to the AMAC group by PSA Peugeot/Citroën and Jaguar Cars Ltd. Since a NIR camera observes at wavelengths which are just outside the visible part of the spectrum, the corresponding images are roughly equivalent to visible ones. The interest of using a thermal (FIR) sensor comes from the following reasons: it is a passive sensor, i.e. it does not rely on an external stimulation (like, for example, the headlights), moreover, particular objects, such as pedestrians, can be easily seen on a cooler background. However, a thermal image has an unnatural appearance and cannot be easily understood by an inexperienced human brain ; besides, a FIR sensor is highly sensitive to weather conditions. This implies that a FIR image complements a NIR one, but a whole night vision system cannot rely only on it. Because a human operator is not able to fully and **fastly** integrate data coming from different sources, the purpose of image fusion is to use a computer in order to perform this integration: image fusion is therefore a man/machine interface problem.

In order to design a fusion procedure, one has to define formally the notion of relevant information: this is a necessary condition for having a quantitative measure which allows to perform the fusion on a computer. Moreover, one should find a fusion operator, acting on some decompositions of the source images, which behaves correctly according to the measure of relevancy and does not introduce any artifacts. As pointed in the image processing literature, sharp variations are very important features for image analysis, this is illustrated by the fact that a human operator is able to recognize an object from only a rough sketch of its contours. Therefore, our goal is to find a fusion operator which preserves as best as possible the objects which have sharp frontiers with the rest of the image. There

are two main scenarios: first, an object is present in one of the two images and not in the other, in that case we want this object to be present without degradation in the fused image ; second, an object is present in the two images, in that case we want the most relevant one (the one which has the sharpest frontier) to be selected and present in the resulting image. As we will see in this thesis, an area-based maximum selection (non-linear) operator applied on the orthogonal wavelet decompositions of the images is a good candidate for fulfilling these requirements.

Obviously, the images, coming from two different sensors, have geometrical differences which do not allow to fuse them directly. Moreover, our data exhibit a strong non-linear distortion which must be taken into account explicitly. The purpose of the first chapter is therefore to deal with this registration problem: we first describe a complete non-linear camera model, then adapt it to our registration problem, and derive least square estimates for its parameters. Experimental results are then given. The second chapter gives an overview of the wavelet theory, since this mathematical tool is extensively used in the remaining part of this thesis. The main subjects are: the continuous wavelet transform, the dyadic wavelet transform and decompositions of functions onto orthogonal wavelet basis. In the last two cases, fast algorithms are presented. This chapter intends to provide an introduction for a reader who is not familiar to wavelet analysis. A more sophisticated reader can probably skip it and refer to it from time to time. The third chapter deals with the image fusion problem and presents some solutions based on orthogonal wavelet decompositions. We first give a short literature survey and discuss the multifocus and multisensor problems, we then focus on the one dimensional case and give some theoretical arguments in favour of a windowed maximum selection as a fusion operator. These results are then extended in two dimensions and experimental results are presented and analysed. Finally, the problem of noise is studied. The goal of the last chapter is to give some perspectives: we study the feasibility of designing a feature-based image fusion procedure using the wavelet maxima representation and discuss the advantages of doing so. The main point is that it allows to see the problem differently and provides a strong theoretical background in which the fusion operation can be performed. However, more research is necessary. Finally, the appendices contain additional details to the first chapter, a discussion about the design of an automatic registration procedure and a short mathematical complement.

Chapter 1

Image registration in presence of non-linear distortion

Introduction

Due to some differences (e.g. position, internal parameters, quality, ...) between the two cameras, a same pixel in the two images does not correspond to the same physical object. Obviously, this problem should be corrected if we want to perform an efficient image fusion. The literature is relatively abundant on this subject (e.g. [Flusser94, Hsieh97, Ventura90, Zheng93]): this is a required preprocessing step for some remote sensing tasks (e.g. satellite imaging) or stereovision. However, they often assume that the transformation that maps a pixel in one image to another is linear, i.e. a combination of the three basic operations: rotation, translation and scaling. Moreover, they do not take into account that the images can have different physical origins (e.g. most of the time the two cameras of a stereovision system are identical and observe at the same wavelength). The multisensor case has already been studied in [Li95a, Li96a, Li96b], in which some automatic feature-based procedures are presented. However, they focus more on correcting the feature inconsistencies (due to the different grey-scale characteristics of the two images) than on modelising the (potential) non-linear distortion. The fact that our data does not allow us to neglect the lens distortion (see figure 1.5, for example) has motivated us to have a look at the field of camera calibration, in which they use camera models which explicitly take into account this type of distortion, see (notably) [Shih95].

The model described here has been used and presented in [Prescott97, Weng92, Sid-Ahmed90] (the main reference is [Weng92]). The chapter is organized as follows: we first present a common linear camera model, then introduce the mathematical modelisation of the lens distortion and discuss the assumptions under which it is usable for solving our registration problem (e.g. only one of the two cameras should exhibit some distortion). We then focus on estimating the model

parameters using a set of control points extracted “by eye” (this is done via a classical mean square/maximum likelihood approach) and present some experimental results.

1.1 A simple (distortion-free) camera model

Let us consider a point $M = (x, y, z)$ in the world coordinate system and its coordinates (x', y', z') in the camera-centered coordinate system. The origin of the camera system is supposed to coincide with the optical center of the camera, its z' -axis coincide with the optical axis and the images plane is supposed to be parallel to the plane $(x'$ -axis, y' -axis) and situated at a distance f (focal distance) of the origin. The relationship between the world coordinates and the camera coordinates is given by

$$\begin{pmatrix} x' \\ y' \\ z' \end{pmatrix} = \begin{pmatrix} \alpha_{11} & \alpha_{12} & \alpha_{13} \\ \alpha_{21} & \alpha_{22} & \alpha_{23} \\ \alpha_{31} & \alpha_{32} & \alpha_{33} \end{pmatrix} \begin{pmatrix} x \\ y \\ z \end{pmatrix} + \begin{pmatrix} \tau_x \\ \tau_y \\ \tau_z \end{pmatrix} \quad (1.1)$$

where (α_{ij}) is a rotation matrix defined by the camera orientation. An application of the well-known Thalès theorem gives the corresponding two-dimensional coordinates in the image plane

$$u = f \frac{x'}{z'}, \quad v = f \frac{y'}{z'} \quad (1.2)$$

1.2 Mathematical model of the lens distortion

Due to several types of imperfections in the manufacturing of lenses, equation (1.2) does not hold and must be replaced by an equation which explicitly takes into account the non-linear positional error

$$u' = u + \nu_u(u, v), \quad v' = v + \nu_v(u, v)$$

where u and v are the (unknown) distortion-free coordinates given by equation (1.2) and u' and v' the corresponding distorted coordinates. This section is a summary of the beginning of [Weng92]. We introduce three types of distortions: the radial, decentering and thin-prism distortions. The complete model is a combination of the three.

1.2.1 Radial distortion

The radial distortion is responsible for an inward or outward displacement of a given point from its ideal location. It is mainly due to some flaws in the lens

(radial) curvature. The radial distortion of a perfectly centered lens is governed by the following equation [Weng92]

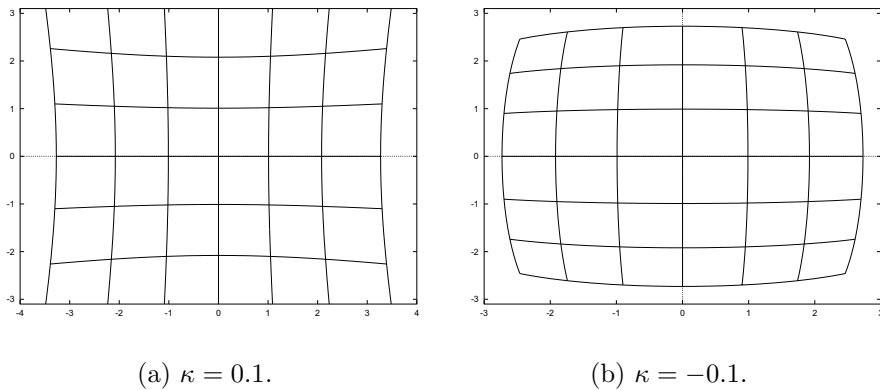
$$\nu_{\rho}^{(r)}(\rho) = \sum_{i=1}^{\infty} \kappa_i \rho^{2i+1}$$

where ρ is the radial distance from the principal point of the camera and the $\{\kappa_i\}$ are the distortion coefficients. For each point in the image plane denoted by its polar coordinates (ρ, ϕ) , the radial distortion corresponds to the distortion along the radial direction. Recalling that $u = \rho \cos \phi$ and $v = \rho \sin \phi$ leads to

$$\begin{aligned} \nu_u^{(r)}(u, v) &= \cos \phi \nu_{\rho}^{(r)}(\rho) \\ &= \cos \phi \rho \sum_{i=1}^{\infty} \kappa_i \rho^{2i} \\ &= u \sum_{i=1}^{\infty} \kappa_i \rho^{2i} \\ &= \kappa_1 u(u^2 + v^2) + O[(u, v)^5] \end{aligned}$$

the same mechanism gives $\nu_v^{(r)}(u, v) = \kappa_1 v(u^2 + v^2) + O[(u, v)^5]$. See also figure 1.1.

Figure 1.1 Radial distortion.



1.2.2 Decentering distortion

The decentering distortion appears because (in general) the optical centers of the different lens elements are not strictly colinear. The decentering distortion has a radial and a tangential component which are governed (respectively) by the

following equations [Weng92]

$$\nu_{\rho}^{(d)} = 3 \sin(\phi - \phi_0) \sum_{i=1}^{\infty} \lambda_i \rho^{2i}$$

and

$$\nu_{\tau}^{(d)} = \cos(\phi - \phi_0) \sum_{i=1}^{\infty} \lambda_i \rho^{2i}$$

where ϕ_0 denotes the angle between the u -axis and the line of maximum tangential distortion. The resulting distortions along the u -axis and the v -axis are given by

$$\begin{pmatrix} \nu_u^{(d)}(u, v) \\ \nu_v^{(d)}(u, v) \end{pmatrix} = \begin{pmatrix} \cos \phi & -\sin \phi \\ \sin \phi & \cos \phi \end{pmatrix} \begin{pmatrix} \nu_{\rho}^{(d)} \\ \nu_{\tau}^{(d)} \end{pmatrix}$$

Therefore,

$$\begin{aligned} \nu_u^{(d)}(u, v) &= (3 \cos \phi \sin(\phi - \phi_0) - \sin \phi \cos(\phi - \phi_0)) \sum_{i=1}^{\infty} \lambda_i \rho^{2i} \\ &= \frac{1}{\rho^2} (3uv \cos \phi_0 - 3u^2 \sin \phi_0 - uv \cos \phi_0 - v^2 \sin \phi_0) \sum_{i=1}^{\infty} \lambda_i \rho^{2i} \\ &= (2uv \cos \phi_0 - (3u^2 + v^2) \sin \phi_0) \sum_{i=1}^{\infty} \lambda_i \rho^{2i-2} \\ &= \mu_1(3u^2 + v^2) + 2\mu_2 uv + O[(u, v)^4] \end{aligned}$$

by letting $\mu_1 = -\lambda_1 \sin \phi_0$ and $\mu_2 = \lambda_2 \cos \phi_0$. The same kind of arguments give

$$\nu_v^{(d)}(u, v) = \mu_2(u^2 + 3v^2) + 2\mu_1 uv + O[(u, v)^4]$$

Figure 1.2 (a) illustrates the decentering distortion for $\xi_1 = 0.02$ and $\xi_2 = 0.03$.

1.2.3 Thin-prism distortion

The thin-prism distortion arises from imperfections in lens design and manufacture and is modeled by the adjunction of a thin prism to the optical system [Weng92]. The thin-prism distortion obeys the following equations

$$\nu_{\rho}^{(d)} = \sin(\phi - \phi_1) \sum_{i=1}^{\infty} \lambda_i \rho^{2i}$$

and

$$\nu_{\tau}^{(d)} = \cos(\phi - \phi_1) \sum_{i=1}^{\infty} \lambda_i \rho^{2i}$$

ϕ_1 is defined as ϕ_0 for the decentering distortion. By using similar techniques as before we end up with

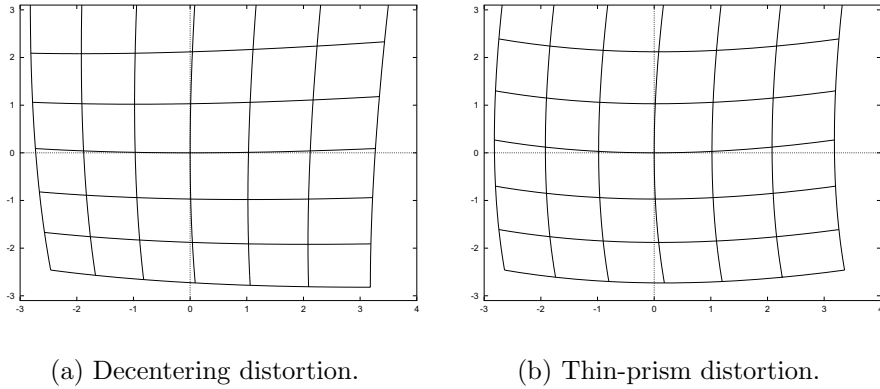
$$\nu_u^{(t)}(u, v) = \xi_1(u^2 + v^2) + O[(u, v)^4]$$

and

$$\nu_v^{(\ell)}(u, v) = \xi_2(u^2 + v^2) + O[(u, v)^4]$$

Figure 1.2 (b) illustrates the thin-prism distortion for $\mu_1 = 0.01$ and $\mu_2 = 0.01$.

Figure 1.2 Decentering and thin-prism distortion.



1.2.4 Complete model

Taking into account the three previous types of distortion, neglecting the terms in $O[(u, v)^p]$, $p \geq 4$ and letting $\varrho_1 = \xi_1 + \mu_1$, $\varrho_2 = \xi_2 + \mu_2$, $\varrho_3 = 2\mu_1$, $\varrho_4 = 2\mu_2$ lead to

$$\nu_u(u, v) \approx (\varrho_1 + \varrho_3)u^2 + \varrho_4uv + \varrho_1v^2 + \kappa_1u(u^2 + v^2)$$

and

$$\nu_v(u, v) \approx \varrho_2u^2 + \varrho_3uv + (\varrho_2 + \varrho_4)v^2 + \kappa_1v(u^2 + v^2)$$

which is a five-parameters (approximate) model.

1.3 Assumptions

This section presents the assumptions under which the previous camera model can be used for solving our image registration problem.

1.3.1 Positions of the cameras

The first assumption concerns the positions of the two camera and can be stated as: the optical axis of the two cameras are parallel, the u -axis, v -axis (NIR) and

the \tilde{u} -axis, \tilde{v} -axis (FIR) are (respectively) parallel and coplanar. Under these assumptions equation (1.1) becomes

$$\begin{pmatrix} x' \\ y' \\ z' \end{pmatrix} = \begin{pmatrix} x \\ y \\ z \end{pmatrix} + \begin{pmatrix} \tau_x \\ \tau_y \\ 0 \end{pmatrix}, \quad \begin{pmatrix} \tilde{x}' \\ \tilde{y}' \\ \tilde{z}' \end{pmatrix} = \begin{pmatrix} x \\ y \\ z \end{pmatrix} + \begin{pmatrix} \tilde{\tau}_x \\ \tilde{\tau}_y \\ 0 \end{pmatrix}$$

1.3.2 Imaged objects

The second assumption deals with the distance of the imaged objects from a camera. It consists in assuming that the imaged objects are situated at a (roughly) constant z coordinate from the optical center of each camera. This allows to rewrite equation (1.2) as

$$u = f \frac{x'}{\text{cte}} = f \frac{x - \tau_x}{\text{cte}}, \quad v = f \frac{y'}{\text{cte}} = f \frac{y - \tau_y}{\text{cte}}$$

for the NIR camera, and

$$\tilde{u} = \tilde{f} \frac{\tilde{x}'}{\text{cte}} = \tilde{f} \frac{\tilde{x} - \tilde{\tau}_x}{\text{cte}}, \quad \tilde{v} = \tilde{f} \frac{\tilde{y}'}{\text{cte}} = \tilde{f} \frac{\tilde{y} - \tilde{\tau}_y}{\text{cte}}$$

for the FIR one. These last equations implies a linear relationship between the (ideal) coordinates in the NIR image and the (ideal) coordinates in the FIR one:

$$\tilde{u} = \alpha u + \beta_u, \quad \tilde{v} = \alpha v + \beta_v$$

where $\alpha = \frac{\tilde{f}}{f}$, $\beta_u = \frac{\tilde{\tau}_x - \tau_x}{\text{cte}}$, and $\beta_v = \frac{\tilde{\tau}_y - \tau_y}{\text{cte}}$.

1.3.3 Distortion of the NIR camera

The last assumption consists in considering that the NIR camera has a neglectable lens distortion. This leads to the following (complete) model

$$\begin{aligned} \tilde{u}' &= \tilde{u} + \nu_{\tilde{u}}(\tilde{u}, \tilde{v}) \\ &= \alpha u + \beta_u + \nu_{\tilde{u}}(\alpha u + \beta_u, \alpha v + \beta_v) \end{aligned} \quad (1.3)$$

Obviously, we also have

$$\tilde{v}' = \alpha v + \beta_v + \nu_{\tilde{v}}(\alpha u + \beta_u, \alpha v + \beta_v) \quad (1.4)$$

Expanding (respectively) equation (1.3) and (1.4) leads to

$$\tilde{u}' = f_u(u, v) = \alpha_1 u^3 + \alpha_2 u v^2 + \alpha_3 u^2 + \alpha_4 v^2 + \alpha_5 u v + \alpha_6 u + \alpha_7 v + \alpha_8 \quad (1.5)$$

and

$$\tilde{v}' = f_v(u, v) = \alpha'_1 v^3 + \alpha'_2 v u^2 + \alpha'_3 u^2 + \alpha'_4 v^2 + \alpha'_5 u v + \alpha'_6 u + \alpha'_7 v + \alpha'_8 \quad (1.6)$$

There exists complicated and highly non-linear relationships between the $\{\alpha_i\}$ and the $\{\alpha'_i\}$. These relationships are ignored and we assume that knowing the parametric form of the model should be sufficient. In the next sections the parameters of f_u and f_v are considered as if they were independant.

1.4 Quadratic model

1.4.1 Model

By neglecting the term of order higher than 3 in equations (1.3) and (1.4) (respectively u^3 , uv^2 and v^3 , vu^2), one ends up with two quadratic polynomials of the form

$$f_u(u, v) = \langle \vec{z}, A\vec{z} \rangle + \langle \vec{b}, \vec{z} \rangle + c, \quad f_v(u, v) = \langle \vec{z}, A'\vec{z} \rangle + \langle \vec{b}', \vec{z} \rangle + c'$$

where $\vec{z} = (u \ v)^T$, $A \in \mathcal{M}_{2 \times 2}(R)$ (symetric), $\vec{b} \in R^2$ and $c \in R$ (same for A' , \vec{b}' and c').

Neglecting these terms means that we do not consider the radial distortion discussed in the previous section. However, as the decentering and the thin-prism distortion also introduce some distortion in the radial direction the model should be able to give reasonable results.

1.4.2 LS/ML estimates of the parameters

Now, given two sets of corresponding control points, $\{u_i, v_i\}$ and $\{\tilde{u}'_i, \tilde{v}'_i\}$, our goal is to find A^* , \vec{b}^* , c^* , A'^* , \vec{b}'^* , c'^* such that

$$\Sigma_u(A^*, \vec{b}^*, c^*) \leq \Sigma(A, \vec{b}, c) \quad \forall A, \vec{b}, c, \quad \Sigma_u(A, \vec{b}, c) = \sum_{i=1}^N (f_u(u_i, v_i) - \tilde{u}'_i)^2$$

and

$$\Sigma_v(A'^*, \vec{b}'^*, c'^*) \leq \Sigma(A', \vec{b}', c') \quad \forall A', \vec{b}', c', \quad \Sigma_v(A', \vec{b}', c') = \sum_{i=1}^N (f_v(u_i, v_i) - \tilde{v}'_i)^2$$

The resulting values are the least square estimates and the maximum likelihood estimates¹ of the model parameters.

Now, A^* , \vec{b}^* and c^* are the solutions of the following equation

$$\begin{pmatrix} \frac{\partial \Sigma_u}{\partial a_{11}} & \frac{\partial \Sigma_u}{\partial a_{22}} & \frac{\partial \Sigma_u}{\partial a_{12}} & \frac{\partial \Sigma_u}{\partial b_1} & \frac{\partial \Sigma_u}{\partial b_2} & \frac{\partial \Sigma_u}{\partial c} \end{pmatrix} = \vec{0}$$

which leads to a linear system of the form

$$Q\vec{x} = \vec{\theta} \tag{1.7}$$

where $\vec{x} = (a_{11} \ a_{22} \ a_{12} \ b_1 \ b_2 \ c)^T$. Finding A'^* , \vec{b}'^* , c'^* (for $f_v(u, v)$) gives the same system except that the right hand side becomes $\vec{\theta}'$ (Q , $\vec{\theta}$ and $\vec{\theta}'$ are given in §A.1). Both systems are solved via the Gauss-Siedel method. Some experimental results are available in §1.6.1.

¹If we assume that the $\{\tilde{u}'_i\}$ are corrupted by a gaussian noise of mathematical expectation 0 and variance σ^2 then the log-likelihood is equal to $-\frac{n}{2} \log 2\pi\sigma^2 - \frac{1}{2\sigma^2} \sum_i (f_u(u_i, v_i) - \tilde{u}'_i)^2$. Therefore, **under this statistical model**, maximizing the likelihood is equivalent to minimize Σ_u . Obviously, the same reasoning holds for Σ_v .

1.5 Third order model

1.5.1 Model

The third order model arises from the fact that we do not neglect the terms of high order in equations (1.5) and (1.6). This leads to

$$f_u(u, v) = d_1 u^3 + d_2 uv^2 + \langle \vec{z}, A\vec{z} \rangle + \langle \vec{b}, \vec{z} \rangle + c$$

and

$$f_v(u, v) = d'_1 v^3 + d'_2 vu^2 + \langle \vec{z}, A'\vec{z} \rangle + \langle \vec{b}', \vec{z} \rangle + c'$$

1.5.2 LS/ML estimates of the parameters

For estimating the model parameters via the least square method (as in the previous section), we need to solve the two following linear systems

$$M\vec{x} = \vec{\vartheta} \tag{1.8}$$

where $\vec{x} = (d_1 \ d_2 \ a_{11} \ a_{22} \ a_{12} \ b_1 \ b_2 \ c)^T$, and

$$M'\vec{x}' = \vec{\vartheta}' \tag{1.9}$$

where $\vec{x}' = (d'_1 \ d'_2 \ a'_{11} \ a'_{22} \ a'_{12} \ b'_1 \ b'_2 \ c')^T$. Note that the bottom right part of both M and M' is equal to Q and that the bottom part of $\vec{\vartheta}$ and $\vec{\vartheta}'$ are respectively equal to $\vec{\theta}$ and $\vec{\theta}'$ (Q , $\vec{\theta}$ and $\vec{\theta}'$ are defined in the previous section). M , M' , $\vec{\vartheta}$ and $\vec{\vartheta}'$ are given in §A.2.

Once again, the two systems are solved using the Gauss-Siedel method. The next section presents some experimental results.

1.6 Experimental results

The estimations presented in this section have been computed using a set of 68 control points extracted by hand. The two sets are uniformly distributed within the image and simulate (as best as the sequence allows it) a calibration grid. This allows to “control” the ill-conditioned nature of the systems.

1.6.1 Quadratic model

The estimated values of the parameters are (see §A.1)

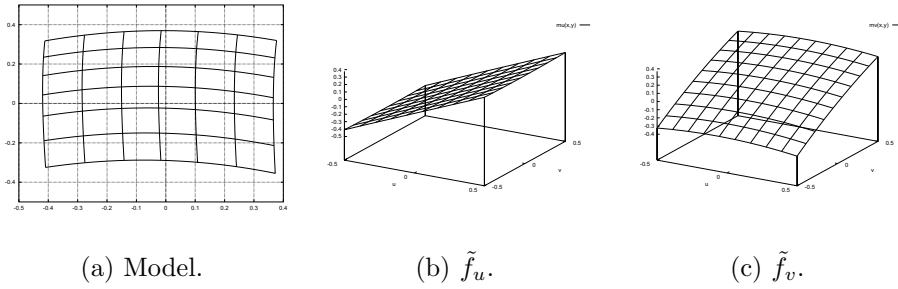
$$\tilde{a}_{11} = -.0063, \tilde{a}_{22} = .0356, \tilde{a}_{12} = .0035, \tilde{b}_1 = .7851, \tilde{b}_2 = .0011, \tilde{c} = -.0251 \tag{1.10}$$

for \tilde{f}_u and

$$\tilde{a}'_{11} = -.2041, \tilde{a}'_{22} = -.1860, \tilde{a}'_{12} = .0160, \tilde{b}'_1 = -.0141, \tilde{b}'_2 = .6583, \tilde{c}' = .0869 \quad (1.11)$$

for \tilde{f}_v . The mean square error² is equal to .0122 for \tilde{f}_u and .0126 for \tilde{f}_v . The resulting (estimated) model is shown on figure 1.3.

Figure 1.3 Estimated quadratic model.



1.6.2 Third order model

The estimated values of the parameters are (see page 103)

$$\begin{aligned} \tilde{d}_1 &= -.1485, & \tilde{d}_2 &= -.0257, & \tilde{a}_{11} &= -.0057, & \tilde{a}_{22} &= .0352, \\ \tilde{a}_{12} &= .0033, & \tilde{b}_1 &= .8085, & \tilde{b}_2 &= .0014, & \tilde{c} &= -.0251 \end{aligned} \quad (1.12)$$

for \tilde{f}_u and (see page 103, as well)

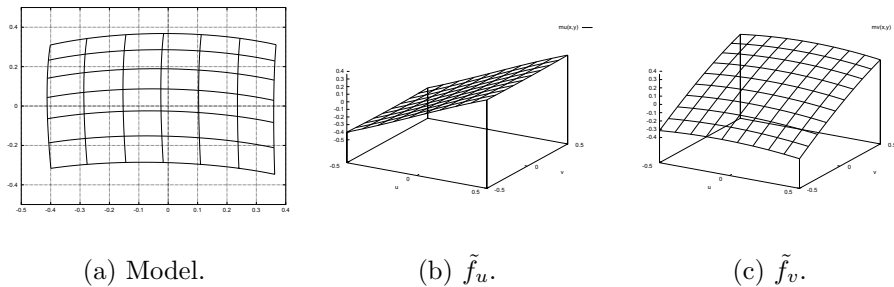
$$\begin{aligned} \tilde{d}'_1 &= -.0669, & \tilde{d}'_2 &= -.0510, & \tilde{a}'_{11} &= -.2047, & \tilde{a}'_{22} &= -.1848, \\ \tilde{a}'_{12} &= .0160, & \tilde{b}'_1 &= -.0143, & \tilde{b}'_2 &= .6715, & \tilde{c}' &= .0869 \end{aligned} \quad (1.13)$$

for \tilde{f}_v , with respective mean square errors equal to .0119 and .0125. The resulting (estimated) model is shown on figure 1.4.

1.7 Image registration

Both on a mean square error and on a “visual” criterion point of view, the two models give roughly equivalent results and lead to reasonable registered images (figure 1.5 shows some examples). As simplicity is a reasonable criteria (for equivalent performances) the quadratic model is the one chosen.

² $\sqrt{\frac{1}{n} \sum_i (\tilde{f}_u(u_i, v_i) - \tilde{u}'_i)^2}$ where $\tilde{f}_u(u, v)$ denotes the estimation of $f_u(u, v)$.

Figure 1.4 Estimated third-order model.

Using the quadratic model, the registration procedure becomes straightforward: for a pixel $(u \ v)^T$ in the registered image we have to take the corresponding pixel $(\tilde{f}_u(u, v) \ \tilde{f}_v(u, v))^T$ in the raw image. Since $(\tilde{f}_u(u, v) \ \tilde{f}_v(u, v))^T$ is not (in general) an integer-valued vector, a bilinear interpolation scheme is used for computing the value at $(u \ v)^T$. Obviously, this interpolation has no physical meaning.

Figure 1.5 Example of registered image.



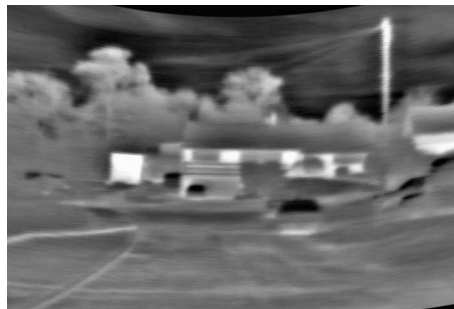
(a) Original NIR.



(b) Original FIR.



(c) Quadratic model.

(d) Third-order model.

Chapter 2

A partial overview of the wavelet theory

Introduction

The last decade has seen the development of a new type of signal representations, known as the wavelet transforms (named after the well-known article of Alex Grossmann and Jean Morlet [Grossmann84]). As in the Fourier analysis, the wavelet transform consists in decomposing a given function onto a set of “building blocks”. However, as opposed to the Fourier transformation (in which the “building blocks” are the well-known complex exponentials), the wavelet transform uses the dilated and translated version of a “mother wavelet” which has convenient properties according to time/frequency localization. As we will see later, this allows to perform a time/frequency analysis of signals which is much more relevant than those provided by other decompositions, e.g. the windowed Fourier transform. In the last few years, the wavelet analysis has been applied successfully to a wide range of problems from pure mathematics to engineering (characterization of some functionnal spaces, study of turbulence, signal processing, ...).

This chapter intends to provide a short introduction to the wavelet theory. The subjects which are addressed are (in chronological order): the continuous wavelet transform, the dyadic wavelet transform, the notions of multiresolution analysis and orthogonal multiresolution analysis (in which orthogonal and non-redundant decompositions arise). Fast algorithms are presented for the dyadic and the orthogonal wavelet transforms. Obviously, this chapter does not pretend to be exhaustive, we have only included the necessary material for understanding the rest of this thesis, so that a reader which is not familiar to wavelets can read it without having to study other references simultaneously.

This chapter has been written using principally [Jawerth93, Daubechies92] and the recent book by Stéphane Mallat: “A Wavelet Tour of Signal Processing”

[Mallat98], which is very complete (not only on a wavelet point of view). Some other “specialized” articles have been used as well.

2.1 Preliminaries

Definition 1 ($L^2(\mathbb{R})$) $L^2(\mathbb{R})$ denotes the space of square integrable functions, i.e.

$$L^2(\mathbb{R}) = \left\{ f / \int_{-\infty}^{+\infty} |f(x)|^2 dx < \infty \right\}$$

provided the scalar product

$$\langle f, g \rangle = \int_{-\infty}^{+\infty} f(x)g^*(x)dx$$

and the associated norm

$$\|f\|^2 = \langle f, f \rangle$$

This space (in association with this scalar product) has a Hilbert space structure (see definition 9, page 123).

Definition 2 (Fourier transform) The Fourier transform¹ of a function $f \in L^2(\mathbb{R})$ is defined as

$$\hat{f}(\xi) = \int_{-\infty}^{+\infty} f(x)e^{-i\xi x} dx$$

and its inverse is given by

$$f(x) = \frac{1}{2\pi} \int_{-\infty}^{+\infty} \hat{f}(\xi)e^{i\xi x} d\xi$$

Many of the results presented in the next sections are dependant on this definition.

Theorem 1 (Poisson sommation formula) For all $f, g \in L^2(\mathbb{R})$, the Poisson sommation formula gives the two equalities

$$\sum_{l=-\infty}^{+\infty} f(x-l) = \sum_{k=-\infty}^{+\infty} \hat{f}(2k\pi)e^{2i\pi kx} \quad (2.1)$$

and

$$\sum_{l=-\infty}^{+\infty} \langle f, \tau_l g \rangle e^{-i\xi l} = \sum_{k=-\infty}^{+\infty} \hat{f}(\xi + 2k\pi)\hat{g}^*(\xi + 2k\pi) \quad (2.2)$$

A proof of this result can be found in [Duong97].

¹In general [Weisstein98], a Fourier transform pair can be defined using two arbitrary constants A and B such that $\hat{f}(\xi) = A \int_{-\infty}^{+\infty} f(x)e^{Bi\xi x} dx$ and $f(x) = \frac{B}{2\pi A} \int_{-\infty}^{+\infty} \hat{f}(\xi)e^{-Bi\xi x} d\xi$.

2.2 The continuous wavelet transform

This section presents the continuous wavelet transform and discusses its basic properties, e.g. time/frequency localization, inversion, redundancy, ... The connections between the continuous transform and other “discrete” wavelet transforms (dyadic or orthogonal wavelet transforms) will be emphasized in the next sections.

2.2.1 Definition and properties

Definition 3 (Continuous wavelet transform) *The continuous wavelet transform of $f \in L^2(\mathbb{R})$ is defined as [Grossmann84, Mallat98, Starck92]*

$$\mathcal{W}_f(a, b) = \langle f, \psi_{a;b} \rangle, \quad \psi_{a;b}(x) = \frac{1}{\sqrt{a}} \psi\left(\frac{x-b}{a}\right) \quad (2.3)$$

where $a > 0^2$ and b are respectively the scale and the translation parameter.

$\psi \in L^2(\mathbb{R})$ is called a wavelet function. This transformation is linear and invariant according to shift and scale. A direct consequence of the Parseval theorem³ is

$$\mathcal{W}_f(a, b) = \frac{1}{2\pi} \langle \hat{f}, \hat{\psi}_{a;b} \rangle, \quad \hat{\psi}_{a;b}(\xi) = \sqrt{a} e^{-i\xi b} \hat{\psi}(a\xi) \quad (2.4)$$

Equations (2.3) and (2.4) imply that the wavelet coefficients contain some information about f coming from both the time and the frequency domains. The wavelet transform is therefore a time/frequency representation as the windowed Fourier transform introduced by Gabor [Gabor46, Feichtinger97], or the Wigner-Ville distribution [Ville48, Hlawatsch92, Mallat98].

Unfortunately, this type of representations is subject to a limitation due to the Weyl-Heisenberg indeterminacy relation⁴ (this is not directly true for the Wigner-Ville distribution but its practical use involves an averaging which leads to a loss of time-frequency resolution [Mallat98]). **In the rest of this thesis, the wavelet function is considered to be real.**

²Other authors ([Daubechies92, Jawerth93] for example) define the transform for all $a \neq 0$. It is therefore necessary to introduce an absolute value in equation (2.3).

³ $\langle f, g \rangle = A \langle \hat{f}, \hat{g} \rangle$, the value of A depends on the definition of the Fourier transform. Here, $A = \frac{1}{2\pi}$.

⁴Also known as the Weyl-Heisenberg uncertainty principle. Here, we use the vocabulary introduced by E. Cornell [Cornell98].

2.2.2 The Weyl-Heisenberg undeterminacy relation

Theorem 2 (Weyl-Heisenberg undeterminacy relation) *Given a function $f \in L^2(\mathbb{R})$ such that $\|f\|^2 = 1$, the Weyl-Heisenberg relation indicates that*

$$\underbrace{\left(\int_{-\infty}^{+\infty} (x - \bar{x})^2 |f(x)|^2 dx \right)}_{\sigma_x^2} \underbrace{\left(\int_{-\infty}^{+\infty} (\xi - \bar{\xi})^2 |\hat{f}(\xi)|^2 d\xi \right)}_{\sigma_\xi^2} \geq A \quad (2.5)$$

Where

- $\bar{x} = \int_{-\infty}^{+\infty} x |f(x)|^2 dx$;
- $\bar{\xi} = \int_{-\infty}^{+\infty} \xi |f(\xi)|^2 d\xi$.

Proofs of this theorem can be found in [Hubbard96, Mallat98] and in almost every books about quantum physics. The value of A also depends on the definition of the Fourier transform, here $A = \frac{1}{4}$. Optimizing equation (2.5) using techniques based on the calculus of variations (see [Duong97] for an introduction) shows that Gauss functions of the form $K(a)e^{-ax^2}$ satisfy the optimum. A direct consequence of the theorem is that a function cannot be simultaneously well localized in both the time and the frequency domain, and it is obviously true for the wavelet function in equation (2.3).

By considering the time-frequency spread of $\psi_{a,b}$, it follows that most of the information contained in $\mathcal{W}_f(a, b)$ comes from the intervals $[b + a\bar{x} - a\sigma_x, b + a\bar{x} + a\sigma_x]$ (time domain) and $[(\bar{\xi} - \sigma_\xi)/a, (\bar{\xi} + \sigma_\xi)/a]$ (frequency domain) [Jawerth93, Mallat98]. These intervals define time-frequency windows, known as Heisenberg boxes, whose areas depend on the translation and scale parameters. From Weyl-Heisenberg relation, the area of a given box has a lower bound: $4\sigma_x\sigma_\xi \geq 2$. However, an interesting property of the wavelet transform is that the dimensions of a given window can be adapted according to the “subject” of interest (as opposite to the windowed Fourier transform). Typically, it consists in using a “good” time resolution for studying the high frequencies and a “good” frequency resolution for the low frequencies.

2.2.3 Inversion of the continuous wavelet transform

Theorem 3 (Calderón identity) *If the wavelet $\psi \in L^2(\mathbb{R})$ satisfies the admissibility condition*

$$C_\psi = \int_0^{+\infty} \frac{|\hat{\psi}(\xi)|^2}{\xi} < \infty$$

then every function $f \in L^2(\mathbb{R})$ is such that

$$f(x) = \frac{1}{C_\psi} \int_0^{+\infty} \int_{-\infty}^{+\infty} \mathcal{W}_f(a, b) \psi_{a,b}(x) \frac{dbda}{a^2}$$

Proofs of this result can be found in [Mallat98, Daubechies92]. This identity has been rediscovered in [Grossmann84] and was known in harmonic analysis since 1964. The admissibility condition requires that $\hat{\psi}(0) = \int_{-\infty}^{+\infty} \psi(x)dx = 0$ which means that the wavelet must be an oscillating function⁵. Note that a given function can also be reconstructed from its wavelet transform using another wavelet [Starck92] $\chi(x)$ if

$$\int_0^{+\infty} \frac{\hat{\chi}(\xi)\hat{\psi}^*(\xi)}{\xi} d\xi < \infty$$

the inversion formula is then given by

$$f(x) = \int_0^{+\infty} \int_{-\infty}^{+\infty} \mathcal{W}(a, b)\chi_{a;b}(x) \frac{dbda}{a^2}$$

2.2.4 Reproducing kernel

Now by inserting the Calderón identity in equation (2.3), we end up with

$$\mathcal{W}_f(a_0, b_0) = \frac{1}{C_\psi} \int_0^{+\infty} \int_{-\infty}^{+\infty} \mathcal{W}_f(a, b)\kappa(a, a_0, b, b_0) \frac{dbda}{a^2} \quad (2.6)$$

where $\kappa(a, a_0, b, b_0) = \langle \psi_{a;b}, \psi_{a_0;b_0} \rangle$ is called a reproducing kernel⁶ [Mallat98]. The modulus of the reproducing kernel measures the correlation between the two wavelets $\psi_{a;b}$ and $\psi_{a_0;b_0}$ and illustrates the redundancy of the continuous wavelet transform. Note that any function $\Phi(a, b)$ is the wavelet transform of some function $f \in L^2(R)$ if and only if it satisfies equation (2.6).

2.2.5 Scaling function

When the wavelet transform is known only for $a < a_0$, f cannot be recovered from its wavelet coefficients. Basically, the Calderón identity is broken into two parts

$$f(x) = \frac{1}{C_\psi} \int_0^{a_0} \int_{-\infty}^{+\infty} \mathcal{W}_f(a, b)\psi_{a;b}(x) \frac{dbda}{a^2} + \frac{1}{C_\psi} \int_{a_0}^{+\infty} \int_{-\infty}^{+\infty} \mathcal{W}_f(a, b)\psi_{a;b}(x) \frac{dbda}{a^2}$$

The role of the scaling function ϕ is to provide the information presents in the second term of the previous equation so that it becomes equal to

$$\int_{-\infty}^{+\infty} \mathcal{L}_f(a_0, b)\phi_{a_0;b}(x)db, \quad \mathcal{L}_f(a, b) = \langle f, \phi_{a;b} \rangle$$

⁵Or the null function which is limited in interest.

⁶If the original function is reconstructed using another wavelet, the reproducing kernel becomes $\kappa(a, a_0, b, b_0) = \langle \chi_{a;b}, \psi_{a_0;b_0} \rangle$.

By using the fact that $\mathcal{W}_f(a, b) = f \otimes \bar{\psi}_a(b)$, $\mathcal{L}_f(a, b) = f \otimes \bar{\phi}_a(b)$ and that

$$\begin{aligned} \int_{-\infty}^{+\infty} \mathcal{W}_f(a, b) \psi_{a,b}(x) db &= \mathcal{W}_f(a, \cdot) \otimes \psi_a(x), \\ \int_{-\infty}^{+\infty} \mathcal{L}_f(a, b) \phi_{a,b}(x) db &= \mathcal{L}_f(a, \cdot) \otimes \phi_a(x) \end{aligned}$$

we end up with

$$f \otimes \bar{\phi}_{a_0} \otimes \phi_{a_0} = f \otimes \Psi(x), \quad \Psi(x) = \int_{a_0}^{+\infty} \bar{\psi}_a \otimes \psi_a(x) \frac{da}{a^2}$$

This leads, via the convolution theorem, to the following constraint on $|\hat{\phi}(\xi)|^2$

$$|\hat{\phi}(\xi)|^2 = \int_1^{+\infty} |\hat{\psi}(a\xi)|^2 \frac{da}{a^2}$$

The phase of $\hat{\phi}(\xi)$ can be arbitrarily chosen [Mallat98].

2.2.6 Examples of wavelets

This subsection is obviously not exhaustive and gives two examples of wavelet given in [Starck92].

Morlet's wavelet

The Morlet's wavelets is a complex wavelet whose real part is given by

$$\Re\{\psi\}(x) = \frac{1}{\sqrt{2\pi}} e^{-\frac{x^2}{2}} \cos 2\pi\nu_0 x$$

and imaginary part by

$$\Im\{\psi\}(x) = \frac{1}{\sqrt{2\pi}} e^{-\frac{x^2}{2}} \sin 2\pi\nu_0 x$$

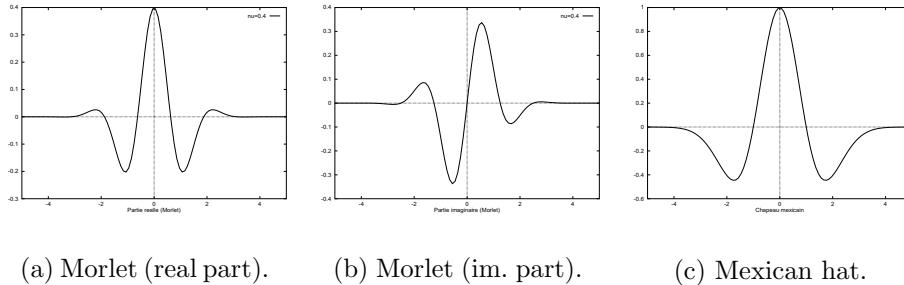
ν_0 is a constant term. For this wavelet, the admissibility condition is not satisfied but if ν_0 is sufficiently large it becomes "pseudo-admissible" [Starck92]. See figure 2.1 (a) & (b) ($\nu = 0.4$).

Mexican hat

The mexican hat is defined as the second derivative of a gaussian, its expression is therefore given by

$$\psi(x) = (1 - x^2) e^{-\frac{x^2}{2}}$$

The well-known property of the Fourier transform: $\frac{d^n f(x)}{dx^n} \Leftrightarrow (i\xi)^n \hat{f}(\xi)$ implies directly that $\hat{\psi}(0) = \int_{-\infty}^{+\infty} \psi(x) dx = 0$ and the fact that the first-order moment of a Gauss function is finite prove that this wavelet is admissible. See figure 2.1 (c).

Figure 2.1 Examples of wavelets.

2.3 Dyadic wavelet transform

A dyadic wavelet transform is obtained by discretizing the scale parameter a according to the dyadic sequence $\{2^j\}_{j \in \mathbb{Z}}$. In order to preserve the translation invariance property of the continuous wavelet transform the translation parameter is not discretized. Under particular conditions, the dyadic wavelet coefficients can be computed using a fast algorithm, known as an *algorithme à trous*.

2.3.1 Definition and inversion formula

Definition 4 (Dyadic wavelet transform) *The dyadic wavelet transform of $f \in L^2(\mathbb{R})$ is defined as*

$$\mathcal{W}_f(2^j, b) = \langle f, \psi_{2^j, b} \rangle, \quad \psi_{2^j, b}(x) = \frac{1}{\sqrt{2^j}} \psi\left(\frac{x-b}{2^j}\right) \quad (2.7)$$

If the frequency plane is completely covered by dilated dyadic wavelets, then the dyadic wavelet transform defines a complete and stable⁷ representation. The following theorem relates the dyadic wavelet transform to the frame theory [Mallat98, Daubechies90, Daubechies92] and gives an inversion formula.

Theorem 4 *If there exists two constants $A, B \in \mathbb{R}^{2+*}$ such that*

$$\forall \xi \in \mathbb{R}, \quad A \leq \sum_{j=-\infty}^{+\infty} |\hat{\psi}(2^j \xi)|^2 \leq B$$

⁷The terms “complete” and “stable” should be understood in a frame theory context [Duffin52, Daubechies90, Mallat98]. Roughly, a sequence $\{\theta_n\}_{n \in \tau}$ is said to be a frame of an Hilbert space \mathcal{H} if there exist $A, B \in \mathbb{R}^{2+*}$ so that $\forall f \in \mathcal{H}, A\|f\|^2 \leq \sum_{n \in \tau} |\langle f, \theta_n \rangle|^2 \leq B\|f\|^2$. This is a necessary and sufficient condition so that the operator $U_f[n] = \langle f, \theta_n \rangle$ is invertible on its image with a bounded inverse. If $A = B$ the frame is said to be tight and if $A = B = 1$ the frame is an orthogonal basis of \mathcal{H} [Daubechies90]. See (notably) [Mallat98, Daubechies90, Daubechies92] for more details.

then

$$A\|f\|^2 \leq \sum_{j=-\infty}^{+\infty} \frac{1}{2^j} \|\mathcal{W}_f(2^j, b)\|^2 \leq B\|f\|^2$$

Moreover, if χ satisfies

$$\forall \xi \in R^+, \quad \sum_{j=-\infty}^{+\infty} \hat{\psi}^*(2^j \xi) \hat{\chi}(2^j \xi) = 1 \quad (2.8)$$

then

$$f(x) = \sum_{j=-\infty}^{+\infty} \int_{-\infty}^{+\infty} \mathcal{W}_f(2^j, b) \chi_{2^j, b}(x) db \quad (2.9)$$

A proof of this theorem can be found in [Mallat98, Daubechies90]. χ denotes the reconstruction wavelet.

2.3.2 Reproducing kernel

As in the continuous case, the dyadic wavelet transform is a redundant representation whose redundancy is illustrated by a reproducing kernel equation. By inserting equation (2.7) in equation (2.9), we end up with

$$\mathcal{W}(2^{j_0}, b_0) = \sum_{j=-\infty}^{+\infty} \int_{-\infty}^{+\infty} \mathcal{W}_f(2^j, b) \kappa(j, j_0, b, b_0) db \quad (2.10)$$

where $\kappa(j, j_0, b, b_0) = \langle \chi_{2^j, b}, \psi_{2^{j_0}, b_0} \rangle$. Another equivalent way⁸ of seeing this reproducing kernel [Mallat92b] consists in using the fact that $\mathcal{W}_f(2^j, b) = f \otimes \bar{\psi}_{2^j}^*(b)$ and that $f(x) = \sum_j \mathcal{W}_f(2^j, \cdot) \otimes \chi_{2^j}(x)$. Inserting the last expression of $f(x)$ in the one of $\mathcal{W}_f(2^{j_0}, b_0)$ gives

$$\mathcal{W}_f(2^{j_0}, b_0) = \sum_{j=-\infty}^{+\infty} \mathcal{W}_f(2^j, \cdot) \otimes \kappa'_{2^j, 2^{j_0}}(b_0), \quad \kappa'_{2^j, 2^{j_0}}(b) = \chi_{2^j} \otimes \bar{\psi}_{2^{j_0}}^*(b) \quad (2.11)$$

2.3.3 Dyadic wavelets and *algorithme à trous*

If the wavelets and scaling functions are properly designed, the dyadic wavelet transform can be computed via a fast algorithm based on filter banks [Mallat98, Mallat92b, Rioul92, Shensa92], known as an *algorithme à trous*. It requires that there exists two discrete filters h and g with $\sum_k h_k = \sqrt{2}$ so that the scaling function ϕ and the wavelet ψ respectively satisfy

$$\hat{\phi}(\xi) = \hat{h}(\xi/2) \hat{\phi}(\xi/2) \quad (2.12)$$

⁸This holds for the continuous wavelet transform as well.

and

$$\hat{\psi}(\xi) = \hat{g}(\xi/2)\hat{\phi}(\xi/2) \quad (2.13)$$

where $\hat{h}(\xi) = \frac{1}{\sqrt{2}} \sum_k h_k e^{-i\xi k}$ is the Fourier transform of the distribution $\frac{1}{\sqrt{2}} \sum_k h_k \delta_k$ (same for $\hat{g}(\xi)$). If $\mathcal{L}_f(2^j, b) = \langle f, \phi_{2^j, b} \rangle$ is known, we can calculate

$$\mathcal{W}_f(2^{j+1}, b) = \langle f, \psi_{2^{j+1}, b} \rangle \quad \text{and} \quad \mathcal{L}_f(2^{j+1}, b) = \langle f, \phi_{2^{j+1}, b} \rangle$$

by using only the discrete filters h and g . Since $\mathcal{L}_f(2^{j+1}, b) = f \otimes \bar{\phi}_{2^{j+1}}(b)$, we have⁹ (from equation (2.12))

$$\begin{aligned} \mathcal{L}_f(2^{j+1}, b) &\Leftrightarrow \hat{f}(\xi)\hat{\phi}_{2^{j+1}}^*(\xi) \\ &= \hat{h}_{2^j}^* \hat{f}(\xi)\hat{\phi}_{2^j}^*(\xi) \\ &\Leftrightarrow \bar{h}_{2^j} \otimes \mathcal{L}_f(2^j, \cdot)(b) \end{aligned} \quad (2.14)$$

The same kind of argument gives

$$\mathcal{W}_f(2^{j+1}, b) = \bar{g}_{2^j} \otimes \mathcal{L}_f(2^j, \cdot)(b) \quad (2.15)$$

h_{2^j} (resp. g_{2^j}) is obtained from h (resp. g) by inserting $2^j - 1$ zeros between the samples of h (resp. g). The pair φ, χ (respectively the scaling function and wavelet) used for reconstructing the signal should as well satisfy two similar equations as (2.12) and (2.13) with filters \tilde{h} and \tilde{g} instead of h and g . Obviously, we must be able to recover $\mathcal{L}_f(2^j, b)$ from $\mathcal{L}_f(2^{j+1}, b)$ and $\mathcal{W}_f(2^{j+1}, b)$. This is done via the following formula

$$\mathcal{L}_f(2^j, b) = \tilde{g}_{2^j} \otimes \mathcal{W}_f(2^{j+1}, \cdot)(b) + \tilde{h}_{2^j} \otimes \mathcal{L}_f(2^{j+1}, \cdot)(b) \quad (2.16)$$

Algorithm 2.1 illustrates the working of the algorithm. Equation (2.15) is equivalent to

$$\mathcal{L}_f(2^j, b) = (\bar{h}_{2^j} \otimes \tilde{h}_{2^j} + \bar{g}_{2^j} \otimes \tilde{g}_{2^j}) \otimes \mathcal{L}_f(2^j, \cdot)(b)$$

Therefore, the required perfect reconstruction introduces the constraint

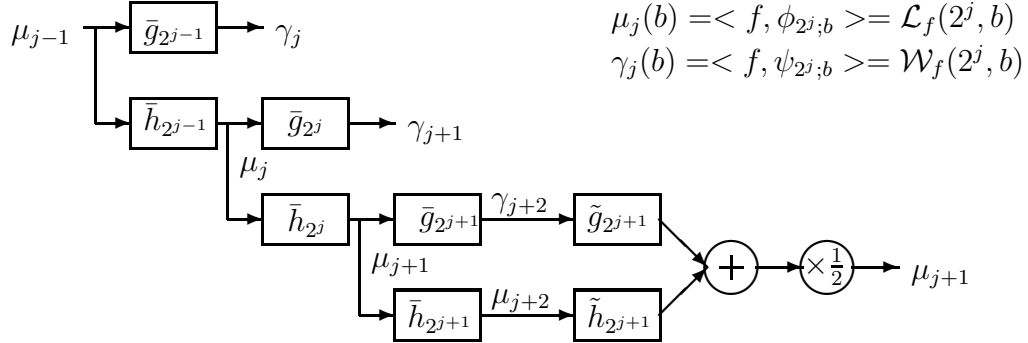
$$\hat{h}^*(\xi)\hat{h}(\xi) + \hat{g}^*(\xi)\hat{g}(\xi) = 1, \quad \forall \xi \in [-\pi, \pi]$$

which is equivalent to condition (2.8) (proof in [Mallat98]).

2.3.4 Practical considerations

In practical cases, i.e. discrete signals of finite duration, the convolutions in equations (2.14), (2.15) and (2.16) are replaced by circular convolutions. Since the scalar product of the discrete sequence with $\phi_{2^{\log_2 N}, k}$ is constant [Mallat98] (N is

⁹The convolution operators in equations (2.14), (2.15) and (2.16) should be understood in a distribution theory context. See [Duong97].

Algorithm 2.1 *Algorithme à trous.*

the length of the signal), the scale only goes from $2^0 = 1$ to $2^{\log_2 N}$. Most of the time, the samples of the discrete input sequence are considered as the average of a function f weighted by $\phi(x - k)$ and give the first approximation required for starting the algorithm. The complexity of the algorithm is in $\mathcal{O}(N \log_2 N)$. Figure 2.2 shows the dyadic wavelet transform of a signal computed by means of the quadratic spline wavelet given in [Mallat92b].

2.4 Multiresolution analysis of $L^2(\mathbb{R})$

The multiresolution analysis introduced by Stéphane Mallat in 1989 [Mallat89a] provides a theoretical context in which non redundant and orthogonal wavelet decompositions arise. However, the definition of a multiresolution analysis does not require any constraint of orthogonality. In this section we focus on the basic properties of a multiresolution analysis and their implications on the pair wavelet/scaling function.

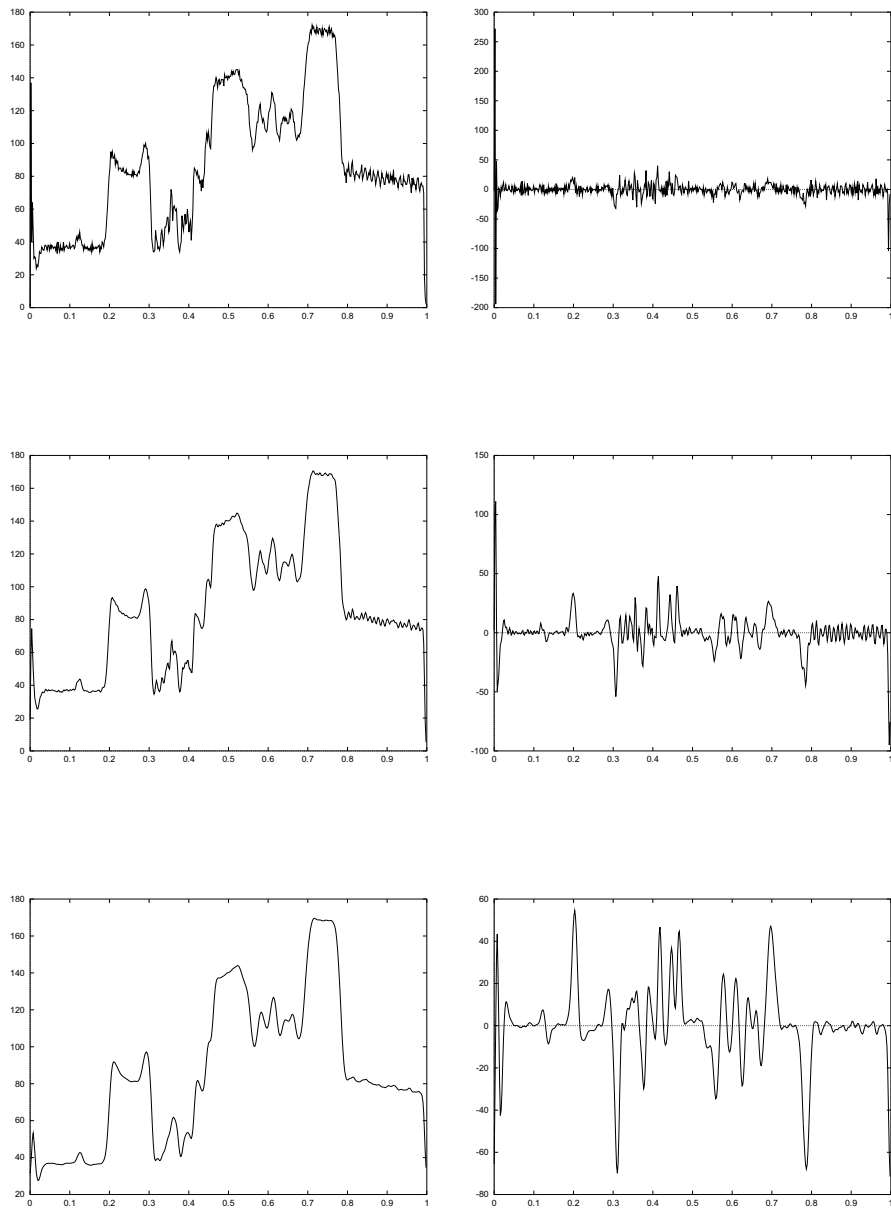
2.4.1 Definition

Definition 5 (Multiresolution analysis) *A multiresolution analysis is a set of closed subspaces V_j of $L^2(\mathbb{R})$, which satisfies the following six properties¹⁰ [Mallat89a, Jawerth93, Hubbard96]*

1. $V_j \subset V_{j+1}, \forall j$.
2. $v(x) \in V_0 \Leftrightarrow v(x - k) \in V_0, \forall k \in \mathbb{Z}$.
3. $v(x) \in V_j \Leftrightarrow v(2x) \in V_{j+1}, \forall j \in \mathbb{Z}$.
4. $\lim_{j \rightarrow -\infty} V_j = \bigcap_{j=-\infty}^{+\infty} V_j = \{0\}$.

¹⁰Some authors [Mallat98, Daubechies92] use $V_{j+1} \subset V_j$ and $f(x) \in V_j \Leftrightarrow f(x/2) \in V_{j+1}$ for (respectively) properties 1 and 3.

Figure 2.2 Beginning of a dyadic wavelet transform.



(e) Scaling coefficients.

(f) Wavelet coefficients.

5. $\lim_{j \rightarrow +\infty} V_j = \bigcup_{j=-\infty}^{+\infty} V_j = L^2(\mathbb{R})$.
6. *There exists a scaling function $\phi \in L^2(\mathbb{R})$ such that $\{\tau_k \phi\}_{k \in \mathbb{Z}}$ is a Riesz basis of V_0 .*

Property 1 (causality property) means that an approximation in V_j contains all the information for computing an approximation at a coarser resolution. Property 2 indicates that V_0 is invariant under integer translations. Property 3 says that the null function is the only common object to all the subspaces V_j , i.e. we lose all the details about f as j goes to $-\infty$. Property 4 means that every functions of $L^2(\mathbb{R})$ can be approximated to an arbitrary precision. The definition of a Riesz basis (property 6) is available page 123. Properties 3 and 6 directly imply that the family $\{\phi_{j;k}\}_{k \in \mathbb{Z}}$ (now $\phi_{j;k}(x)$ stands for $\sqrt{2^j} \phi(2^j x - k)$) forms a Riesz basis of V_j .

Simple examples of multiresolution analysis are: the piecewise constant approximations (related to the Haar wavelet), the Shannon approximations (related to the Shannon wavelet) and the spline approximations, the two first examples defines some orthogonal multiresolutions while the third defines a non-orthogonal one, more details are available in [Mallat98, Jawerth93].

2.4.2 Dilation equation and basic consequences

Theorem 5 (Dilation equation) *Let $\phi \in L^2(\mathbb{R})$ be the scaling function of a multiresolution analysis, then [Jawerth93, Daubechies92]*

$$\exists \{h_k\}_{k \in \mathbb{Z}} / \phi(x) = \sqrt{2} \sum_{k=-\infty}^{+\infty} h_k \phi(2x - k) \quad (2.17)$$

This theorem follows directly from properties 1 and 6: as a function of V_0 (property 6) and because $V_0 \subset V_1$ (property 1), ϕ can be expressed as a linear combination of the basis function of V_1 .

Equation (2.17) is known as a **dilation equation** [Strang94] or a **scaling equation** [Mallat98] and plays a fundamental role in the orthogonal dyadic wavelet theory. Integrating equation (2.17) on both sides implies that $\sum_k h_k = \sqrt{2}$.

Introducing the dilation equation in the Fourier transform of ϕ leads to

$$\hat{\phi}(\xi) = \hat{h}(\xi/2) \hat{\phi}(\xi/2) \quad (2.18)$$

where $\hat{h}(\xi) = \frac{1}{\sqrt{2}} \sum_k h_k e^{-i\xi k}$ denotes the Fourier transform (2π -periodic) of the distribution $\frac{1}{\sqrt{2}} \sum_k h_k \delta_k$. Equation (2.18) can be used recursively and gives (at least formally)

$$\hat{\phi}(\xi) = \prod_{k=1}^{\infty} \hat{h}(\xi/2^k)$$

This product can be interpreted as an infinite cascade of convolutions of the distribution $\frac{1}{\sqrt{2}} \sum_k h_k \delta_k$ by itself, its convergence properties are (notably) studied in [Daubechies88].

2.4.3 Complementary subspaces

Let W_j denotes the subspace complementing V_j in W_{j+1} i.e.

$$V_{j+1} = V_j \oplus W_j$$

where \oplus denotes the direct sum operator. As a consequence of property 5, we have $\bigoplus_{j=-\infty}^{+\infty} W_j = L^2(R)$.

Definition 6 (Wavelet function) *In a multiresolution context, a function ψ is said to be a wavelet function if the family $\{\tau_k \psi\}_{k \in Z}$ is a Riesz basis of the complementary subspace W_0 [Jawerth93].*

As a function of V_1 , the wavelets also obey a dilation equation

$$\psi(x) = \sqrt{2} \sum_{k=-\infty}^{+\infty} g_k \phi(2x - k)$$

which leads to

$$\hat{\psi}(\xi) = \hat{g}(\xi/2) \hat{\phi}(\xi/2) \quad (2.19)$$

and (as in the case of the scaling function) to an infinite product of the form

$$\hat{\psi}(\xi) = \hat{g}(\xi/2) \prod_{k=2}^{+\infty} \hat{h}(\xi/2^k)$$

The family of functions $\{\psi_{j;k}\}_{j,k \in Z^2}$ forms a Riesz basis of $L^2(R)$ [Jawerth93, Mallat98]. As a consequence, every functions of $L^2(R)$ can be written as

$$f(x) = \sum_{j=-\infty}^{+\infty} \sum_{k=-\infty}^{+\infty} \mu_{j;k} \psi_{j;k}(x) \quad (2.20)$$

This equation can be seen as an inverse wavelet transform where the scale and the translation parameters have been discretized.

2.5 Orthogonal multiresolution analysis

2.5.1 Definition and perfect reconstruction constraint

Definition 7 (Orthogonal multiresolution analysis) *An orthogonal multiresolution analysis is a multiresolution analysis such that for all $j \in Z$, W_j is the orthogonal complement of V_j in V_{j+1} [Jawerth93, Daubechies92].*

A sufficient condition for a multiresolution to be orthogonal is given by [Jawerth93]

$$V_0 \perp W_0 \text{ i.e. } \langle \phi, \tau_k \psi \rangle = 0, \forall k \in Z \quad (2.21)$$

A consequence of this definition is the existence of an unique scaling function ϕ so that the family $\{\tau_k \phi\}_{k \in Z}$ forms an orthogonal basis of V_0 [Mallat89a], i.e.

$$\langle \phi, \tau_k \phi \rangle = \delta_{0,k}, \forall k \in Z \quad (2.22)$$

Now, the families $\{\phi_{j;k}\}_{k \in Z}$, $\{\psi_{j;k}\}_{k \in Z}$ and $\{\psi_{j;k}\}_{j,k \in Z^2}$ form orthogonal basis of (respectively) V_j , W_j and $L^2(R)$ (proof in [Mallat98]). Hence, in this context, equation (2.20) can be written as

$$f(x) = \sum_{j=-\infty}^{+\infty} \sum_{k=-\infty}^{+\infty} \langle f, \psi_{j;k} \rangle \psi_{j;k}(x)$$

By using the Poisson formula (equation (2.2)), equation (2.22) is equivalent to

$$F(\xi) = \sum_{k=-\infty}^{+\infty} |\hat{\phi}(\xi + 2k\pi)|^2 = 1 \quad (2.23)$$

Since (from equation (2.18) and from the fact that both $F(\xi)$ and $\hat{h}(\xi)$ are 2π -periodic)

$$\begin{aligned} F(2\xi) &= \sum_{k=-\infty}^{+\infty} |\hat{\phi}(2\xi + 2k\pi)|^2 \\ &= \sum_{k=-\infty}^{+\infty} |\hat{h}(\xi + k\pi)|^2 |\hat{\phi}(\xi + k\pi)|^2 \\ &= \sum_{k=-\infty}^{+\infty} |\hat{h}(\xi + 2k\pi)|^2 |\hat{\phi}(\xi + 2k\pi)|^2 \\ &\quad + \sum_{k=-\infty}^{+\infty} |\hat{h}(\xi + \pi + k\pi)|^2 |\hat{\phi}(\xi + \pi + k\pi)|^2 \\ &= |\hat{h}(\xi)|^2 F(\xi) + |\hat{h}(\xi + \pi)|^2 F(\xi + \pi) \end{aligned}$$

we end up with the following theorem [Jawerth93, Mallat98, Daubechies88].

Theorem 6 (Perfect reconstruction) *Let $\phi \in L^2(R)$ be the scaling function of an orthogonal multiresolution, then $\hat{h}(\xi)$ satisfies¹¹*

$$|\hat{h}(\xi)|^2 + |\hat{h}(\xi + \pi)|^2 = 1 \quad (2.24)$$

¹¹Note that the right hand side depends on the definition of $\hat{h}(\xi)$. Here: $\hat{h}(\xi) = \frac{1}{\sqrt{2}} \sum_k h_k e^{-i\xi k}$. Other authors [Daubechies88, Mallat98] end up with the right hand side equals to 2.

This constraint is fundamental for the design of orthogonal wavelets and connects wavelets to the conjugate quadrature filters (tree-structured subband coders with exact reconstruction [Smith86]) theory¹² [Daubechies88, Mallat98, Cohen92a]. Note that equation (2.24) is a sufficient condition so that $\phi \in L^2(R)$ [Cohen92a].

2.5.2 Relation between $\hat{h}(\xi)$ and $\hat{g}(\xi)$

Now consider the sufficient condition for a multiresolution to be orthogonal (equation (2.21)), again from Poisson formula it is equivalent to

$$G(\xi) = \sum_{k=-\infty}^{+\infty} \hat{\phi}(\xi + 2k\pi) \hat{\psi}^*(\xi + 2k\pi) = 0$$

which leads to (from equations (2.18), (2.19) and (2.23))

$$\begin{aligned} G(2\xi) &= \sum_{k=-\infty}^{+\infty} \hat{\phi}(2\xi + 2k\pi) \hat{\psi}^*(2\xi + 2k\pi) \\ &= \sum_{k=-\infty}^{+\infty} \hat{h}(\xi + k\pi) \hat{g}^*(\xi + k\pi) |\hat{\phi}(\xi + k\pi)|^2 \\ &= \sum_{k=-\infty}^{+\infty} \hat{h}(\xi + 2k\pi) \hat{g}^*(\xi + 2k\pi) |\hat{\phi}(\xi + 2k\pi)|^2 \\ &+ \sum_{k=-\infty}^{+\infty} \hat{h}(\xi + \pi + 2k\pi) \hat{g}^*(\xi + \pi + 2k\pi) |\hat{\phi}(\xi + \pi + 2k\pi)|^2 \\ &= \hat{h}(\xi) \hat{g}^*(\xi) + \hat{h}(\xi + \pi) \hat{g}^*(\xi + \pi) = 0 \end{aligned}$$

This implies the following relation [Jawerth93]

$$\hat{g}(\xi) = \alpha(\xi) \hat{h}^*(\xi + \pi)$$

where $\alpha(\xi)$ is a 2π -periodic function such that $\alpha(\xi) = -\alpha(\xi + \pi)$. Now, from Parseval theorem, equation (2.22) can be written as

$$\frac{1}{2\pi} \int_{-\infty}^{+\infty} |\hat{h}(\xi/2)|^2 |\hat{\phi}(\xi/2)|^2 e^{-i\xi k} dx = \delta_{0,k}, \quad \forall k \in Z \quad (2.25)$$

Since

$$\begin{aligned} \langle \psi, \tau_k \psi \rangle &= \frac{1}{2\pi} \int_{-\infty}^{+\infty} |\hat{\psi}(\xi)|^2 e^{-i\xi k} d\xi \\ &= \int_{-\infty}^{+\infty} |\hat{g}(\xi/2)|^2 |\hat{\phi}(\xi/2)|^2 e^{-i\xi k} d\xi \end{aligned}$$

¹²For every orthogonal bases of compactly supported wavelets, there exists a pair of discrete filters which defines a subband coder allowing perfect reconstruction [Cohen92a] (the opposite is not generally true).

$$\begin{aligned}
&= \int_{-\infty}^{+\infty} |\alpha(\xi/2)|^2 |\hat{h}(\xi/2 + \pi)|^2 |\hat{\phi}(\xi/2)|^2 e^{-i\xi k} d\xi \\
&= \int_{-\infty}^{+\infty} |\alpha(\xi/2)|^2 |\hat{h}(\xi/2)|^2 |\hat{\phi}(\xi/2)|^2 e^{-i\xi k} d\xi
\end{aligned}$$

the orthogonality of the wavelet is implied by the orthogonality of the scaling function if $|\alpha(\xi)|^2 = 1$. We then impose the following constraint: if the scaling function has a compact support, i.e. $\hat{h}(\xi)$ is a trigonometric polynomial, the wavelet must have a compact support. This constraint requires that $\alpha(\xi)$ is a trigonometric polynomial as well. The only trigonometric polynomials which have these two properties are of the form

$$\alpha(\xi) = K e^{-i(2k+1)\xi}$$

with $|K| = 1$. Choosing $K = \pm 1$ implies that if the coefficients $\{h_k\}_{k \in \mathbb{Z}}$ are real, then the coefficients $\{g_k\}_{k \in \mathbb{Z}}$ are also real. The ‘‘classical’’ choice [Jawerth93, Daubechies88] is $\alpha(\xi) = -e^{-i\xi}$ and leads to

$$\begin{aligned}
\hat{g}(\xi) &= -e^{-i\xi} \hat{h}^*(\xi + \pi) & (2.26) \\
&= -e^{-i\xi} \sum_{-\infty}^{+\infty} h_k^* e^{i(\xi+\pi)k} \\
&= - \sum_{k=-\infty}^{+\infty} (-1)^k h_k^* e^{-i\xi(1-k)} \\
&= \sum_{l=-\infty}^{\infty} (-1)^l h_{1-l}^* e^{-i\xi l}
\end{aligned}$$

hence

$$g_k = (-1)^k h_{1-k}^* \quad (2.27)$$

Other authors (notably) [Mallat98] choose $\alpha(\xi) = e^{-i\xi}$ and then end up with $g_k = (-1)^{1-k} h_{1-k}^*$ instead of equation (2.27).

2.5.3 Extension: biorthogonal multiresolution analysis

The notion of biorthogonal multiresolution analysis [Cohen92a, Jawerth93] generalizes the idea of multiresolution analysis by using different scaling function/wavelet pairs for respectively the decomposition and the reconstruction of the signal. The idea consists in defining two ladders of closed subspaces¹³

$$\dots \subset V_{-j} \subset \dots \subset V_{-1} \subset V_0 \subset V_1 \subset \dots \subset V_j \subset \dots$$

and

$$\dots \subset \tilde{V}_{-j} \subset \dots \subset \tilde{V}_{-1} \subset \tilde{V}_0 \subset \tilde{V}_1 \subset \dots \subset \tilde{V}_j \subset \dots$$

¹³As in the simple multiresolution case some authors ([Cohen92a] notably) are using $\dots \supset V_j \supset V_{j+1} \supset \dots$ and $\dots \supset \tilde{V}_j \supset \tilde{V}_{j+1} \supset \dots$ instead of the previous definition.

such that they respectively lead to a multiresolution analysis and a dual multiresolution analysis. Moreover, it is required that

$$\tilde{W}_j \perp V_j \text{ and } W_j \perp \tilde{V}_j$$

so that $\{\psi_{j;k}\}_{j,k \in \mathbb{Z}^2}$ and $\{\tilde{\psi}_{j;k}\}_{j,k \in \mathbb{Z}^2}$ define two dual Riesz basis of $L^2(R)$. By mimicing the orthogonal case, it is possible to derive conditions on the four filters $h, g, \tilde{h}, \tilde{g}$ such that they lead to a perfect reconstruction subband coding scheme (with different analysis and synthesis filters). For more precisions the reader is sent to (notably) [Cohen92a, Mallat98].

Finally, every function $f \in L^2(R)$ can be expressed as [Cohen92a]

$$f(x) = \sum_{j=-\infty}^{+\infty} \sum_{k=-\infty}^{+\infty} \langle f, \psi_{j;k} \rangle \tilde{\psi}_{j;k}(x) = \sum_{j=-\infty}^{+\infty} \sum_{k=-\infty}^{+\infty} \langle f, \tilde{\psi}_{j;k} \rangle \psi_{j;k}(x)$$

which illustrates the fact that the role of the two basis can be interchanged. The interest of building biorthogonal multiresolution analysis comes from the fact that more freedom is allowed in the design of the wavelets/filters and that it becomes possible to create symmetric wavelets.

2.6 Orthogonal wavelets and fast algorithm

2.6.1 Fast orthogonal wavelet transform

Now let $\mu_{j;k} = \langle f, \phi_{j;k} \rangle = \mathcal{L}_f(2^{-j}, 2^{-j}k)$ and $\gamma_{j;k} = \langle f, \psi_{j;k} \rangle = \mathcal{W}_f(2^{-j}, 2^{-j}k)$. Generalizing the scaling equation (2.17) gives

$$\begin{aligned} \phi_{j;k}(x) &= \sum_{l=-\infty}^{+\infty} h_l \phi_{j+1;2k+l}(x) \\ &= \sum_{m=-\infty}^{+\infty} h_{m-2k} \phi_{j+1;m} \end{aligned}$$

Putting this last equation in the expression of $\mu_{j;k}$ leads to

$$\begin{aligned} \mu_{j;k} &= \sum_{l=-\infty}^{+\infty} h_{l-2k} \langle f, \phi_{j+1;l} \rangle \\ &= \sum_{l=-\infty}^{+\infty} \bar{h}_{2k-l} \mu_{j+1;l} = \bar{h} \otimes \mu_{j+1}[2k] \end{aligned} \quad (2.28)$$

The same kind of arguments gives

$$\gamma_{j;k} = \bar{g} \otimes \mu_{j+1}[2k] \quad (2.29)$$

Equations (2.28) and (2.29) are discrete convolutions followed by a downsampling operation. We come back to the $\mu_{j+1;k}$ from the $\mu_{j;k}$ and the $\gamma_{j;k}$ by inserting

$$f_{j+1}(x) = \underbrace{\sum_{l=-\infty}^{+\infty} \mu_{j;l} \phi_{j;l}(x)}_{\in V_j} + \underbrace{\sum_{l=-\infty}^{+\infty} \gamma_{j;l} \psi_{j;l}(x)}_{\in W_j}$$

in $\mu_{j+1;k} = \langle f, \phi_{j+1;k} \rangle = \langle f_{j+1}, \phi_{j+1;k} \rangle$. Hence (and from the orthogonality of the scaling function),

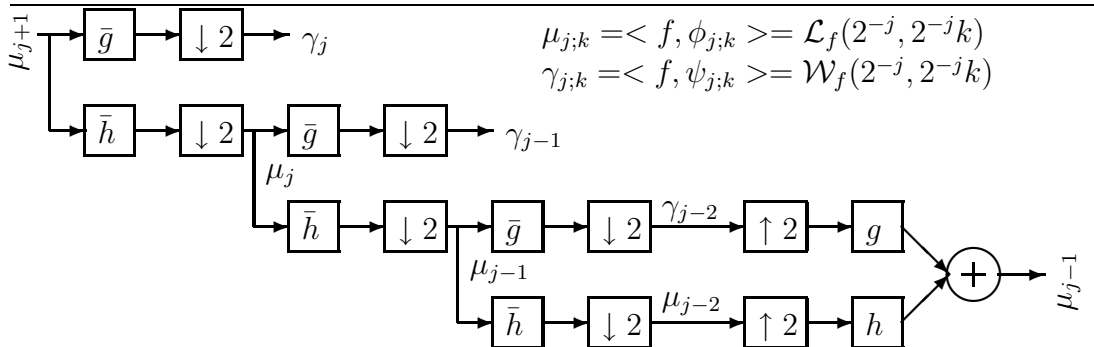
$$\begin{aligned} \mu_{j+1;k} &= \sum_{l=-\infty}^{+\infty} \mu_{j;l} \sum_{m=-\infty}^{+\infty} h_{m-2l} \langle \phi_{j+1;m}, \phi_{j+1;k} \rangle \\ &+ \sum_{l=-\infty}^{+\infty} \gamma_{j;l} \sum_{m=-\infty}^{+\infty} g_{m-2l} \langle \phi_{j+1;m}, \phi_{j+1;k} \rangle \end{aligned} \quad (2.30)$$

$$\begin{aligned} &= \sum_{l=-\infty}^{+\infty} \mu_{j;l} \sum_{m=-\infty}^{+\infty} h_{m-2l} \delta_{k,m} + \sum_{l=-\infty}^{+\infty} \gamma_{j;l} \sum_{m=-\infty}^{+\infty} g_{m-2l} \delta_{k,m} \\ &= \sum_{l=-\infty}^{+\infty} \mu_{j;l} h_{k-2l} + \sum_{l=-\infty}^{+\infty} \gamma_{j;l} g_{k-2l} \end{aligned} \quad (2.31)$$

The first and second terms of this last equation are discrete convolutions preceded by an upsampling operation (insert one zero between every sample). See algorithm 2.2.

Equations (2.28), (2.29) and (2.31) define a perfect reconstruction decimated fil-

Algorithm 2.2 Fast decimated filter bank algorithm.



ter banks (perfect reconstruction subband coder). If we note $\hat{\mu}_j(\xi) = \sum_k \mu_{j;k} e^{-i\xi k}$ the discrete Fourier transform of the sequence $\{\mu_{j;k}\}_{k \in \mathbb{Z}}$ (same for $\hat{\gamma}_j(\xi)$) we have: $\hat{\mu}_j(\xi) = \hat{h}^*(\xi/2) \hat{\mu}_{j+1}(\xi/2)$, $\hat{\gamma}_j(\xi) = \hat{g}^*(\xi/2) \hat{\mu}_{j+1}(\xi/2)$ and $\hat{\mu}_{j+1}(\xi) = \hat{h}(\xi) \hat{\mu}_j(2\xi) + \hat{g}(\xi) \hat{\gamma}_j(2\xi)$. Therefore,

$$\hat{\mu}_{j+1}(\xi) = (\hat{h}(\xi) \hat{h}^*(\xi) + \hat{g}(\xi) \hat{g}^*(\xi)) \hat{\mu}_{j+1}(\xi)$$

The perfect reconstruction constraint is then given by $\hat{h}(\xi)\hat{h}^*(\xi) + \hat{g}(\xi)\hat{g}^*(\xi) = 1$ or in “Z-transform” notation

$$H(e^{i\xi})H(e^{-i\xi}) + G(e^{i\xi})G(e^{-i\xi}) = 1$$

this condition is equivalent to equation (2.24), using the expression of $\hat{g}(\xi)$ derived in §2.5.2, and (roughly) to the condition derived in [Smith86].

2.6.2 Practical considerations

There exists different ways of modifying the fast wavelet transform algorithm for dealing with practical signals, i.e. sampled signals of finite duration. Most of the time, (as in the *algorithme à trous* case), the samples are interpreted such that they gives $\mu_{0;k}$. Note that the complexity of the algorithm is in $\mathcal{O}(\log_2 N)$ (faster than the fast Fourier transform— $\mathcal{O}(N \log_2 N)$).

Zero padding

The most intuitive way of dealing with the border problem consists in assuming that the function vanishes outside the sampling interval i.e. $\in L^2([0, N])$. The fast wavelet transform algorithm is therefore applied without modification. However, the signal is interpreted as if it was discontinuous at $x = 0$ and $x = N$: large coefficients are created in the neighbourhood of this points and significant errors may appear during the reconstruction process.

Periodic wavelets

A better solution consists in using a proper orthogonal basis of $L^2([0, N])$. For example, an orthogonal basis of $L^2([0, N])$ can be constructed by periodizing an orthogonal wavelet basis of $L^2(\mathbb{R})$. By using the periodic extension of a function $f \in L^2([0, N])$ i.e.

$$f^{(\pi)}(x) = \sum_{k=-\infty}^{\infty} f(x + kN)$$

it can be shown¹⁴ [Mallat98] that the family

$$\{\psi_{j;k}^{(\pi)}\}_{j,k \in \mathbb{Z}^2}, \quad \psi_{j;k}^{(\pi)}(x) = \sqrt{2^j} \sum_{l=-\infty}^{+\infty} \psi(2^j x - k + 2^j lN)$$

forms an orthogonal basis of $L^2([0, N])$ such that

$$\langle \psi_{j;k}^{(\pi)}, \psi_{j';k'}^{(\pi)} \rangle_{L^2([0,N])} = \delta_{j,j'} \delta_{k,k'}$$

¹⁴The proof is based on using the fact that $f(x) = f^{(\pi)}(x)$, $\forall x \in [0, N]$, $f \in L^2([0, N])$ and on periodizing the decomposition $\sum_j \sum_k \langle f, \psi_{j;k} \rangle \psi_{j;k}(x)$.

and

$$f(x) = \sum_{j=-\infty}^{+\infty} \sum_{k=-\infty}^{+\infty} \langle f, \psi_{j;k}^{(\pi)} \rangle_{L^2([0,N])} \psi_{j;k}^{(\pi)}(x)$$

This is similar to consider a wavelet decomposition on a torus instead on the the real line [Jawerth93] and the main modification is to replace the convolution operators in equations (2.28), (2.29) and (2.31) by circular convolutions. However, the problem of creating large coefficients in the neighbourhood of 0 and N is not avoided since there is no guarantee that $f(0) = f(N)$.

Boundary wavelets

Using boundary wavelets avoids to create large wavelet coefficients at the border. Basically, it consists in using modified wavelets functions, which have as many vanishing moments as the original, for processing the borders. For a proper presentation, the reader is sent to [Cohen92b, Cohen93, Mallat98].

Note that folded wavelets are usable if the corresponding basis of $L^2(R)$ is constructed using symmetric or antisymmetric wavelets. This cannot occur in the one-dimensional orthogonal case, but can happen for biorthogonal wavelets. This solution preserves the continuity at the border but acts as if the signal had a discontinuous first-order derivative in the neighbourhood of 0 and N .

2.6.3 Examples of orthogonal wavelets

This subsection gives some important properties that a wavelet function may have (this list has been taken from [Jawerth93]) and presents a few families of orthogonal wavelet. Pointers to articles in which biorthogonal wavelets are constructed are also given.

Properties of a wavelet function

Orthogonality. The orthogonality is convenient to have in many situations. First, it directly links the L^2 -norm of a function to a norm on its wavelet coefficients. Second, the fast wavelet transform is a unitary transformation ($W^{-1} = W^\dagger$) which means that the condition number of the transformation ($\|W\| \|W^{-1}\|$) is equal to 1 (optimal case), i.e. stable numerical computations are possible. Moreover, if the multiresolution is orthogonal the projection operators onto the different subspaces (V_j, W_j) yield optimal approximations in the L^2 sense.

Compact support. If the wavelet has a compact support the filter h and g have a finite impulse response. Obviously, this is convenient for implementing the fast wavelet transform. However, if the wavelet does not have a compact support,

a fast decay is required so that h and g can be reasonably approximated using FIR filters.

Rational coefficients. For efficient computations, it can be interesting that the coefficients of h and g are rational or dyadic rational. Binary shifts are much faster than floating point operations.

Symmetry. If the scaling function and wavelet are symmetric, the filters h and g have generalized linear phase. The absence of this property can lead to phase distortion.

Regularity. As pointed in the works of Yves Meyer [Meyer90] and David Donoho [Donoho91a] the regularity of the multiresolution analysis is crucial for many applications such as data compression, statistical estimation, ... In the biorthogonal case, the regularity of the primary multiresolution is more important than the regularity of the dual one [Jawerth93].

Number of vanishing moments. The number of vanishing moments is connected to the regularity of the wavelet and vice versa [Meyer90].

Analytic expressions. In some case, it can be useful to have analytic expressions for the scaling function and wavelet.

Interpolation. If the scaling function satisfies

$$\phi(k) = \delta_k, \quad k \in Z$$

then the computation of the first scaling coefficients (required for starting the fast wavelet transform) is trivial and the assumption discussed in §2.6.2 is valid.

Obviously, a given multiresolution cannot satisfies all these properties (e.g. orthogonality, compact support and symmetry are exclusive properties in one dimension except for the Haar wavelet) and it is necessary to make a trade-off between them.

Some families of orthogonal wavelets

The Haar transform. The Haar transform has been invented in 1910, long before the invention of the terms “wavelet” and “multiresolution”. Some books about image processing present it as a curiosity [Gonzales92]. The Haar transform corresponds to an orthogonal multiresolution, associated with the following scaling function and wavelet

$$\phi(x) = \chi_{[0,1]}(x), \quad \psi(x) = \chi_{[0,1/2]}(x) - \chi_{[1/2,1]}(x)$$

The discrete filter h is then equal to $\{1, 1\}$. However, the Haar transform is not very used in practice because the analysing functions are too discontinuous. Note that the Haar wavelet is a particular case of a Daubechies wavelet for $N = 1$.

The Shannon wavelet. The Shannon wavelet is constructed from the Shannon multiresolution approximations which approximates functions by their restrictions to low frequency intervals. The scaling function is then a cardinal sine and the wavelet is equal to [Jawerth93]

$$\psi(x) = \frac{\sin 2\pi x - \sin \pi x}{\pi x}$$

This wavelet is C^∞ but it has a very slow time decay which makes it not suitable for practical purpose.

Meyer and Battle-Lemarié. A more interesting example is given by the Meyer wavelet and scaling function [Meyer90] which are C^∞ and have faster than polynomial decay (this makes them more suitable for practical purpose according to the compact support property). ϕ and ψ are respectively symmetric around 0 and $\frac{1}{2}$ and ψ as an infinite number of vanishing moments (see [Meyer90] for more details). The Battle-Lemarié wavelets are created by orthogonalizing B -spline functions and have exponential decay. A Battle-Lemarié wavelet with N vanishing moments is a piecewise polynomial of degree $N - 1$ belonging to C^{N-2} . See [Battle87, Lemarié88, Meyer90, Mallat98].

Daubechies wavelets. The first non-trivial compactly supported and orthogonal wavelet basis have been constructed by Ingrid Daubechies [Daubechies88]. A Daubechies scaling function/wavelet pair of order M satisfies the two following dilation equations

$$\phi(x) = \sqrt{2} \sum_{k=0}^{2M-1} h_k \phi(2x - k)$$

and

$$\psi(x) = \sqrt{2} \sum_{k=-2M+2}^1 g_k \phi(2x - k)$$

The coefficients $\{h_k\}$ (the $\{g_k\}$ are then given by (2.27)) are determined by solving the following $2M$ equations

$$\frac{1}{2} \sum_{l=0}^{2M-1} h_l h_{l-2k} = \delta_k, \quad k = 0, \dots, M-1$$

and

$$\sum_{l=0}^{2M-1} (-1)^{l+1} l^k h_l = 0, \quad k = 0, \dots, M-1$$

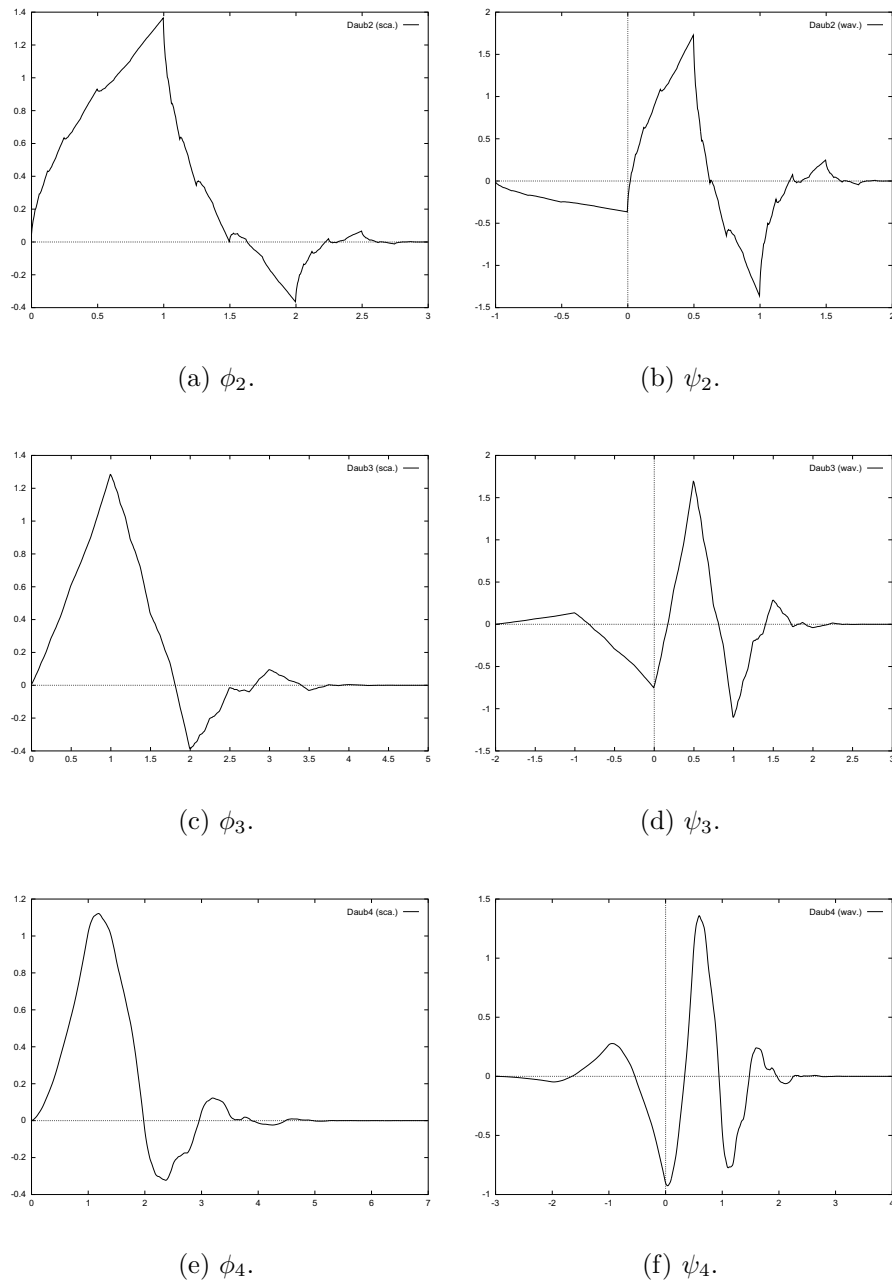
The first set of equations is a reformulation of equation (2.24) via the Wiener-Kintchine theorem¹⁵. The second set of equations expresses the fact that ψ must have M vanishing moments, i.e.

$$\int_{-\infty}^{+\infty} x^k \psi(x) dx = 0, \quad k = 0, \dots, M - 1$$

The resolution of this system of equations is done by finding a trigonometric polynomial $\hat{h}(\xi)$ satisfying equation (2.24) and having a root of multiplicity M at $\xi = \pi$. This is done by means of spectral factorization techniques (see—notably— [Daubechies88, Bourges94, Mallat98]). The regularity of the multiresolution analysis increases as N increases (roughly like $0.2075M$ for large M [Jawerth93, Meyer94]). However, these wavelets cannot be symmetric (except for $M = 1$ which corresponds to the Haar wavelet). Figure 2.3 presents some scaling functions and wavelets of the Daubechies family. These functions have been generated using a cascade algorithm [Delyon93, Bourges94] which (roughly) consists in applying the inverse wavelet transform algorithm on respectively the $\{h_k\}$ and the $\{g_k\}$. The filter coefficients for $M = 2, \dots, 10$ are available in [Daubechies88] (table 1, page 980).

Other orthogonal wavelet basis have been built using this philosophy. An interesting example is the coiflets constructed by Ronald Coifman [Beylkin91]. For this family, the scaling function also has some vanishing moments (except the first one) and these functions leads to discrete filters having $3M - 1$ non-zero coefficients. See [Beylkin91]. Other families of orthogonal and biorthogonal wavelets are (notably) designed in [Cohen92a, Vetterli92], [Mallat98] provides an up-to-date exposition on the subject.

¹⁵For discrete-time signals: $\mathcal{F}\{\sum_l f_l f_{l-k}\} = |\hat{f}(\xi)|^2$ where $\hat{f}(\xi) = \sum_k f_k e^{-i\xi k}$.

Figure 2.3 Some of the Daubechies scaling functions and wavelets.

Chapter 3

Image fusion in orthogonal wavelet basis

Introduction

The image fusion problem can be stated as follows: given two images containing complementary information, we want to build a new image which exhibits the relevant information present in both original images. Obviously, this problem can be expressed in a more general way where more than two images are available. An image fusion procedure is a low-level image processing task which aims at preparing higher-level processing. For example, a human brain is not able to fully and fastly integrate data coming from different sources. In that case, an image fusion operation prepares the data so that they are more easily understandable for a human operator, e.g. the driver of a car at night. Another field, known as data fusion [Bloch94, Bloch96], also exploits multisensor data (not necessarily images) in order to access higher-level cognitive functions, e.g. decision making. An example of application is target recognition via the Dempster-Shafer theory [Janez97, Shafer76].

In order to design an image fusion algorithm, one has to define clearly what a “relevant information” is, and to find a fusion operator (acting on some “convenient decompositions” of the source images) which has a correct behavior according to this definition. A simple fusion algorithm can consist in performing a pixel-by-pixel averaging of the source images but, as we will see later, this is not a correct solution. Here, the fusion problem is seen as a sharpest singularity selection problem and this task is performed by applying a non-linear operator on the decompositions of the images onto an orthogonal wavelet basis, i.e.

$$f(x) = \sum_{j=-\infty}^{+\infty} \sum_{k=-\infty}^{+\infty} \vartheta(\gamma_{j;k}^{(1)}, \gamma_{j;k}^{(2)}) \psi_{j;k}(x)$$

where $\gamma_{j;k}^{(1)}$ and $\gamma_{j;k}^{(2)}$ denote the coefficients of the (orthogonal) wavelet decompositions of the two source functions/images.

The chapter is organized as follows: we first give a short literature survey, then state the problem of image fusion in both multifocus and multisensor contexts and study the limitations of an approach based on linear operators or operators acting directly on the images. We then study the behavior of the wavelet coefficients of some one-dimensional signals containing isolated Hölder-0 singularities, and derive a one-dimensional fusion operator which is relevant in the context of sharpest singularity selection. These results are extended to the two-dimensional case and some experimental results are presented for both multifocus and multisensor data. Finally, we theoretically study the design of a fusion operator which takes into account the presence of a gaussian white noise.

3.1 Previous work and literature survey

Different methods have been proposed for performing image fusion tasks in a multisensor context. Before the coming of wavelet based techniques, other multiscale decompositions have been used such as: the Laplace pyramid [Burt83, Jahne95] (also known as the difference of low-pass—DoLP—pyramid) or the ratio of low-pass (RoLP) pyramid [Toet89, Toet92]. These different methods have been explored in a previous MSc thesis by Philip Cotterel [Cotterel97] where DoLP-and-RoLP-based fusion algorithms are tested and reasonable results are obtained. Note that a morphological-difference-pyramid-based fusion scheme has also been implemented and tested. For more details, the reader is sent to [Cotterel97]. The main differences between this work and the current thesis concern the registration procedure (they were mapping the NIR image onto the FIR one while we are doing the opposite) and obviously the absence of wavelets.

Concerning wavelet based techniques, Wilson *and al* [Wilson95] proposed an image fusion algorithm for the AVIRIS sensor¹ which is based on an empirical perceptual-based fusion operator (“optimal” for a resolution of 1024×1280 and for an average viewing distance of 61 cm) applied on the wavelet decompositions of the images to be fused. Finally, the work of Li *and al* [Li95b] is very close to the current one: they introduce a pixel-by-pixel maximum selection rule and an area-based maximum selection rule (both acting on the wavelet decompositions of the images to be fused) and empirically test their performances on a wide range of fusion problems (multifocus, MRI-PET, Landsat-Spot, Landsat-Seasat and visible-thermal images) with different classes of wavelets. There also exists some difficult-to-find references, foreseen on the internet, which are ignored since we have not been able to get sufficient precisions for localizing them.

¹Airborne Visible/Infrared Imaging Spectrometer. This sensor simultaneously records information in hundred of spectral bands and produces fully registered images, for more details see [Wilson95, Porter87].

3.2 Multifocus and multisensor data

3.2.1 The multifocus problem

The multifocus problem is probably the easiest to deal with. Basically, a scene, which contains different objects situated at different distances from the camera, is imaged. For a given image, only one object in the scene is in focus. In general, test images are generated from a scene containing two objects. We then have to fuse two images in which the two scenarios: blurred/clear and clear/blurred occur for (respectively) the two objects. This problem is relatively easy because (contrary to the multisensor case) we have an idea of the result we want: an image containing the two well-focused objects. Moreover, the multifocus pairs are perfectly registered. This allows us to test the fusion procedure without introducing any artifacts due to registration problems.

We have used two sets of data, coming from the internet:

1. Two objects: a can and some text coming from www.lehigh.edu/zhz3/IF_example1.html.
2. Two clocks (used in [Li95b]) coming from vivaldi.ece.ucsb.edu/projects/registration/fusion.html.

Figure 3.1 shows the two pairs of test images.

3.2.2 The multisensor problem

The multisensor problem is trickier than the multifocus one for two main reasons: first, we do not have a clear idea of the desired result and second, the two (or more) images do not have the same “nature” (the first reason is probably a consequence of the second one). Since the two images depend on totally different physical properties of the imaged objects (reflection of light for the NIR image and temperature for the FIR—thermal—one), an object can, for example, be bright on a dark background in one of the two images and dark on a bright background in the other one (this scenario cannot occur in the multifocus case). This problem is illustrated in figures 3.9 (page 68) and 3.10 (page 69), e.g. the trees. Figure 3.2 shows a typical NIR/FIR pair. Studying figure 3.2 gives us an idea of the desired result. Basically, we want the “well-defined” objects (in some sense which is to be defined) present in the FIR image (e.g. the trees, the post, . . .) and those present in the NIR one (e.g. the bottom right car, the window, . . .) to be visible without any degradation in the fused image. An informal definition of a “well-defined” object can be based on the sharpness of its frontier since sharp transitions/contours are very important attributes for image analysis (both on a “human” and a “machine” point of view) [Gonzales92, Jahne95, Deriche, Meyer94].

Figure 3.1 Examples of multifocus data.

(a) The “can” pair.



(c) The “clocks” pair.

Figure 3.2 Example of multisensor data.



(a) NIR image.

(b) FIR image.

3.3 Linear operators

As stated in the introduction (page 49), the simplest fusion algorithm consists in using a linear (or non-linear) operator acting directly on the image without transforming it. The most popular one is the pixel-by-pixel averaging which implies a loss of contrast if an object is visible in only one of the two images, or if its NIR and thermal properties are not compatible e.g. it is bright in the NIR image and dark in the FIR one. Therefore, this kind of operator is not usable for both multifocus (local blurring also implies a loss of intensity) and multisensor data. Concerning the non-linear operators acting directly on the image, one can use a maximum-based selection which provides reasonable results when the different frames are seen independently. However, the fused images seem to be very unstable and highly sensitive to registration problems [Cotterel97].

3.4 Wavelet transform of some Hölder-0 singularities

The two next subsections give some formal arguments which explain the relevancy of using an area-based maximum selection rule for image fusion. As discussed in §3.2.2, an object is said to be well-defined if it has a sharp frontier with the “outside world”. This frontier can be modelised by the presence of a Hölder-0 singularity. Its degree of smoothness (expressed as a convolution with a gaussian operator) gives a measure of its saliency. Here, we focus on the one-dimensional

problem: we first study the wavelet coefficients of a sharp Hölder-0 singularity, then introduce a smoothed singularity model and finally study the consequences of the smoothing on its wavelet coefficients.

3.4.1 Sharp Hölder-0 singularity

A sharp Hölder-0 singularity corresponds to a Heaviside-like singularity of the form $f(x) = \tau_\nu U(x)$ where

$$U(x) = \begin{cases} 1 & \text{if } x \geq 0 \\ 0 & \text{otherwise} \end{cases}$$

We consider an orthogonal wavelet ψ with at least one vanishing moment, such that

$$\text{supp}\psi = [a, b] \Leftrightarrow \text{supp}\psi_{j;k} = [a/2^j + k, b/2^j + k]$$

$\psi_{j;k}$ should be understood in a multiresolution context (see §2.4.1). The wavelet coefficients $\gamma_{j;k} = \langle f, \psi_{j;k} \rangle$ are then equal to

$$\gamma_{j;k} = \begin{cases} \int_\nu^{b/2^j+k} \psi_{j;k}^*(x) dx & \text{if } [\nu - b/2^j, \nu - a/2^j] \\ 0 & \text{otherwise} \end{cases}$$

Hence, the wavelet coefficients vanish if the support of the wavelet does not overlap the singularity (this is a direct consequence of the fact that ψ has at least one vanishing moment).

3.4.2 Smooth Hölder-0 singularity

We now consider a smooth Hölder-0 singularity model expressed as follows

$$f(x) = \tau_\nu U \otimes g_\sigma(x)$$

where $g_\sigma(x)$ denotes the normalized Gauss function $\frac{1}{\sqrt{2\pi}\sigma} e^{-\frac{x^2}{2\sigma^2}}$. This model is commonly used e.g. [Mallat92a, Mallat92b] (or [Blaska94, Blaska97] where it is used to model the blurring effect of an imaging system). It can easily be shown that $f(x) = \tau_\nu \Phi_\sigma(x)$ where Φ_σ is the Erf function corresponding to g_σ [Weisstein98], i.e.

$$\Phi_\sigma(x) = \frac{1}{\sqrt{2\pi}\sigma} \int_{-\infty}^x e^{-\frac{y^2}{2\sigma^2}} dy$$

For $|x - \nu| \gg \sigma$, $\tau_\nu \Psi(x)$ is approximately constant (equal to 0 or 1 depending on $\text{sign}(x - \nu)$), therefore $\gamma_{j;k} \approx 0$ for $a/2^j + k - \nu \gg \sigma$ or $\nu - b/2^j - k \gg \sigma$. Now, let us forget (for a short moment) the discretization of the wavelet transform parameters and recall that $\mathcal{W}_f(a, b) = f \otimes \bar{\psi}_{a,b}$. In our particular case, we have

$$\begin{aligned} \mathcal{W}_f(a, b) &= \tau_\nu U \otimes g_\sigma \otimes \bar{\psi}_a(b) \\ &= g_\sigma \otimes \mathcal{W}_{\tau_\nu U}(a, \cdot)(b) \end{aligned}$$

Hence, the gaussian convolution operator smoothes, spreads and decreases the amplitude of the wavelet coefficients of $\tau_\nu U(x)$ in the neighbourhood of the singularity, i.e. the presence of a singularity introduces a “burst” of non zero wavelet coefficients and, as σ increases, the maximum wavelet coefficient (in terms of absolute value) in the neighbourhood of the singularity tends to decrease. Formally,

$$\sup_{b \in \Omega} |\mathcal{W}_{\tau_\nu \Phi_{\sigma_1}}(a, b)| > \sup_{b \in \Omega} |\mathcal{W}_{\tau_\nu \Phi_{\sigma_2}}(a, b)|, \quad \sigma_1 < \sigma_2 \quad (3.1)$$

Ω denotes the neighbourhood of ν . If we re-introduce the “multiresolution sampling”, we end up with

$$\gamma_{j;k} = g_\sigma \otimes \mathcal{W}_{\tau_\nu U}(2^{-j}, \cdot)[2^{-j}k]$$

Unfortunately, in this case, the lack of translation invariance [Coifman95] does not guarantee that property (3.1) is preserved by the sampling of the wavelet coefficients. However, as shown on figure 3.3, it seems reasonable to consider that for $\sigma_1 \ll \sigma_2$, there will be at least one wavelet coefficient coming from the sharpest singularity which will be greater than those coming from the smoothest one, in the neighbourhood of ν .

Another way of interpreting the previous results can be done via the following theorem (proved in [Mallat98]).

Theorem 7 *A wavelet ψ with a fast decay has n vanishing moments if and only if there exists θ (a smoothing operator) with a fast decay such that*

$$\psi(x) = (-1)^n \frac{d^n \theta(x)}{dx^n}$$

As a consequence

$$W_f(a, b) = a^n \frac{d}{db^n} (f \otimes \bar{\theta}_a)(b)$$

where $\theta_a(x) = a^{-\frac{1}{2}} \theta(x/a)$. Moreover, ψ has no more than n vanishing moments if and only if $\int_{-\infty}^{+\infty} \theta(x) dx \neq 0$.

Therefore the wavelet coefficients (forgetting again the discretization of a and b) can be expressed as

$$\begin{aligned} \mathcal{W}_f(a, b) &= a^n \frac{d^n}{db^n} (\tau_\nu U \otimes g_\sigma \otimes \bar{\theta}_a)(b) \\ &= a^n \frac{d^{n-1}}{db^{n-1}} (\tau_\nu g_\sigma \otimes \bar{\theta}_a)(b) \\ &= a^n \tau_\nu \frac{d^{n-1}}{db^{n-1}} \lambda_{\sigma;a}(b) \end{aligned}$$

Where $\lambda_{\sigma;a}$ is a infinitely differentiable low-pass filter, such that

$$\int_{-\infty}^{+\infty} (x - \bar{x})^2 \lambda_{\sigma;a}(x) dx$$

is an increasing function of σ (for a fixed value of a). We therefore have

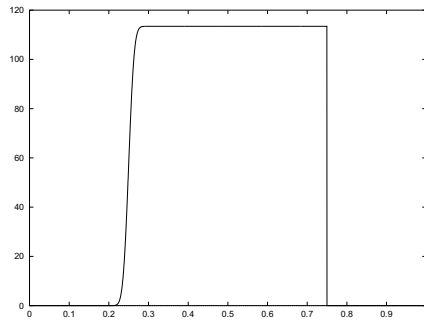
$$\sup_{b \in \Omega} \frac{d^{n-1}}{db^{n-1}} \lambda_{\sigma_1;a}(b) > \sup_{b \in \Omega} \frac{d^{n-1}}{db^{n-1}} \lambda_{\sigma_2;a}(b), \quad \sigma_1 < \sigma_2$$

Which is equivalent to property (3.1). Re-introducing the discretization occuring in the multiresolution context gives

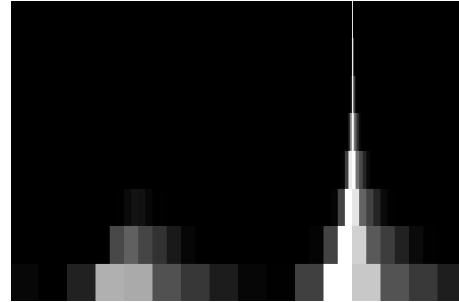
$$\gamma_{j;k} = 2^{-nj} \frac{d^{n-1}}{db^{n-1}} \lambda_{\sigma;2^j}(b) \Big|_{b=2^{-j}k}$$

and is interpreted as before, i.e. the lack of translation invariance does not guarantee that the maximum amplitude wavelet coefficient (over Ω) is sampled.

Figure 3.3 Wavelet transform of some Hölder-0 singularities (Daubechies-8).



(a) Original signal.



(b) Its wavelet decomposition.

3.5 Sharpest singularity selection

In this section, we derive a one-dimensional fusion operator from the results previously discussed and generalize them to a whole class of functions belonging to Besov spaces (see §D.3). We then give a formal definition of the windowed maximum selection rule and discuss its limitations.

3.5.1 Piecewise regular functions

Requiring that ψ has n vanishing moments allows us to extend the results derived in the previous section to piecewise polynomial signals. Since $\int_{-\infty}^{+\infty} x^k \psi(x) dx = 0$, $\forall k \in \{0, n-1\}$, we have

$$\int_{-\infty}^{+\infty} \sum_{k=0}^{n-1} \alpha_k x^k \psi(x) dx = \sum_{k=0}^{n-1} \alpha_k \int_{-\infty}^{+\infty} x^k \psi(x) dx = 0$$

If the wavelet has a compact support and as soon as $\psi_{j;k}$ does not overlap any singularity, $\gamma_{j;k} = 0$. This implies that piecewise polynomial signals have the same kind of behavior than the piecewise constant signals studied in §3.4, i.e. they generate “bursts” of non zero wavelet coefficients in the neighbourhood of the singularities. Moreover, as the number of vanishing moments increases, the regularity of the multiresolution (in Yves Meyer sense [Meyer90]) increases and makes the wavelet basis suitable for studying functions belonging to Besov spaces which behave roughly like piecewise polynomial signals: they are efficiently characterized by a few non-zero wavelet coefficients [Meyer94]. In other words, an orthogonal wavelet basis provides an optimal “point of view” in which the relevant information (sharp variations) can be easily discriminated from the rest². This assertion is the basis of David Donoho’s work (for denoising purpose, see 3.9.1) and justifies the relevancy of using orthogonal wavelet decompositions for image fusion: the “relevant information” is better seen in an orthogonal wavelet basis than in any others.

3.5.2 Windowed maximum operator

Property (3.1) and the assumption that it is satisfied in a multiresolution context allow us to design a simple fusion operator which aims at selecting the sharpest singularity at a given “location”. Basically, it consists in studying the absolute values of the wavelet coefficients over a given window and to keep the wavelet coefficient which corresponds to the highest absolute value within the window. Formally,

$$\gamma_{j;k}^{(f)} = \begin{cases} \gamma_{j;k}^{(1)} & \text{if } \max_{l \in \Omega} |\gamma_{j;l}^{(1)}| \geq \max_{l \in \Omega} |\gamma_{j;l}^{(2)}| \\ \gamma_{j;k}^{(2)} & \text{otherwise} \end{cases}$$

Ω denotes the window. Since the blurring of a Hölder-0 singularity by a gaussian operator implies a decreasing of the maximum wavelet coefficients in the neighbourhood of that singularity, the windowed maximum operator performs a singularity selection based on their sharpness. Moreover, the fusion does not

²We translate Yves Meyer ([Meyer94], fourth chapter, p. 183): “Wavelets allows to represent very efficiently signals which are relatively regular and which contain isolated singularities. These signals belong to $B_{p,p}^{\frac{1}{p}}$, $\forall p > 0$.”

take into account the regular parts of the signal, which are “coded” in the dilated and translated wavelets.

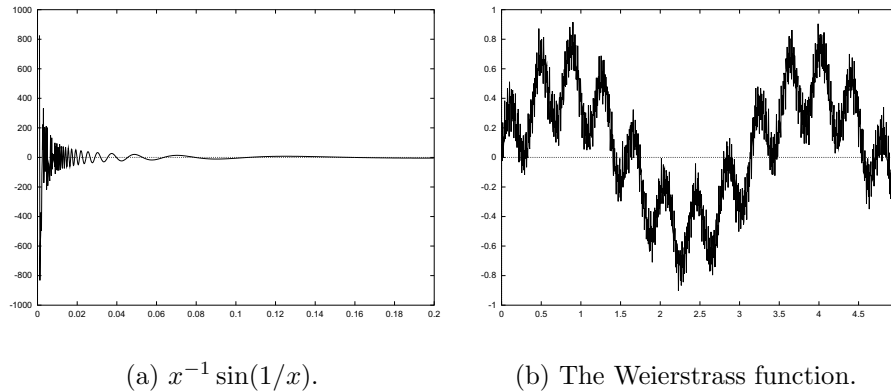
3.5.3 Limitations

In the previous sections we have implicitly assumed that the singularities contained in the signal are isolated, i.e. sufficiently far away from each other. If we consider some functions with non isolated singularities like $x^{-1} \sin(1/x)$ [Farge93] (see figure 3.4 (a)) or the (globally fractal) Lebesgue-Weierstrass function [Farge93, Lamoureux94, Meyer94] (see figure 3.4 (b)),

$$\sum_{k=1}^{\infty} \frac{1}{2^k} \sin 2^{n^2} x$$

which is continuous but nowhere differentiable, the windowed maximum selection rule is likely to give improper or uncontrolled results. However, the study of the relationships between wavelets (not necessarily orthogonal) and (multi)fractal signals is beyond the scope of this thesis, the reader is (notably) sent to [Farge93, Mallat92a, Hwang93, Mallat98, Meyer94] for more details. Other limitations due to the multisensor origins of the data are to be discussed in §3.7.3.

Figure 3.4 Examples of signals with non-isolated singularities.



3.6 Bi(multi)dimensional wavelet transform

This section generalizes the notion of wavelet transform and orthogonal multiresolution analysis in two dimensions. We first (briefly) introduce the spaces $L^2(\mathbb{R}^n)$ and $L^p(\mathbb{R}^n)$, then defines the continuous wavelet transform on $L^2(\mathbb{R}^2)$ and build

orthogonal multiresolution analysis of $L^2(\mathbb{R}^2)$ by means of separable wavelet basis. Obviously, these extensions are necessary for being able to use the wavelet analysis in an image processing context.

3.6.1 Spaces: $L^2(\mathbb{R}^2)$, $L^2(\mathbb{R}^n)$ and $L^p(\mathbb{R}^n)$

The spaces $L^2(\mathbb{R}^2)$, $L^2(\mathbb{R}^n)$ and $L^p(\mathbb{R}^n)$ are “natural extensions” of $L^2(\mathbb{R})$ (space of square integrable function of one variable, see §2.1). $L^2(\mathbb{R}^2)$, the space of square integrable functions of two variables, is defined as

$$L^2(\mathbb{R}^2) = \left\{ f / \int_{-\infty}^{+\infty} \int_{-\infty}^{+\infty} |f(x, y)|^2 dx dy < \infty \right\}, \quad f, g \in L^2(\mathbb{R}^2)$$

provided the following scalar product and the following norm

$$\langle f, g \rangle_{L^2(\mathbb{R}^2)} = \int_{-\infty}^{+\infty} \int_{-\infty}^{+\infty} f(x, y) g^*(x, y) dx dy, \quad \|f\|_{L^2(\mathbb{R}^2)}^2 = \langle f, f \rangle_{L^2(\mathbb{R}^2)}$$

Obviously, the more general space $L^2(\mathbb{R}^n)$ is defined as

$$L^2(\mathbb{R}^n) = \left\{ f / \int_{\mathbb{R}^n} |f(\vec{z})|^2 d\vec{z} < \infty \right\}, \quad \vec{z} \in \mathbb{R}^n \quad (3.2)$$

with

$$\langle f, g \rangle_{L^2(\mathbb{R}^n)} = \int_{\mathbb{R}^n} f(\vec{z}) g^*(\vec{z}) d\vec{z}, \quad \|f\|_{L^2(\mathbb{R}^n)}^2 = \langle f, f \rangle_{L^2(\mathbb{R}^n)}$$

Finally, $L^p(\mathbb{R}^n)$ is defined (for $1 \leq p \leq \infty$) by replacing 2 by p in equation (3.2) and the norm operator becomes (with the usual modification for $p = \infty$)

$$\|f\|_{L^p(\mathbb{R}^n)} = \left(\int_{\mathbb{R}^n} |f(\vec{z})|^p d\vec{z} \right)^{\frac{1}{p}}$$

The concepts of wavelet transform and multiresolution analysis can be easily generalized for $L^2(\mathbb{R}^n)$ (see the next subsection for $L^2(\mathbb{R}^2)$), but the generalization for $L^p(\mathbb{R}^n)$ is trickier³, the reader is (notably) sent to [Meyer90].

3.6.2 Continuous wavelet transform on $L^2(\mathbb{R}^2)$

The continuous wavelet transform of a function f of two variables belonging to $L^2(\mathbb{R}^2)$ is a straightforward generalization of the one-dimensional case presented in §2.3. Formally, given a wavelet Ψ

$$\mathcal{W}_f(a, b, b') = \langle f, \Psi_{a;b;b'} \rangle_{L^2(\mathbb{R}^2)}, \quad \Psi_{a;b;b'}(x, y) = \frac{1}{a} \Psi \left(\frac{x-b}{a}, \frac{y-b'}{a} \right)$$

The reader is (notably) sent to [Mallat98] for more details (including the wavelet transform using wavelets with different spatial orientations).

³In that general case, we have to deal with some paradoxical behaviors e.g. if we directly use an orthogonal decomposition of the form $f(x) = \sum_j \sum_k \langle f, \psi_{j;k} \rangle \psi_{j;k}(x)$ (ψ is supposed to have at least one vanishing moment) on $f(x) = 1$ ($f \in L^\infty(\mathbb{R})$) we end up with $\langle f, \psi_{j;k} \rangle = 0$, $\forall j, k \in \mathbb{Z}^2$ and hence with $1 = 0$! See [Meyer90] for more details.

3.6.3 Multiresolution analysis of $L^2(R^2)$

A simple way of building an orthogonal multiresolution of $L^2(R^2)$ consists in using separable wavelet basis which is done via the following theorem (notably proved in [Mallat98]).

Theorem 8 (Separable multiresolution) *Let ϕ and ψ (respectively) be the scaling function and the wavelet generating an orthogonal multiresolution on $L^2(R)$ and define*

$$\Psi^{(1)}(x, y) = \phi(x)\psi(y), \quad \Psi^{(2)}(x, y) = \psi(x)\phi(y), \quad \Psi^{(3)}(x, y) = \psi(x)\psi(y)$$

For $\alpha \in \{1, 3\}$

$$\Psi_{j;k;k'}^{(\alpha)} = 2^j \Psi^{(\alpha)}(2^j x - k, 2^j y - k')$$

Then the families $\{\Psi_{j;k;k'}^{(\alpha)}\}_{\alpha \in \{1,3\}, k,k' \in \mathbb{Z}^2}$ and $\{\Psi_{j,k,k'}^{(\alpha)}\}_{\alpha \in \{1,3\}, j,k,k' \in \mathbb{Z}^3}$ (respectively) form orthogonal basis of W_j^2 and $L^2(R^2)$.

The wavelet transform of an image is then organized as shown on figure 3.5. For example, the coefficients $\gamma_{j;k;k'}^{(1)} = \langle f, \Psi_{j;k;k'}^{(1)} \rangle$ correspond to the one dimensional scalar product of f with $\phi_{j;k}$ according to the rows and to the scalar product of f with $\psi_{j;k'}$ according to the columns of the image. As discussed in [Bourges94, Starck92]: $\gamma_{j;k;k'}^{(1)}$ corresponds to the horizontal low frequencies and to the vertical high frequencies (vertical details) of $\mu_{j+1;k;k'} = \langle f, \Phi_{j+1,k,k'} \rangle$ ($\Phi(x, y) = \phi(x)\phi(y)$), while $\gamma_{j;k;k'}^{(2)}$ and $\gamma_{j,k,k'}^{(3)}$ respectively correspond to its horizontal high/vertical low and horizontal high/vertical high frequencies (horizontal and diagonal details). The algorithm for computing the wavelet coefficients of an image becomes a straightforward extension of the decimated filter banks algorithm used in one dimension (see §2.6.1). Basically, it consists in applying the one dimensional algorithm on the rows followed by the same operation on the columns (the order does not matter) for each scale, i.e. for computing the wavelet coefficients at scale j from the scaling coefficients at scale $j + 1$. Note that it is possible to create non-separable wavelet basis of $L^2(R^2)$ [Kovačević92], but in spite of their interesting properties e.g. orthogonal, compactly supported and symmetric wavelets (which is not possible in the one dimensional case), they are not very used in practice. Figure 3.6 shows the wavelet decompositions of some images.

3.7 Wavelet based image fusion

3.7.1 Extension of the results derived in §3.4

The purpose of this subsection is to generalize the results derived in §3.4 (for the one dimensional case) in two dimensions. This will allow us to define the

Figure 3.5 Organization of a two-dimensional wavelet decomposition.

Φ		...	$\Psi^{(2)}(\vec{z}) =$ $\psi(x)\phi(y)$ “High-Low”
		...	
		...	
$\Psi^{(1)}(\vec{z}) =$ $\phi(x)\psi(y)$ “Low-High”		$\Psi^{(3)}(\vec{z}) =$ $\psi(x)\psi(y)$ “High-High”	

$\vec{z} = (x \ y)^T$

fusion operator in the next subsection. As in the one-dimensional case, if the analysed function is singular at $(\nu \ \nu')^T$, in the direction of the wavelet, the corresponding coefficients are going to be large (in the neighbourhood of $(\nu \ \nu')^T$). This is illustrated by using theorem 7 (page 55) which implies that each wavelets $(\{\psi^{(\alpha)}\}_{\alpha=1,2,3})$ is the n^{th} -order partial derivative of a smoothing operator, i.e.

$$\Psi^{(1)}(x, y) = (-1)^n \frac{\partial^n}{\partial y^n} \Theta^{(1)}, \quad \Psi^{(2)}(x, y) = (-1)^n \frac{\partial^n}{\partial x^n} \Theta^{(2)}$$

and

$$\Psi^{(3)}(x, y) = (-1)^{2n} \frac{\partial^n}{\partial x^n} \frac{\partial^n}{\partial y^n} \Theta^{(3)}$$

where $\Theta^{(1)}(x, y) = \phi(x)\theta(y)$, $\Theta^{(2)}(x, y) = \theta(x)\phi(y)$ and $\Theta^{(3)}(x, y) = \theta(x)\theta(y)$. This directly implies that the wavelet coefficients correspond to the partial derivatives of f smoothed by $\Theta^{(\alpha)}$ (properly scaled).

$$\mathcal{W}_f^{(1)} = a^n \frac{\partial^n}{\partial b'^n} (f \otimes \bar{\Theta}_a^{(1)})(b, b'), \quad \mathcal{W}_f^{(2)} = a^n \frac{\partial^n}{\partial b^n} (f \otimes \bar{\Theta}_a^{(2)})(b, b')$$

and

$$\mathcal{W}_f^{(3)} = a^{2n} \frac{\partial^n}{\partial b^n} \frac{\partial^n}{\partial b'^n} (f \otimes \bar{\Theta}_a^{(3)})(b, b')$$

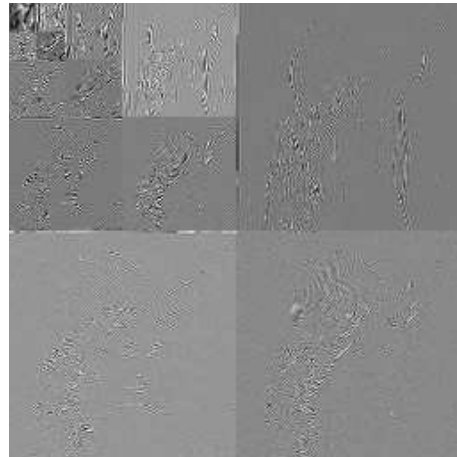
Hence, the more f is singular in the wavelet direction, the more $\sup_{\Omega} |\mathcal{W}_f^{(\alpha)}(a, b, b')|$ is large (Ω denotes the two-dimensional neighbourhood of $(\nu \ \nu')^T$). Considering a two-dimensional gaussian operator of the form $(2\pi\sigma^2)^{-1} e^{-(x^2+y^2)/(2\sigma^2)}$ and using the fact that $\mathcal{W}_f^{(\alpha)}(a, b, b') = f \otimes \bar{\psi}_a^{(\alpha)}(b, b')$ leads to

$$\begin{aligned} \mathcal{W}_{f \otimes g_\sigma}^{(\alpha)} &= f \otimes g_\sigma \otimes \bar{\Psi}_a^{(\alpha)}(b, b') \\ &= g_\sigma \otimes \mathcal{W}_f^{(\alpha)}(a, b, b') \end{aligned}$$

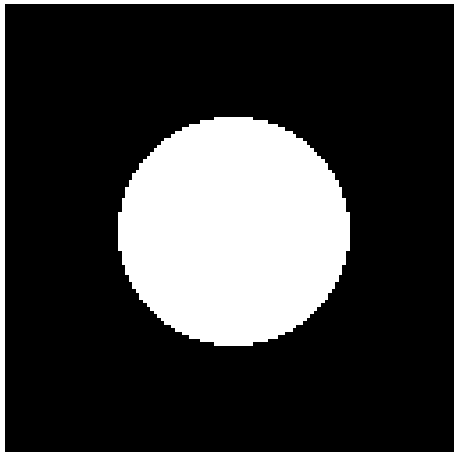
Figure 3.6 Wavelet decompositions of some images (Daubechies-8).



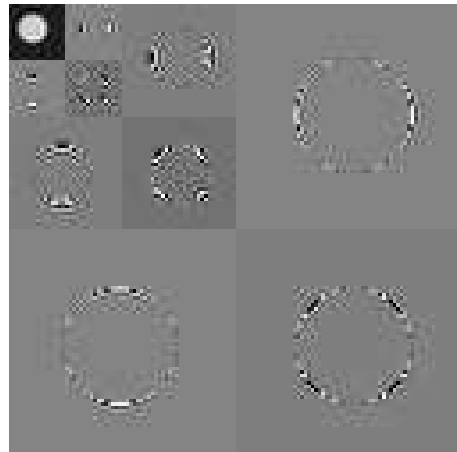
(a) "Lenna".



(b) Its wavelet decomposition.



(c) A disk.



(d) Its wavelet decomposition.

Therefore, the effect of a gaussian smoothing operator is to decrease (at least) the maximum amplitude coefficient (in Ω), to spread and to smooth the wavelet coefficients. As in one dimension we end up with

$$\sup_{b,b' \in \Omega} |\mathcal{W}_{f \otimes g_{\sigma_1}}^{(1)}(a, b, b')| > \sup_{b,b' \in \Omega} |\mathcal{W}_{f \otimes g_{\sigma_2}}^{(1)}(a, b, b')|, \quad \sigma_1 < \sigma_2 \quad (3.3)$$

However, the lack of translation invariance, introduced by the sampling of the translation parameters ($b = 2^{-j}k$ and $b' = 2^{-j}k'$) implies that the maximum absolute value wavelet coefficient on Ω is not necessarily sampled. Generalization to piecewise regular images (or geometrical images [Meyer94]) done using the same arguments as in §3.4.

3.7.2 Area based maximum selection

Since the presence of a singularity is responsible for a “burst” of non zeros wavelet coefficients, we propose (as in [Li95b]) to realize the fusion using an area-based maximum selection. Basically, it consists in studying the absolute value of the wavelet coefficients within a square window⁴ centered on the coefficient of interest (in both images) and to choose the one which corresponds to the highest maximum value in this area. This operator behaves correctly, according to what we want to select i.e. sharp transitions. Moreover, it is not sensitive to (small) imperfections (which are likely to occur) in the registration process. Since we study the neighbourhood of a given wavelet coefficient, it is not required that two singularities (having the same origins in the “outside-world”) have to be perfectly aligned (however, this assertion should be an assumption because the lack of translation invariance does not allow to interpret the wavelet coefficients easily).

The relevancy of this operator for the multifocus problem is obvious since the two images have the same nature: the presence of a local blurring decreases the amplitude of the wavelet coefficients in the blurred area. Concerning the multisensor problem, its relevancy is less obvious because (as already discuss in §3.2.2) the two images are resulting from completely different physical phenomenons. However, if an object has a sharper frontier in one of the two images, then its frontier will be the one chosen and since its regular parts are “coded” in the dilated/translated wavelet functions, we perform a kind of object selection, which is what we want (see figure 3.7).

3.7.3 Limitations

In spite of the interesting properties of the operator, some problems may crop up. For example, if an object is not “physically homogeneous”: consider a bar heated

⁴The size of the window has been empirically set to 3×3 . Moreover, since the image is subsampled from 2^j to 2^{j-1} , the dimensions of the window do not need to be adapted for taking into account that the scaling coefficients are more and more smoothed.

up on only one side (say the right side), the resulting thermal image will be bright on the hot side and relatively dark on the cool side (the left one). Now, consider that the same bar is lighted up from behind: this gives a visible image which corresponds to a black rectangle on a bright background. On a fusion point of view, these two images are not compatible: on one hand, if the hot side of the bar has a sharper frontier in the thermal image than in the visible one, it will be taken from the thermal image, on the other hand the other (left/cool) side will be taken from the visible image. Therefore, in that particular case, we have not performed an object selection but built an incomprehensible composite object. Figure 3.7 ((d), (e) & (f)) illustrates this problem. However, extensive experimental tests have shown that this kind of scenario rarely occurs in practice.

As in the one dimensional case (§3.5.3), we have implicitly assumed that the singularities present in an image are isolated, the fusion operator may fail to fuse correctly some objects with a fractal frontier or may behave improperly if some objects have a fractal texture (however, do we know what the correct result is?).

Figure 3.7 Example of correct and failed object selection.



(c) Object selection.



(d) Visible image.

(e) Thermal image.

(f) Objects merging.

3.8 Experimental results

3.8.1 Multifocus image fusion

Figure 3.8 shows the results of the fusion operator applied on both the “can” and the “clocks” pairs of images. On a visual point of view, the resulting images seem reasonable, i.e. the well-focused objects present in both images are present without any (visual) degradation in the fused images. In the multifocus case, we are able to have a quantitative estimate of the algorithm performances. As proposed in [Li95b], a reference image can be created by manual cut and paste⁵ and the performances of the algorithm are evaluated using the following measure

$$\rho = \sqrt{\frac{1}{N^2} \sum_{i,j} (f^*[i,j] - f[i,j])^2}$$

where f^* denotes the manually fused image. The fusion has been performed using a Daubechies wavelet with 8 null moments and a popularity filter. The values lying outside $[0, 255]$ have been clipped. In the “can” case, the performance measure is equal to 3.5175, while in the “clocks” case, we have $\rho = 3.7077$. These results are roughly equivalent to those provided in [Li95b]. Moreover, extensive experimental tests, involving different orthogonal and biorthogonal wavelets [Antonini92, Cohen92a, Daubechies88, Beylkin91, Vetterli92], have shown that the performances of the fusion algorithm are not affected by the wavelet, as soon as the multiresolution analysis is sufficiently regular.

3.8.2 Multisensor image fusion

Figure 3.9, 3.10 and 3.11 present some experimental results in the multisensor case. The NIR/FIR pairs have been taken from the sequence and correspond to the frames $\{050, 053\}$, $\{100, 103\}$, $\{200, 203\}$, $\{300, 303\}$, \dots , $\{600, 603\}$. This set of images is representative of the kind of scenari available within the sequence. As shown on the three figures, the results given by the fusion algorithm are reasonable: it gives (most of the time) an image which integrates the relevant information available in the two source images. The tests have been performed using a Daubechies-8 wavelet, the area-based maximum selection and a popularity filter [Li95b]. In what follows, we analyse briefly the results.

Figure 3.9

The object selection is well-illustrated on many frames. For example, the fused image, corresponding to $\{050, 053\}$, contains the bottom-right car and the house window coming from the NIR image while the trees and the post have been taken

⁵However, this manual cut and paste is tricky to do, even for a human operator.

Figure 3.8 Experimental results on multifocus data.



(c) Fusion (“can”).



(f) Fusion (“clocks”).

from the FIR one ; the bottom-right part of the road is coming from the NIR image as well. This object selection has been performed for all the frames in this figure (e.g. the road marks and the bareer of the house in $\{200, 203\}$, the “mysterious square” in the three frames, ...). Moreover, the fused images are easily understandable, in comparison to the raw FIR ones, and contain more information than the raw NIR ones.

Figure 3.10

On this figure, the comments are roughly the same: the object selection has been correctly performed (e.g. the bin in $\{300, 303\}$, the bareer, the house and the trees in $\{350, 353\}$, the road sign in $\{400, 403\}$, ...). As in figure 3.9, the fusion gives reasonable results and leads to understandable images which takes into account the relevant information coming from both the NIR and the FIR images.

Figure 3.11

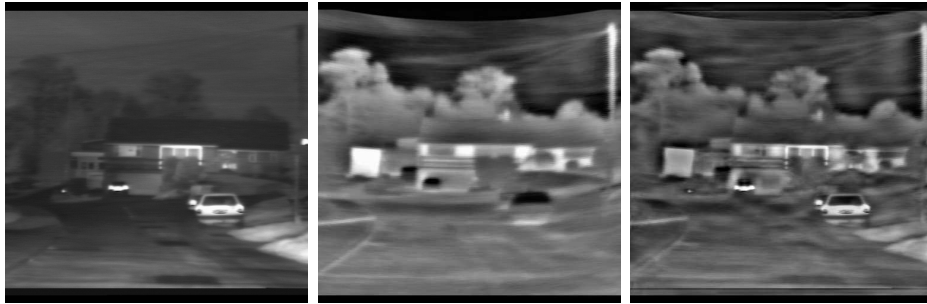
Figure 3.11 provides two interesting examples. For the first pair ($\{500, 503\}$), the NIR image contains no useful information almost everywhere in its bottom part, while the FIR image shows the border of the road (useful, when driving at night!) and a sort of house. However, the frontier between the sky and the trees is better defined in the NIR image than in the FIR one. The resulting image is a good fusion example: the bottom part of the fused image contains all the useful information available in the FIR image, and the frontier between the sky and the tree has been taken from the NIR image. The pair $\{600, 603\}$ exhibits some artifacts in the top part, we think that this is mainly a consequence of a “bar”-like problem (see §3.7.3). Due to the sunset, the trees in the NIR image are dark on a bright background (lighted up from behind). Moreover, they have been “eroded” because of the over-exposition. The FIR image, as a thermal one, is not subject to this problem. Hence, the two images are incompatible and a composite object is built by the fusion process. However, this situation is not likely to occur when driving at night (not at sunset) and just concerns the top part of the image (which is not very important when driving).

Experimental tests have also shown (as in the multifocus case) that the results are not affected by the wavelet as soon as it has a sufficient number of vanishing moments. For example, a Daubechies wavelet with only 2 vanishing moments leads to a pertubated fused image.

3.9 Denoising in the wavelet space

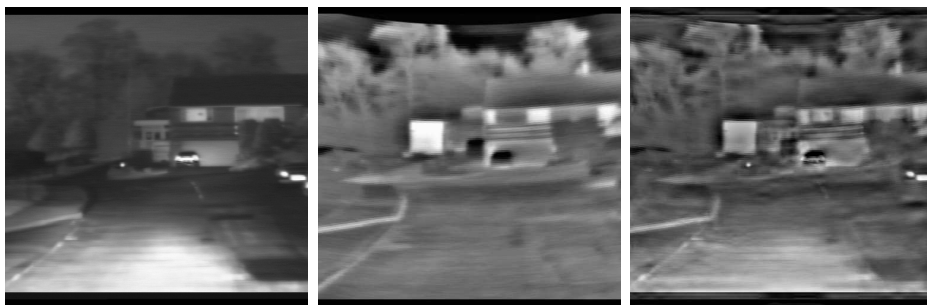
Since the beginning of the chapter, we have not spoken about noise: it does not seem to disturb the fusion process, **in the case of our data** which are of good

Figure 3.9 Experimental results on multisensor data.



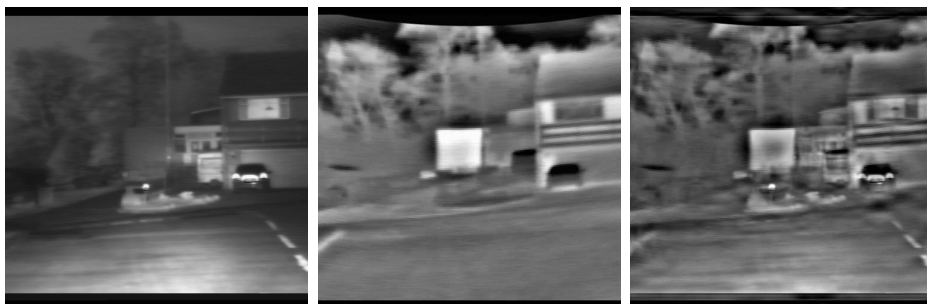
(a) NIR-050.

(b) FIR-053.



(d) NIR-100.

(e) FIR-103.



(g) NIR-200.

(h) FIR-203.

Figure 3.10 More experimental results on multisensor data.



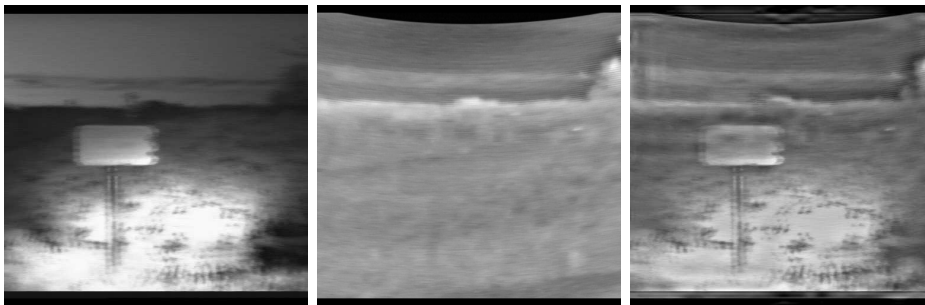
(a) NIR-300.

(b) FIR-303.



(d) NIR-350.

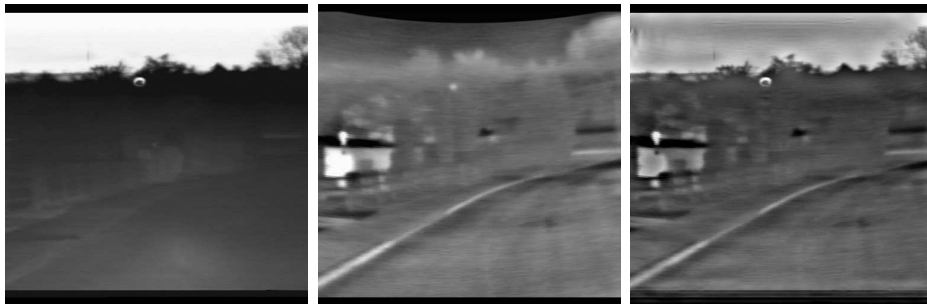
(e) FIR-353.



(g) NIR-400.

(h) FIR-403.

Figure 3.11 Still more experimental results on multisensor data.



(a) NIR-500.

(b) FIR-503.



(d) NIR-600.

(e) FIR-603.

quality i.e. nearly noise-free. This section is devoted to signal/image fusion in a noisy environment. We first introduce the well-known denoising algorithm(s) proposed by David Donoho *and al* [Donoho91b, Donoho92, Donoho94, Donoho95], then study the feasibility of image fusion in a noisy environment and finally, we present a few other methods of denoising.

3.9.1 Denoising via wavelet shrinkage

The purpose of denoising is to estimate a real function f from a set of corrupted measurements. A simple statistical model consists in considering that the samples are corrupted by an additive gaussian white noise i.e.

$$G_k = f_k + \sigma B_k, \quad B_k \text{ follows } \mathcal{N}(0, 1) \text{ iid, } \sigma \in \mathbb{R}^+$$

In a orthogonal basis of $l^2(\{0, N-1\})$ e.g. $\{\theta_k\}_{k \in \{0, N-1\}}$, the expansion of a gaussian white noise remains a gaussian white noise [Carré98, Mallat98] (in all this section, $\langle \cdot, \cdot \rangle$ and $\|\cdot\|$ should be understood in a $l^2(\{0, N-1\})$ sense).

Proof:

$$E[\langle B, \theta_k \rangle] = \sum_{l=0}^{N-1} E[B_l] \theta_k^*[l] = 0$$

and

$$\begin{aligned} COV[\langle B, \theta_k \rangle, \langle B, \theta_l \rangle] &= E[\langle B, \theta_k \rangle \langle B, \theta_l \rangle^*] \\ &= \sum_{m=0}^{N-1} \sum_{n=0}^N \underbrace{E[B_k B_l]}_{\delta_{m,n}} \theta_k^*[m] \theta_l[n] \\ &= \sum_{m=0}^{N-1} \theta_k^*[m] \theta_l[m] = \langle \theta_k, \theta_l \rangle^* = \delta_{k,l} \end{aligned}$$

Since a linear combination of iid gaussian random variables gives a gaussian random variable, and since the absence of correlation $COV(X, Y) = 0$, $X \neq Y$ implies (for gaussian random variables) the independance of the two variables, we have $\langle B, \theta_k \rangle$ follows $\mathcal{N}(0, 1)$ iid. In what follows, we present the two main philosophies for building some estimates of f , namely: coefficients attenuation (“implemented” via a soft thresholding) and coefficients selection (hard thresholding). The next two subsections summarize the ideas developed in [Mallat98].

Coefficients attenuation

From the noisy signal G , we construct an estimator of the form

$$\tilde{F} = \sum_{k=0}^{N-1} \langle G, \theta_k \rangle \lambda[k] \theta_k$$

Here, we focus on non-linear estimators that depends on the realisation of G . We now consider the mean square error⁶

$$E[\|f - \tilde{F}\|^2] = \sum_{k=0}^{N-1} E[\underbrace{|\langle f, \theta_k \rangle - \langle G, \theta_k \rangle \lambda[k]|^2}_{\varepsilon}]$$

Since $\langle G, \theta_k \rangle = \langle f, \theta_k \rangle + \sigma \langle B, \theta_k \rangle$, we have

$$\begin{aligned} \varepsilon &= E[|\langle f, \theta_k \rangle (1 - \lambda[k]) - \sigma \langle B, \theta_k \rangle \lambda[k]|^2] \\ &= |\langle f, \theta_k \rangle|^2 (1 - \lambda[k])^2 + \sigma^2 \lambda[k]^2 \end{aligned}$$

because $E[\langle B, \theta_k \rangle] = 0$ and $E[|\langle B, \theta_k \rangle|^2] = 1$. By solving $\frac{\partial \varepsilon}{\partial \lambda[k]} = 0$, one derives that ε is a minimum for

$$\lambda[k] = \frac{|\langle f, \theta_k \rangle|^2}{|\langle f, \theta_k \rangle|^2 + \sigma^2} \quad (3.4)$$

leading to the mean square error

$$E[\|f - \tilde{F}\|^2] = \sum_{k=0}^{N-1} \frac{|\langle f, \theta_k \rangle|^2 \sigma^2}{|\langle f, \theta_k \rangle|^2 + \sigma^2}$$

Note that equation (3.4) can be seen as a “generalized” Wiener filter. If the basis functions $\{\theta\}_{k \in \{0, N-1\}}$ were the complex exponentials of Fourier analysis we would end up with

$$\lambda[k] = \frac{1}{1 + \frac{\sigma^2}{|f[k]|^2}}$$

which is precisely the expression of the Wiener filter [Gonzales92] for a point spread function equal to δ .

Coefficients selection

A coefficient selection is performed by requiring that $\lambda[k]$ takes binary values, i.e. the estimator consists in selecting a subset of the noisy coefficients of G . In that case, it is obvious that the mean square error (still equal to: $E[\|f - \tilde{F}\|^2] = |\langle f, \theta_k \rangle|^2 (1 - \lambda[k])^2 + \sigma^2 \lambda[k]^2$) is minimized by an operator of the form

$$\lambda[k] = \begin{cases} 1 & \text{if } |\langle f, \theta_k \rangle|^2 \geq \sigma^2 \\ 0 & \text{otherwise} \end{cases}$$

⁶Recall that an orthonormal basis of an abstract Hilbert space is a particular case of a Riesz basis with $A = B = 1$ [Daubechies92], therefore $\|f\|^2 = \sum_k |\langle f, e_k \rangle|^2$ (see definition 10, page 123, as well).

The mean square error produced by this ideal selection procedure

$$E[\|f - \tilde{F}\|^2] = \sum_{k=0}^{N-1} \min(|\langle f, \theta_k \rangle|^2, \sigma^2) \quad (3.5)$$

remains of the same order than the one introduced by the attenuation operator [Mallat98]. Obviously, because of our lack of knowledge about $\langle f, \theta_k \rangle$, the ideal coefficients attenuation and selection cannot be implemented. However, since the work of David Donoho (see notably [Donoho94]), it is known that the performances of some thresholding estimators (applied on the empirical wavelet decomposition) are closed to the ones of the ideal procedures previously discussed.

Denoising in orthogonal wavelet basis

We have not yet spoken about denoising in orthogonal wavelet basis. Basically, the choice of the basis in which a non-linear operator is applied is crucial. The best (non-linear) approximation of a function f (with M vectors) in an orthogonal basis is given by

$$f_M = \sum_{|\langle f, \theta_k \rangle| \geq \sigma} \langle f, \theta_k \rangle \theta_k$$

while the approximation error is equal to

$$\|f - f_M\|^2 = \sum_{|\langle f, \theta_k \rangle| < \sigma} |\langle f, \theta_k \rangle|^2$$

For the ideal selection procedure previously discussed, the mean square error (equation (3.5)) can therefore be written as

$$E[\|f - \tilde{F}\|^2] = \|f - f_M\|^2 + M\sigma^2$$

hence, the mean square error is small only if the approximation error and $M\sigma^2$ are both small, i.e. we want a basis in which the function f is coded by a few large coefficients which characterize it relevantly. This, for example, eliminates the complex exponential basis for estimating a function containing some singularities: this type of signals generates non-neglectible coefficients in all the Fourier spectrum. The convenience of using orthogonal wavelet basis comes from the fact that a r -regularly (in the sense defined by Yves Meyer [Meyer90]) orthogonal wavelet basis provides unconditionnal basis for a wide range of smoothness spaces [Meyer90] (namely: Hölder, Sobolev, Besov spaces, ...). For example, piecewise regular functions, i.e. functions containing isolated singularities (belonging to the Besov space(s)), are efficiently approximated with a few large coefficients [Donoho91a, Mallat98], see §D.3. The only *a priori* knowledge about the desired result is the order of a given Besov-norm and the implementation of the algorithm does not depend on its parameters (α, p, q) [Meyer94].

The last problem deals with the necessity of approximating the ideal operators and estimating their parameters (e.g. σ). For example, a hard-thresholding operator

$$\tilde{F} = \sum_{k=0}^{N-1} \Lambda(\langle G, \theta_k \rangle) \theta_k, \quad \Lambda(x) = \begin{cases} x & \text{if } |x| \geq T \\ 0 & \text{otherwise} \end{cases} \quad (3.6)$$

with⁷ $T = \sigma\sqrt{\log N}$, produces a mean square error which remains within a $2 \log N$ factor of the ideal error and is asymptotically optimal in a minimax sense [Donoho92]. The reader is notably sent to [Mallat98, Donoho95] for some discussions on the operators (e.g. hard/soft thresholding) and the threshold choices.

3.9.2 Image fusion in a noisy environment

Using the tools previously discussed, it becomes relatively straightforward to design a fusion algorithm which takes into account the presence of noise in the image. Basically it consist in applying simultaneously the denoising algorithm and the area-based maximum selection.

Denoising algorithm

The denoising algorithm, as presented by David Donoho, works as follows. It is first required to apply a discrete orthogonal wavelet transform (possibly on the interval [Cohen92b, Cohen93, Mallat98]) in order to obtain the empirical wavelet coefficients. Then, we need to estimate σ using the median-based estimator discussed in §3.9.1 and apply the soft/hard (see equation (3.6)) thresholding non-linearity:

$$\Lambda(x) = \begin{cases} x - T & \text{if } x \geq T \\ x + T & \text{if } x \leq -T \\ 0 & \text{otherwise} \end{cases}$$

Finally, we get the estimation of f by applying an inverse transform algorithm on the thresholded empirical coefficients. Some experimental results are (notably) available in [Mallat98]. The algorithm can easily be extended to images (again via separable basis) but it is (by definition) likely to suppress some interesting information on textural parts (especially if they cannot be considered as being piecewise regular e.g. fractal textures often present in natural scenes).

⁷In practice, the noise variance is not known and need to be estimated. This is done by using $\tilde{\sigma} = MED/.6745$ where MED denotes the median of the absolute values of the empirical wavelet coefficients at the finest scale (recall that $\int_{-.6745\sigma}^{+.6745\sigma} g_{\sigma}(x)dx = .5$ [Daintith89]). When f is piecewise smooth, it generates only a small number of non vanishing coefficients at the finest scale (the wavelet overlaps the singularities for only a few values of the translation parameter) and the median is not very sensitive to a few outliers.

Fusion algorithm

For saving computational time it, is not recommended to apply the denoising algorithm before applying the fusion scheme i.e. consider it as a preprocessing task, because it will require two superfluous wavelet transform/inverse wavelet transform operations. It is therefore better to merge the denoising and the fusion operators in a single one (discussed just after). The complete algorithm works as follows: we first compute the empirical coefficients of the images to be fused, then estimate the noise variance in each ones and apply the modified area-based maximum selection operator, defined as follows

$$\gamma_{j;k}^{(f)} = \begin{cases} \gamma_{j;k}^{(1)} & \text{if } \max_{l \in \Omega} |\Lambda^{(1)}(\gamma_{j;l}^{(1)})| \geq \max_{l \in \Omega} |\Lambda^{(2)}(\gamma_{j;l}^{(2)})| \\ \gamma_{j;k}^{(2)} & \text{otherwise} \end{cases}$$

where $\Lambda^{(1)}$ and $\Lambda^{(2)}$ denote the hard/soft thresholding non-linearities associated with each image i.e. dependant on $\tilde{\sigma}^{(1)}$ and $\tilde{\sigma}^{(2)}$. Taking the inverse transform gives the (estimated) fused image. Experimental results are not available but since the operator has been built on a strong theoretical background (which has been extensively tested in the litterature), we believe that it is likely to give reasonable results.

3.9.3 Other wavelet-based denoising methods

The purpose of this subsection is to give a few pointers on other works which also use the wavelet transform for denoising purpose. Most of them are based on undecimated transformations and use their redundancy for producing better approximations of a given function. The translation invariant denoising of Ronald Coifman [Coifman95] consists in applying a threshold-based denoising for different shifts of the original signal. Some artifacts (e.g. Gibbs effect in the neighbourhood of the singularities) are then attenuated by averaging the different results. Philippe Carré *and al* [Carré98] also introduces a translation invariant denoising based on the *algorithme à trous*. Other authors [Mallat92a, Mallat92b, Lu93] propose some denoising methods based on the wavelet maxima representation (discussed in the next chapter). Note that some articles (notably [Carré98]) deal with the removal of colored noise problem.

Chapter 4

Feature-based image fusion

Introduction

Multiscale edges have been introduced in order to deal with the problem of noise while performing a contour extraction task, e.g. [Bergholm87]. A popular strategy consists in using a detection operator which is the first or second order of a low-pass filter (e.g. gaussian filter [Canny86] or the exponential filter [Deriche87]) in order to reduce the noise and carry out the edge detection. Obviously, this method have a fundamental disadvantage: the “good” localization and “good” detection criteria [Canny86] (see B.1.1) are dual and cannot be simultaneously arbitrary small. In order to overcome this limitation, Fredrik Bergholm [Bergholm87] has proposed a procedure, known as “edge focusing”, which consists in computing the output of the Canny detector for different values of σ (i.e. scales) and detecting the edges using a coarse-to-fine tracking.

This philosophy has been retained for designing feature-based image representations¹, using “classical” multiscale decompositions (e.g [Hummel89]) or the wavelet transform [Mallat91, Mallat92a, Mallat92b]. These representations allow to reconstruct an approximation of the original image from its multiscale edges (the uniqueness and stability of these representations is notably adressed in [Berman91, Berman92, Berman93, Meyer94]). Because of this reconstruction, it has been foreseen by Stéphane Mallat [Mallat92b] that many image processing tasks could be implemented using edge-based algorithms.

The purpose of this chapter is to study the feasibility of a feature-based image fusion procedure using the wavelet maxima representation. The chapter is organized as follows: we first introduce the multiscale edge detection procedure, then present the reconstruction algorithm, and discuss the possible design of a fusion operator in this context. The main references are [Mallat92a, Mallat92b, Lu93].

¹Known as adaptive quasi-linear representations (AQLR).

4.1 Multiscale edges

In this section, we only focus on the wavelet maxima representation. Information about the zero-crossing representation are available (notably) in [Mallat91]. Theorem 7 (page 55) implies that a wavelet having one vanishing moment corresponds to the first order derivative of a smoothing operator. Formally,

$$\psi(x) = -\frac{d\theta}{dx}$$

The dyadic wavelet transform (the use of a dyadic wavelet transform is motivated by its translation invariance and its redundancy) can therefore be interpreted as

$$W_f(2^j, b) = 2^j \frac{d}{db} (f \otimes \bar{\theta}_{2^j})(b)$$

As j increases, $W_f(2^j, b)$ is smoother. For example, if θ is a Gauss function, one ends up with a multiscale Canny operator. Under this condition the dyadic wavelet transform provides a multiscale gradient from which the points of sharp variation can be extracted.

4.1.1 Quadratic spline wavelet

For being able to use the *algorithme à trous* (see §2.3.3), it is required that

$$\hat{\phi}(\xi) = \hat{h}(\xi/2)\hat{\phi}(\xi/2) \text{ and } \hat{\psi}(\xi) = \hat{g}(\xi/2)\hat{\phi}(\xi/2)$$

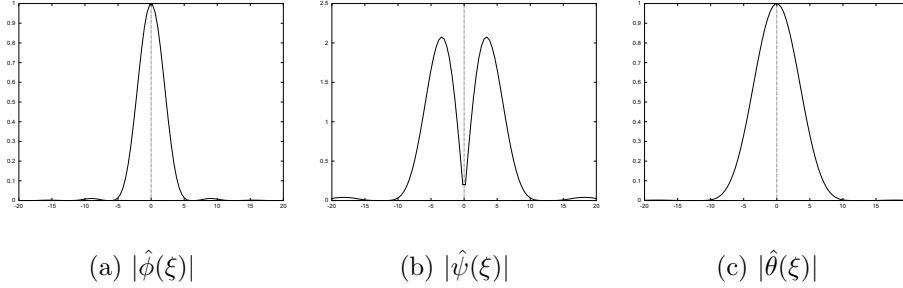
where $\hat{h}(\xi)$ and $\hat{g}(\xi)$ are the Fourier transform of two discrete filters (the same constraints should be satisfied by $\hat{\phi}(\xi)$ and $\hat{\psi}(\xi)$). Since ψ should be the first order of a smoothing operator, $\hat{\psi}(\xi)$ must have a zero of order 1 at $\xi = 0$. Because $\hat{\phi}(0) = 0$ the constraint is moved onto $\hat{g}(\xi)$. Moreover, $\hat{h}(\xi)$ is chosen such that $\psi(x)$ is antisymmetrical, is as regular as possible and has a small compact support. Stéphane Mallat [Mallat92b] has proposed the following family of filters

$$\hat{h}(\xi) = \hat{h}(\xi) = e^{\frac{i\xi}{2}} \cos(\xi/2)^{2n+1}, \quad \hat{g}(\xi) = 4ie^{\frac{i\xi}{2}} \sin(\xi/2) \text{ and } \hat{\hat{g}}(\xi) = \frac{1 - |\hat{h}(\xi)|^2}{\hat{g}(\xi)}$$

This leads to the filter coefficients, available in [Mallat92b] (table 1, page 728), and to the following scaling function, wavelet and smoothing operator

$$\hat{\phi}(\xi) = \text{sinc}(\xi/2)^{2n+1}, \quad \hat{\psi}(\xi) = i\xi \text{sinc}(\xi/4)^{2n+2} \text{ and } \hat{\theta}(\xi) = \text{sinc}(\xi/4)^{2n+2}$$

note that $\text{sinc}x = \frac{\sin x}{x}$. Choosing $2n + 1 = 3$ leads to a scaling function and a smoothing operator which are respectively a cubic and a quadratic spline. Figure 4.1 shows the modulus of their Fourier transforms.

Figure 4.1 Quadratic spline wavelet.

4.1.2 *Algorithme à trous* in two dimensions

In two dimensions, the dyadic wavelet transform is (most of the time) defined by using two spatially oriented separable wavelets [Mallat98]

$$\Psi^{(1)}(x, y) = \psi(x)\phi(y) = -\frac{\partial}{\partial x}\Theta^{(1)}, \quad \Psi^{(2)}(x, y) = \phi(x)\psi(y) = -\frac{\partial}{\partial y}\Theta^{(2)} \quad (4.1)$$

and a separable scaling function $\Phi(x, y) = \phi(x)\phi(y)$. The resulting algorithm becomes (roughly) a straightforward extension of the one dimensional case (§2.3.3) which consists in iteratively applying separable filters on the scaling coefficients for obtaining the scaling and wavelet coefficients at the next scale. As usual, for practical images, the first coefficients are given by the grey-scale values of the original image (see 2.3.4). Figure 4.2 shows the dyadic wavelet transform of the “lenna” image, computed using the scaling function/wavelet pair presented in the previous subsection. More details are available in [Mallat92b, Mallat98].

4.1.3 Contours extraction

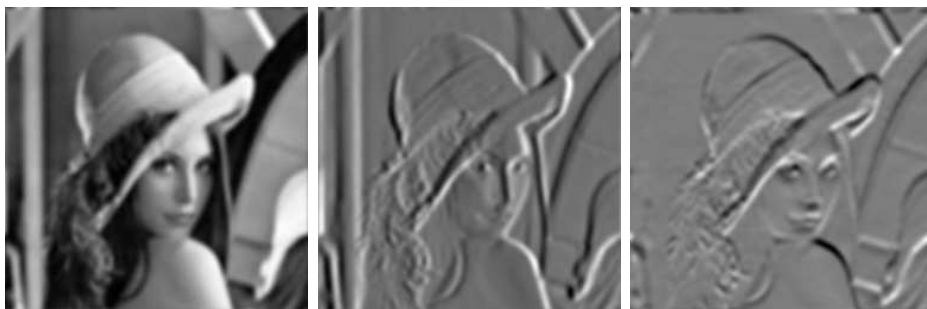
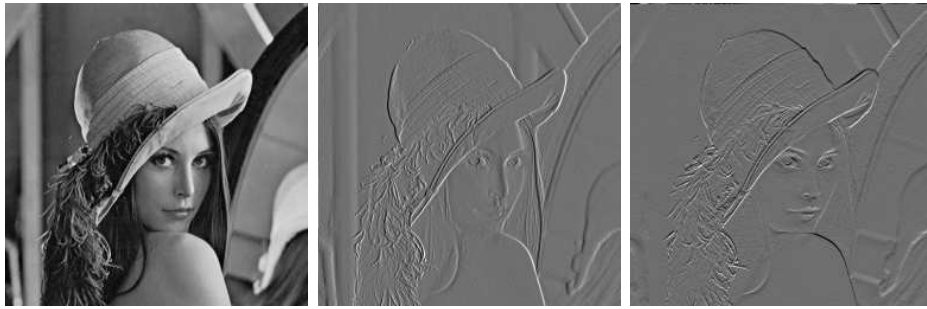
From the definition of $\Psi^{(1)}$ and $\Psi^{(2)}$, it directly follows that the wavelet coefficients are proportionnal to the gradient of the image smoothed by Θ_{2^j} ($\Theta^{(1)} \approx \Theta^{(2)}$ [Mallat92b]) i.e.

$$\begin{pmatrix} \mathcal{W}_f^{(1)}(2^j, b, b') \\ \mathcal{W}_f^{(2)}(2^j, b, b') \end{pmatrix} = \begin{pmatrix} 2^j \frac{\partial}{\partial b}(f \otimes \bar{\Theta}_{2^j})(b, b') \\ 2^j \frac{\partial}{\partial b'}(f \otimes \bar{\Theta}_{2^j})(b, b') \end{pmatrix} = 2^j \vec{\nabla} f \otimes \bar{\Theta}_{2^j}(b, b')$$

This information can therefore be used (as in a classical edge detector) for extracting the multiscale edges. The modulus of the gradient is proportionnal to the modulus of the wavelet coefficients

$$|\vec{\nabla} f \otimes \bar{\Theta}_{2^j}(b, b')| \propto \sqrt{|\mathcal{W}_f^{(1)}(2^j, b, b')|^2 + |\mathcal{W}_f^{(2)}(2^j, b, b')|^2}$$

Figure 4.2 Beginning of a two-dimensional dyadic wavelet transform.



(g) Scaling coeff.

(h) Wave. co. ($\Psi^{(1)}$).(i) Wave. co. ($\Psi^{(2)}$).

and its orientation is given by

$$\alpha(2^j, b, b') = \tan^{-1} \frac{\mathcal{W}_f^{(2)}(2^j, b, b')}{\mathcal{W}_f^{(1)}(2^j, b, b')}$$

The detection consists in two main steps: it is first necessary to extract the local maxima of the gradient norm in the gradient direction and secondly, to suppress the non-significant local maxima via a thresholding operation. This last operation is often implemented using an hysteresis thresholding (more details are available in [Deriche] and in §B.1 as well).

The set of values,

$$\Omega = \{ \{ (b_k \ b'_k)^T, (\mathcal{W}_f^{(1)}(2^j, b_k, b'_k) \ \mathcal{W}_f^{(2)}(2^j, b_k, b'_k))^T \}_{k=1, \dots, N_j} \}_{j \in Z}$$

where $(b_k \ b'_k)^T$ denotes the coordinates of a local maximum, is called the wavelet maxima representation of the image. For a digital $N \times N$ image, the wavelet maxima representation obviously becomes

$$\Omega = \{ \{ (i_k \ i'_k)^T, (\mathcal{W}_f^{(1)}(2^j, i_k, i'_k) \ \mathcal{W}_f^{(2)}(2^j, i_k, i'_k))^T \}_{k=1, \dots, N_j} \}_{j=0, \dots, \log_2 N}$$

where $(i_k \ i'_k)^T$ is an integer-valued vector. See figure 4.3.

4.2 Reconstruction from local maxima

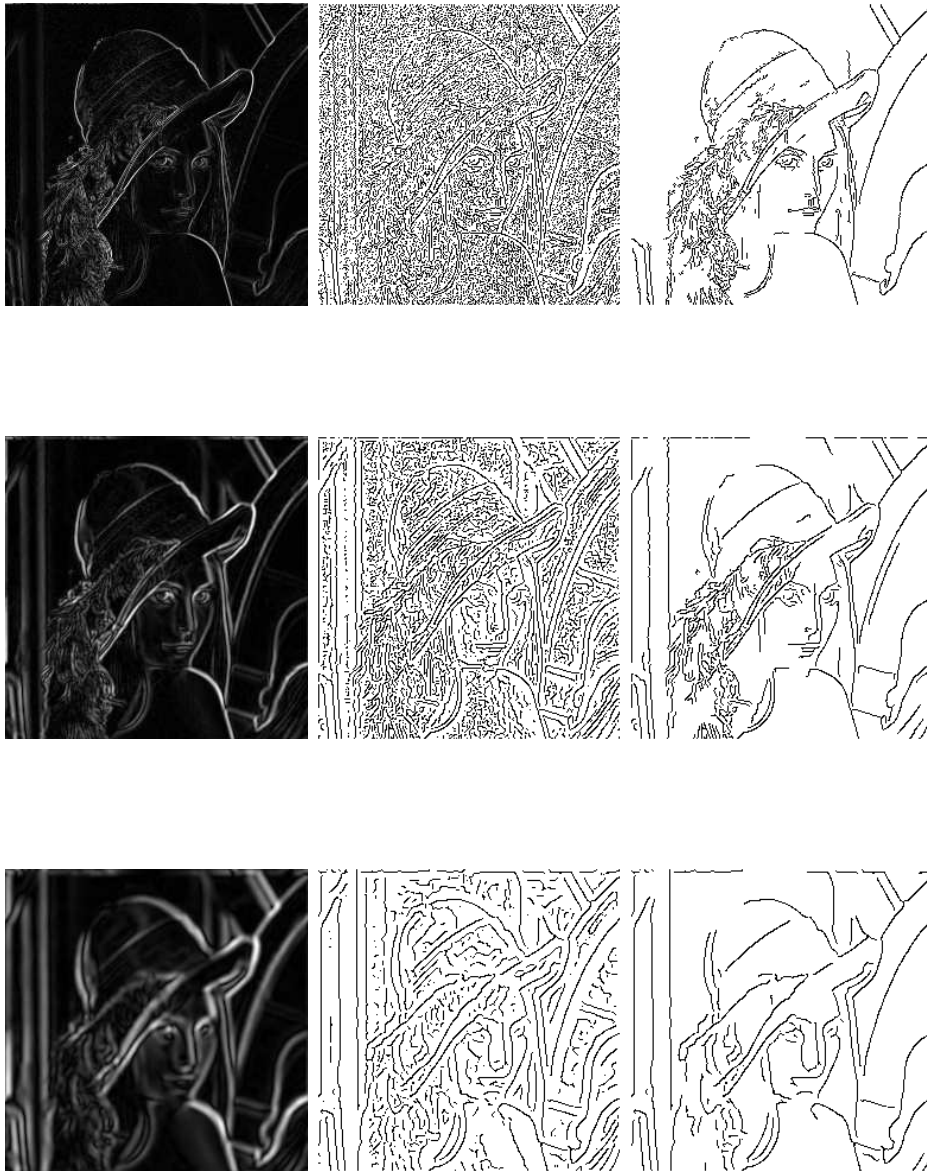
As pointed in (notably) [Berman91, Meyer94], the wavelet maxima representation does not characterize uniquely a given function f . However, two functions having the same local maxima differ mainly and only slightly on their high-frequency content, which makes the reconstruction suitable for practical purposes [Mallat98, Meyer94]. Here, we shortly present the alternate projection algorithm, introduced in Stéphane Mallat's articles. However, other alternative algorithms have been proposed in [Carmora, Cvetković95]. We restrict ourselves to the one dimensional case, since the two dimensional algorithm is a straightforward extension and is fully presented in [Mallat92b].

4.2.1 The alternate projection algorithm

Basically, our goal is to find a sequence of functions $\{g_j\}_{j \in Z}$ such that: it is the wavelet transform of a function of $L^2(R)$, it has the same wavelet maxima as \mathcal{W}_f and **not more**. As pointed in [Mallat92b], this last condition (not more) is not convex and cannot be implemented easily, thus it is relaxed and replaced by requiring the following Sobolev norm to be minimum

$$\|\{g_j\}_{j \in Z}\|_K^2 = \sum_j \|g_j\|_{L^2(R)}^2 + 2^{2j} \left\| \frac{dg_j}{dx} \right\|_{L^2(R)}^2$$

Figure 4.3 Multiscale edges extracted from the “lenna” image.



(g) Gradient norm.

(h) Local maxima.

(i) Hysteresis thresh.

The constraint on $\|dg_j/dx\|_{L^2(R)}^2$ allows to control the appearance of spurious maxima and the multiplication by 2^j express the fact that g_j should be smoother as j increases. Let K be the set of all the sequences $\{g_j\}_{j \in \mathbb{Z}}$ such that $\|\{g_j\}_{j \in \mathbb{Z}}\|_K$ is finite. Let V denote the space of all the sequences $\{g_j\}_{j \in \mathbb{Z}}$ such that their are the wavelet transform of a function belonging to $L^2(R)$ i.e. such that the sequence $\{g_j\}_{j \in \mathbb{Z}}$ satisfies the reproducing kernel equation (equation (2.10) or (2.11)). Let Γ be the set of sequences $\{g_k\}_{j \in \mathbb{Z}}$ such that for all j and for all maxima position x_k we have

$$W_f(2^j, x_k) = g_j(x_k)$$

The alternate projection algorithm converges to a sequence $\{g_j^*\}_{j \in \mathbb{Z}}$, lying in $\Lambda = V \cap \Gamma$, by alternatively project the current sequence onto V and Γ . Starting from the initial guess $\{g_j\}_{j \in \mathbb{Z}}^{(0)} \in V$ (in general $g_j(x) = 0, \forall j$), the algorithm is simply expressed as

$$\{g_j\}_{j \in \mathbb{Z}}^{(k+1)} = P_V(P_\Gamma(\{g_j\}_{j \in \mathbb{Z}}^{(k)}))$$

where P_V and P_Γ are respectively the orthogonal projectors that project a set of functions of K onto (respectively) V and Γ .

P_V is simply equal to $W \circ W^{-1}$ where W denotes the wavelet transform operator, i.e. P_V is implemented by taking the inverse wavelet transform of $\{g_j\}_{j \in \mathbb{Z}} \in K$ followed by a wavelet transform. The P_Γ operator is trickier, it transforms a sequence in $\{g_j\}_{j \in \mathbb{Z}} \in K$ into a sequence $\{h_j\}_{j \in \mathbb{Z}} \in \Gamma$ such that its K -norm is minimum. After solving a simple problem of calculus of variation [Mallat98] (again!), one finds that $h_j(x) = \epsilon_j(x) + g_j(x)$ where

$$\epsilon_j(x) = \alpha e^{2-jx} + \beta e^{-2-jx}, \quad x \in [x_k, x_{k+1}]$$

x_i and x_{i+1} are the abscissa of two consecutive local maxima and α, β should be chosen such that

$$\begin{cases} \epsilon_j(x_k) &= \mathcal{W}_f(2^j, x_k) - g_j(x_k) \\ \epsilon_j(x_{k+1}) &= \mathcal{W}_f(2^j, x_{k+1}) - g_j(x_{k+1}) \end{cases}$$

An implementation of P_Γ is available page 122. For more details (stability of the reconstruction, rate of convergence, ...) the reader is sent to the articles already cited in this subsection.

4.2.2 Practical considerations

Even if the representation is not unique, the algorithm is suitable for practical purpose. Figure 4.4, presents some experimental results on the ‘‘lenna’’ image. On a visual point of vue there is no difference between images (a) and (b) (image (b) has been reconstructed using all the wavelet maxima of the original one). If we consider only the significant maxima, we loose some textural information, but the reconstructed images still approximate correctly the original image ((c)

and (d) have been computed by considering smaller sets of local maxima). This phenomenon is stated in [Mallat98], as well. Our experiments also suggest that 15 to 30 iterations are required for building a reasonable approximation of an image. Obviously, due to its iterative nature, the reconstruction algorithm is computationally intensive and is not suitable (in its direct form) for real-time processing.

4.3 Image fusion

4.3.1 Estimation of K , α and σ

An interesting property of the wavelet maxima representation is that it allows to estimate some of the parameters that characterize an isolated singularity². The following theorem, proved in [Meyer90], relates the decay of the wavelet coefficients to the Hölder regularity (see definition page 124) of the original function.

Theorem 9 *A function f is uniformly Hölder- α over the interval $[a, b]$ if and only if there exists $K > 0$ such that*

$$\forall c \in [a, b], |\mathcal{W}_f(2^j, c)| \leq K2^{j\alpha}$$

This theorem also holds for tempered distributions, e.g. δ . As a basic consequence: if a function is uniformly Hölder- α ($\alpha < 0$) the amplitude of the wavelet coefficients decrease as j increase, while if $\alpha > 0$ the coefficients increase with the scale parameter. Now, if we reintroduce the gaussian model discussed in §3.4.2, i.e. the function f contains an isolated Hölder- α singularity at $\nu \in [a, b]$ smoothed by a gaussian operator, we have

$$\mathcal{W}_{f \otimes g_\sigma}(2^j, c) = 2^j \frac{d}{dc} (f \otimes g_\sigma \otimes \bar{\theta}_{2^j})(c)$$

Assuming that $g_\sigma \otimes \bar{\theta}_{2^j} \approx \bar{\theta}_\Sigma$, $\Sigma = \sqrt{\sigma^2 + 2^{2j}}$ leads to

$$\mathcal{W}_{f \otimes g_\sigma}(2^j, c) \approx \frac{2^j}{\Sigma} \mathcal{W}_f(\Sigma, c)$$

Therefore, if f is Hölder- α over $[a, b]$, we end up with

$$\exists K > 0, \forall c \in [a, b], |\mathcal{W}_{f \otimes g_\sigma}(2^j, c)| \leq K2^j \Sigma^{\alpha-1}$$

Which can be rewritten as

$$\log_2 |\mathcal{W}_{f \otimes g_\sigma}(2^j, c)| \leq \log_2 K + j + \frac{\alpha - 1}{2} \log_2(\sigma^2 + 2^{2j}) \quad (4.2)$$

²The non-isolated singularities case is notably addressed in [Mallat92a, Hwang93].

Figure 4.4 Reconstruction via the alternate projection algorithm.



(a) Original image.



(b) Reconstruction from all the local maxima (30 it.).



(c) Reconstruction from a subset of the local maxima (30 it.).



(d) Reconstruction from a smaller subset of the local maxima (30 it.).

Given the wavelet maxima trace $\{c_j, |\mathcal{W}_{f \otimes g_\sigma}(2^j, c_j)|\}_{1 \leq j \leq J}$ of the singularity at $\nu \in [a, b]$, Stéphane Mallat (in [Mallat92a, Mallat92b]) proposes to estimate K , α and σ by finding their values such that equation (4.2) is as close as possible of an equality. This is done by optimizing

$$\Delta = \sum_{j=1}^J \left(\log_2 |\mathcal{W}_{f \otimes g_\sigma}(2^j, c_j)| - \log_2 K - j - \frac{\alpha - 1}{2} \log_2(\sigma^2 + 2^{2j}) \right)^2$$

using a gradient descent method, e.g.

$$\begin{pmatrix} K^{(k+1)} \\ \alpha^{(k+1)} \\ \sigma^{(k+1)} \end{pmatrix} = \begin{pmatrix} K^{(k)} \\ \alpha^{(k)} \\ \sigma^{(k)} \end{pmatrix} + \rho \begin{pmatrix} \partial \Delta / \partial K \\ \partial \Delta / \partial \alpha \\ \partial \Delta / \partial \sigma \end{pmatrix}$$

where $K^{(0)}$, $\alpha^{(0)}$ and $\sigma^{(0)}$ are chosen arbitrarily. These parameters express different characteristics of the singularity: K is related to its amplitude, α to its type and σ to its degree of smoothness. However, the raw wavelet maxima representation is not sufficient for estimating these values, since we need to access the wavelet maxima trace of the singularity, i.e. we need to link the wavelet maxima across scales. This representation, known as the wavelet maxima tree, is briefly presented in the next subsection.

4.3.2 The wavelet maxima tree

In order to link the wavelet maxima across scales one can use an *ad hoc* algorithm, as the one proposed in [Mallat92b]. Basically, it consists in linking two successive wavelet maxima if they are close to each other and if their corresponding values are of the same sign and of the same order. However, smarter algorithms can be found in the litterature such as the one in [Lu93]. From the sets of wavelet maxima at scales j and $j + 1$

$$\Omega_j = \{c_k^{(j)}, \mathcal{W}_f(2^j, c_k^{(j)})\}_{k=1, \dots, N_j}, \quad \Omega_{j+1} = \{c_k^{(j+1)}, \mathcal{W}_f(2^j, c_k^{(j+1)})\}_{k=1, \dots, N_{j+1}}$$

Jian Lu proposes a measure of interaction based on the reproducing kernel corresponding to the wavelet (recall equations (2.10) and (2.11))

$$\Gamma(c_k^{(j+1)}, c_l^{(j)}) = \mathcal{W}_f(2^{j+1}, c_k^{(j+1)}) \kappa'_{2^{j+1}, 2^j}(c_k^{(j+1)} - c_l^{(j)})$$

The wavelet maxima tree is then constructed recursively using a coarse-to-fine strategy. For a given maxima at scale j , the maxima at scale $j + 1$ which maximizes $\Gamma(c_k^{(j+1)}, c_l^{(j)})$ is marked as its parent node. The main child of a parent node at scale $j + 1$ is the one which maximizes $\Gamma(c_l^{(j)}, c_k^{(j+1)})$ among its children. A main branch connects a maxima to the tip end of the tree and provides the

approximation of the trace of a wavelet maxima required for estimating the parameters discussed in the previous subsection. Note that this algorithm works only if the smoothing operator θ is a good approximation of a Gauss function, this implies that the behavior of the wavelet maxima is convenient, e.g. it satisfies a causality property (any feature at a coarser scale must have its origin at a finer scale), see [Bergholm87, Lu93]. This algorithm also requires to estimate the reproducing kernel of the wavelet transform. A more detailed presentation is available in [Lu93].

4.3.3 Signal fusion

Once the maxima tree has been built, one can estimate the parameters that characterize the different singularities present in the signal. This information may be used for denoising purpose: a gaussian white noise creates non-significant wavelet maxima which can be eliminated via a thresholding operation, moreover, it introduces singularities whose Hölder exponent are negative [Mallat92a] (we are therefore able to identify them under the assumption that the original signal contains only some Hölder- $(\alpha \geq 0)$ singularities). The remaining main branches, in the two signals, should be matched and selected in order to build the fused one. For example, a matching criterion can be designed by taking into account the distance between two main branches present in the two signals and their corresponding estimated Hölder exponents. While a selection operator (between two associated main branches) can be based on the estimation of K (amplitude) and σ (degree of smoothness).

4.3.4 Extension to images

The extensions of the previous results and algorithms to the two-dimensional case are **not** straightforward (!). The algorithm used for building the wavelet maxima tree becomes trickier (notably because the convenient behavior of the one-dimensional wavelet maxima is not preserved when considering two-dimensional signals). Once again, the reader is sent to [Lu93] for a detailed description of the two-dimensional algorithm. Moreover, the matching procedure may be more complicated because it has to take into account the geometric properties of the multiscale contours. In that case, more research is necessary. However, we hope that the theoretical arguments discussed in this chapter are sufficient for motivating further studies.

Conclusion

This thesis provides some solutions to the problems involved in the design of an image fusion algorithm. We have first provided a complete model for solving the registration problem, which leads to reasonable experimental results. Concerning this problem, the next step is the automatisisation of the whole registration procedure. However, it is highly recommended to simplify the problem (for example, by using some reference objects) in order to get a reliable algorithm. Secondly, we have introduced an area-based maximum selection rule for performing the image fusion and obtained reasonable experimental results, as well. However, it may be interesting to go deeper in the theoretical explanations of the (relative) success of the method. We believe that it can help improving the quality of the fused images by giving other operators (see the discussion in the next paragraph). Obviously, this fusion operator (associated with the fast wavelet transform algorithm) is suitable for fast computations. Finally, we have discussed the mathematical tools required for designing a feature-oriented image fusion algorithm. On this subject, more research is necessary but we hope that the arguments developed in this work are sufficient to motivate further studies.

When reading (again!) the last chapter of Yves Meyer's book [Meyer94] ("Compression des données et restauration d'images bruitées"), one can find some indications which (indirectly) explain the relevancy of performing the image fusion in an orthogonal wavelet basis. Basically, an orthogonal wavelet basis is optimal for representing the relevant information contained in a signal (in the work of David Donoho and for the fusion problem the relevant information are the sharp transitions) compared to the rest (noise, texture and regular parts of the signal). The philosophy of the fusion algorithm, presented in this thesis, is then to use a "convenient point of view", in which the sharp variations are efficiently discriminated and to use this property in order to perform the fusion by considering only the relevant information. We believe that the works of Yves Meyer and David Donoho are good starting points for trying to demonstrate the optimality of using orthogonal wavelet decompositions for solving the fusion problem (for particular but convenient classes of functions).

Bibliography

- [Anh96] V. ANH, J.Y. SHI, H.T. TSUI, *Scaling Theorem for Zero Crossings of Bandlimited Signals*, IEEE Transactions on Pattern Analysis and Machine Intelligence, Vol. 18, No. 3, 1996.
- [Antonini92] M. ANTONINI, M. BARLAUD, P. MATHIEUR, I. DAUBECHIES, *Image Coding Using Wavelet Transform*, IEEE Transactions on Image Processing, Vol. 1, No. 2, 1992.
- [1] I. ASIMOV, *The Complete Robot: the Definitive Collection of Robot Stories* (“Sally”, p. 19), Harper Collins Publisher, 1982.
- [Barnard93] H.J. BARNARD, *Efficient Signal Extension for Subband/Wavelet Decomposition of Arbitrary Length Signals*, Proceeding of the SPIE 2094, 1993.
- [Battle87] G. BATTLE, *A Block Spin Construction of Ondelettes*, Communications on Mathematical Physics, No. 110, 1987.
- [Benveniste90] A. BENVENISTE, *Multiscale Signal Processing: from QMF to Wavelets*, Rapport de Recherche INRIA No. 1299, 1990.
- [Bergholm87] F. BERGHOLM, *Edge Focusing*, IEEE Transactions on Pattern Analysis and Machine Intelligence, Vol. 9, No. 6, 1987.
- [Berman91] Z. BERMAN, *The Uniqueness Question of Discrete Wavelet Maxima Representation*, Technical Research Report, University of Maryland, 1991.
- [Berman92] Z. BERMAN, *Generalizations and Properties of the Multiscale Maxima and Zero-Crossings Representations*, PhD Thesis (University of Maryland), 1992.
- [Berman93] Z. BERMAN, J.S. BARAS, *Properties of the Multiscale Maxima and Zero Crossings Representations*, IEEE Transactions on Signal Processing, Vol. 41, No. 12, 1993.
- [Beylkin] G. BEYLKIN, *On the Representation of Operators in Bases of Compactly Supported Wavelets*, SIAM Journal on Numerical Analysis, Vol. 6, No. 6.

- [Beylkin91] G. BEYLKIN, R. COIFMAN, V. ROKHLIN, *Fast Wavelet Transform and Numerical Algorithms I*, Communication on Pure and Applied Mathematics, No. 44, 1991.
- [Blaska94] T. BLASKA, R. DERICHE, *Recovering and Characterizing Image Features Using an Efficient Model Based Approach*, rapport de recherche INRIA No. 2422, 1994.
- [Blaska97] T. BLASKA, *Approche par modèles en vision précoce*, Thèse de Doctorat (Université de Nice-Sophia Antipolis, France), 1997.
- [Bloch94] I. BLOCH, H. MAITRE, *Fusion de données en traitement d'image: modèles d'information et décision*, Traitement du Signal, Vol. 11, No. 6, 1994.
- [Bloch96] I. BLOCH, *Information Combination Operators for Data Fusion: A Comparative Review and Classification*, IEEE Transactions on Systems, Man and Cybernetics (Part A: Systems and Humans), Vol. 26, No. 1, 1996.
- [Bourges94] M. BOURGES-SÉVENIER, *Réalisation d'une bibliothèque C de fonctions ondelettes*, rapport de recherche INRIA No. 2362, 1994.
- [Burns86] B. BURNS, A.R. HASSON, E.M. RISEMAN, *Extracting Straight Lines*, IEEE Transactions on Pattern Analysis and Machine Intelligence, Vol. 8, No. 7, 1986.
- [Burt83] P.J. BURT, E.H. ADELSON, *The Laplacian Pyramid as a Compact Image Code*, IEEE Transactions on Communications, Vol. 31, No. 4, 1983.
- [Canny86] J. CANNY, *A Computational Approach to Edge Detection*, IEEE Transactions on Pattern Analysis and Machine Intelligence, Vol. 8, No. 6, 1986.
- [Carmora] R.A. CARMORA, *Extrema Reconstruction and Spline Smoothing, Variations on an Algorithm of Mallat & Zhong*, Technical Report, Princeton University.
- [Carmora93] R.A. CARMORA, *Wavelet Identification of Transients in Noisy Time Series*, Lecture Notes (Meeting of the Interface'93), 1993.
- [Carmora95] R.A. CARMORA, W.L. HWANG, B. TORRÉSANI, *Characterization of Signals by the Ridges of their Wavelet Transform*, 1995.
- [Carré98] P. CARRÉ, P. SIMARD, D. BOICHU, C. FERNANDEZ, *Débruitage par transformée en ondelettes non-décimée: extension aux acquisitions multiples*, Preprint, 1998.

- [Chang97] S-H. CHANG, F-H. CHENG, W-H. HSU, G-Z. WU, *Fast Algorithm for Point Pattern Matching: Invariant to Translation, Rotation and Scale*, Pattern Recognition, Vol. 30, No. 2, 1997.
- [Chatterjee97] C. CHATTERJEE, V.P. ROYCHOWDHURY, E.K.P. CHONG, *A Non-linear Gauss-Siedel Algorithm for Noncoplanar and Coplanar Camera Calibration with Convergence Analysis*, Computer Vision and Image Understanding, Vol. 67, No. 1, 1997.
- [Chuang96] G.C.H. CHUANG, J. KUO, *Wavelet Descriptor of Planar Curves: Theory and Applications*, IEEE Transactions on Image Processing, Vol. 5, No. 1, 1996.
- [Cohen92a] A. COHEN, I. DAUBECHIES, J-C. FAUVEAU, *Biorthogonal Bases of Compactly Supported Wavelets*, Communications on Pure and Applied Mathematics, No. 45, 1992.
- [Cohen92b] A. COHEN, I. DAUBECHIES, B. JAWERTH, P. VIAL, *Multiresolution Analysis, Wavelets and Fast Algorithms on the Interval*, Comptes rendus de l'académie des sciences de Paris, Vol. 316, 1992.
- [Cohen93] A. COHEN, I. DAUBECHIES, P. VIAL, *Wavelet Bases on the Interval and Fast Algorithms*, Journal of Applied and Computing Harmonic Analysis, Vol. 1, 1993.
- [Coifman95] R.R. COIFMAN, D.L. DONOHO, *Translation Invariant De-Noising*, Technical Report No. 475, Stanford University, 1995.
- [Cornell98] E. CORNELL, K. WIEMAN, *La condensation de Bose-Einstein*, Pour la Science (édition française de Scientific American), No. 247, 1998.
- [Cotterel97] P. COTTEREL, *Fusion of NIR and FIR Images for Night Vision*, MSc Thesis (Cranfield University, School of Mechanical Engineering, Applied Mathematics and Computing Group), 1997.
- [Cox] G.S. COX, G. DE JAGER, *A Survey of Point Pattern Matching Techniques and a New Approach to Point Pattern Recognition*, Department of Electrical Engineering, University of Cape Town.
- [Cvetković95] Z. CVETKOVIĆ, M. VETTERLI, *Discrete-Time Wavelet Extrema Representation: Design and Consistent Reconstruction*, IEEE Transaction on Signal Processing, Vol. 43, No. 3, 1995.
- [Daintith89] J. DAINTITH, R.D. NELSON, *The Penguin Dictionary of Mathematics*, Penguin Books, 1989.

- [Daubechies88] I. DAUBECHIES, *Orthonormal Basis of Compactly Supported Wavelets*, Communications on Pure and Applied Mathematics, No. 41, 1988.
- [Daubechies90] I. DAUBECHIES, *The Wavelet Transform, Time-Frequency Localization and Signal Analysis*, IEEE Transactions on Information Theory, Vol. 36, No. 5, 1990.
- [Daubechies92] I. DAUBECHIES, *Ten Lectures on Wavelets*, SIAM, 1992.
- [Delyon93] B. DELYON, *Ondelettes orthogonales et biorthogonales*, rapport de recherche INRIA No. 1985, 1993.
- [Deriche87] R. DERICHE, *Using Canny's Criteria to Derive a Recursively Implemented Optimal Edge Detector*, International Journal of Computer Vision, Vol. 1, No. 1, 1987.
- [Deriche90] R. DERICHE, *Fast Algorithm for Low-Level Vision*, IEEE Transactions on Pattern Analysis and Machine Intelligence, Vol. 12, No. 1, 1990.
- [Deriche] R. DERICHE, *Techniques d'extraction de contours*, available at www.inria.fr/robotvis/personnel/der/Demo/Features/features.html.
- [Devore88] R.A. DEVORE, V.A. POPOV, *Interpolation of Besov Spaces*, Transactions of the American Mathematical Society, Vol. 305, No. 1, 1988.
- [Devore92] R.A. DEVORE, B.J. LUCIER, *Wavelets*, Acta Numerica, Vol. 1, 1992.
- [Donoho91a] D.L. DONOHO, *Unconditional Bases are Optimal Bases for Data Compression and for Statistical Estimation*, Paper presented as *Wavelets + Decision Theory = Optimal Smoothing* at the "Wavelet and Applications" workshop (Luminy, France) and at the workshop on "Trends in the Analysis of Curve Data" (University of Heidelberg), 1991.
- [Donoho91b] D.L. DONOHO, I.M. JOHNSTONE, *Minimax Estimation via Wavelet Shrinkage*, IMS Special Invited Lecture at the Annual Meeting of the Institute of Mathematical Statistics of Atlanta, 1991.
- [Donoho92] D.L. DONOHO, I.M. JOHNSTONE, G. KERKYACHARIAN, D. PICARD, *Wavelet Shrinkage: Asymptotia?*, presented at the Oberwolfach Meeting "Mathematische Stochastik", 1992.
- [Donoho94] D.L. DONOHO, I.M. JOHNSTONE, *Adapting to Unknown Smoothness via Wavelet Shrinkage*, 1994, available at www.mathsoft.com/wavelets.html.
- [Donoho95] D.L. DONOHO, *De-Noising by Soft Thresholding*, IEEE Transactions on Information Theory, Vol. 41, No. 3, 1995.

- [Duffin52] R.J. DUFFIN, A.C. SCHAEFFER, *A Class of Nonharmonic Fourier Series*, Transactions of the American Mathematical Society, No. 72, 1952.
- [Duong97] T. HA DUONG, *Cours de l'unité de valeur: techniques mathématiques de l'ingénieur (MT12)*, Université de Technologie de Compiègne, 1997.
- [Falkenauer98] E. FALKENAUER, *Genetic Algorithms and Grouping Problems*, John Wiley and Sons, 1998.
- [Farge93] M. FARGE, J.C.R. HUNT, J.C. VASSILICOS, *Wavelets, Fractals and Fourier Transforms*, The Institute of Mathematics & its Applications Conference Series, Clarendon Press, 1993.
- [Feichtinger97] H.G. FEICHTINGER, T. STROHMER, *Gabor Analysis and Algorithms, Theory and Applications*, Birkhauser, 1997.
- [Flusser94] J. FLUSSER, T. SUK, *A Moment-Based Approach to Registration of Images with Affine Geometric Distortion*, IEEE Transactions on Geoscience And Remote Sensing, Vol. 32, No. 2, 1994.
- [Frazier85] M. FRAZIER, B. JAWERTH, *Decomposition of Besov Spaces*, Indiana University Mathematical Journal, Vol. 34, No. 4, 1985.
- [Gabor46] D. GABOR, *Theory of Communication*, Journal of the IEE (London), Vol. 93, No. 3, 1946.
- [Gonzales92] R.C. GONZALES, R.E. WOODS, *Digital Image Processing*, Addison-Wesley, 1992.
- [Grosky90] W.I. GROSKY, L.A. TAMBURINO, *A Unified Approach to the Linear Camera Calibration Problem*, IEEE Transactions on Pattern Analysis and Machine Intelligence, Vol. 12, No. 7, 1990.
- [Grossmann84] A. GROSSMANN, J. MORLET, *Decomposition of Hardy Functions into Square Integrable Wavelet of Constant Shape*, SIAM Journal of Mathematical Analysis, Vol. 15, No. 4, 1984.
- [Hill93] D.L.G. HILL, D.J. HAWKES, N.A. HARRISON, C.F. RUFF, *A Strategy for Automated Multimodality Image Registration Incorporating Anatomical Knowledge and Imager Characteristics*, Proceedings of Information Processing in Medial Imaging, Flagstaff, 1993.
- [Hlawatsch92] F. HLAWATSCH, G.F. BOUDREAUX-BARTELS, *Linear and Quadratic Time-Frequency Signal Representations*, IEEE Signal Processing Magazine, April 1992.

- [Hsieh97] J-W. HSIEH, H-Y.M. LIAO, K-C. FAN, M-T. KO, Y-P. HUNG, *Image Registration Using a New Edge-Based Approach*, Computer Vision and Image Understanding, Vol. 67, No. 2, 1997.
- [Hubbard96] B. BURKE HUBBARD, *Ondes et ondelettes, la saga d'un outil mathématique*, Pour la Science (Diffusion Belin), 1996.
- [Hummel89] R. HUMMEL, R. MONIOT, *Reconstruction from Zero Crossing in Scale Space*, IEEE Transactions on Acoustics, Speech and Signal Processing, Vol. 37, No. 12, 1989.
- [Hwang93] W-L. HWANG, S. MALLAT, *Characterization of Self-Similar Multifractals with Wavelet Maxima*, Technical Report No. 641, Courant Institute of Mathematical Sciences, New York University, 1993.
- [Jahne95] B. JAHNE, *Digital Image Processing: Concepts, Algorithms, and Scientific Applications*, Springer-Verlag, 1995.
- [Janez97] F. JANEZ, *Rappels sur la théorie de l'évidence*, Rapport de Recherche ONERA, 1997.
- [Jawerth93] B. JAWERTH, W. SWELDENS, *Overview of Wavelet Based Multiresolution Analysis*, 1993, available at www.mathsoft.com/wavelets.html.
- [Kolmogorov57] A.N. KOLMOGOROV, S.V. FOMIN, *Elements of the Theory of Functions and Functionnal Analysis (Vol. 1: Metric and Normed Spaces)*, Translated from the First Russian Edition by L. BORON, Graylock Press, 1957.
- [Kolmogorov61] A.N. KOLMOGOROV, S.V. FOMIN, *Elements of the Theory of Functions and Functionnal Analysis (Vol. 2: Measure, Lebesgue Integral, Hilbert Spaces)*, Translated from the First Russian Edition by H. KAMEL and H. KOUM, Graylock Press, 1961.
- [Kovačević92] J. KOVAČEVIĆ, M. VETTERLI, *Nonseparable Multidimensionnal Perfect Reconstruction Filter Banks and Wavelet Bases for R^n* , IEEE Transactions on Information Theory, Vol. 38, No. 2, 1992.
- [Lakhal96] J. LAKHAL, L. LITZER, *A Parallelization of the Deriche Filter: a Theoretical Study and an Implementation on the MapStar System*, Proceedings of the International Conference on Parallel Computing and Distributed Processing Techniques (PDPTA'96), 1996.
- [Lamoureux94] C. LAMOUREUX, *Cours de mathématiques : tome 1 (première année d'études)*, Ecole Centrale Paris, 1994.

- [Lee95] J-S. LEE, Y-N. SUN, C-H. CHEN, *Multiscale Corner Detector by Using Wavelet Transform*, IEEE Transactions on Image Processing, Vol. 4, No. 1, 1995.
- [Lemarié88] P.G. LEMARIÉ, *Ondelettes à localisation exponentielle*, Journal des mathématiques pures et appliquées, No. 67, 1988.
- [Li95a] H. LI, B.S. MANJUNATH, S.K. MITRA, *A Contour-Based Approach to Multisensor Image Registration*, IEEE Transactions on Image Processing, Vol. 4, No. 3, 1995.
- [Li95b] H. LI, B.S. MANJUNATH, S.K. MITRA, *Multisensor Image Fusion Using the Wavelet Transform*, Graphical Models and Image Processing, Vol. 57, No. 3, 1995.
- [Li96a] H.H. LI, Y-T. ZHOU, *A Wavelet-Based Point Feature Extractor for Multi-Sensor Images Registration*, Proceedings of the SPIE, Vol. 2762, 1996.
- [Li96b] H.H. LI, Y-T. ZHOU, *Automatic Visual/IR image registration*, Optical Engineering, Vol. 35, No. 5, 1996.
- [Liu91] Y. LIU, T.S. HUANG, *Determining Straight Lines Correspondences From Intensity Images*, Pattern Recognition, Vol. 24, No. 6, 1991.
- [Lu93] J. LU, *Signal Recovery and Noise Reduction with Wavelets*, PhD Thesis (Thayer School of Engineering, Dartmouth College), 1993.
- [Mallat89a] S. MALLAT, *A Theory for Multiresolution Signal Decomposition: The Wavelet Representation*, IEEE Transactions on Pattern Analysis and Machine Intelligence, Vol. 11, No. 7, 1989.
- [Mallat89b] S. MALLAT, *Multifrequency Channel Decompositions of Images and Wavelet Models*, IEEE Transactions on Acoustics, Speech and Signal Processing, Vol. 37, No. 12, 1989.
- [Mallat91] S. MALLAT, *Zero Crossings of a Wavelet Transform*, IEEE Transactions on Information Theory, Vol. 17, No. 4, 1991.
- [Mallat92a] S. MALLAT, W.L. HWANG, *Singularity Detection and Processing with Wavelets*, IEEE Transactions on Information Theory, Vol. 38, No. 2, 1992.
- [Mallat92b] S. MALLAT, S. ZHONG, *Characterization of Signals from Multiscale Edges*, IEEE Transactions on Pattern Analysis and Machine Intelligence, Vol. 14, No. 7, 1992.

- [Mallat98] S. MALLAT, *A Wavelet Tour of Signal Processing*, Academic Press, 1998.
- [Meyer90] Y. MEYER, *Ondelettes et opérateur (Vol. 1: ondelettes)*, Hermann, 1990.
- [Meyer94] Y. MEYER, *Les ondelettes: algorithmes et applications*, Armand Colin, 1994.
- [Nandhakumar88] N. NANDHAKUMAR, J.K. AGGARVAL, *Integrated Analysis of Thermal and Visible Images for Scene Interpretation*, IEEE Transactions on Pattern Analysis and Machine Intelligence, Vol. 10, No. 4, 1988.
- [Olkkonen96] H. OLKKONEN, P. PESOLA, *Gaussian Pyramid Wavelet Transform for Multiresolution Analysis of Images*, Graphical Models and Image Processing, Vol. 58, No. 4, 1996.
- [Perrier] V. PERRIER, C. BASDEVANT, *Besov Norms in Terms of the Continuous Wavelet Transform, Application to Structure Functions*, available at www.mathsoft.com/wavelets.html.
- [Porter87] W. PORTER, H.T. ENMARK, *A System Overview of the Airborne Visible/Infrared Imaging Spectrometer (AVIRIS)*, Proceeding of the SPIE, No. 834, 1987.
- [Prescott97] B. PRESCOTT, G.F. MCLEAN, *Line Based Correction of Radial Lens Distortion*, Graphical Models and Image Processing, Vol. 59, No. 1, 1997.
- [Riesz55] F. RIESZ, B. SZ.-NAGY, *Functionnal Anlysis*, Translated from the Second French Edition by L. BORON, Frederic Ungar Publishing, 1955.
- [Rioul91] O. RIOUL, M. VETTERLI, *Wavelets and Signal Processing*, IEEE Signal Processing Magazine, October 1991.
- [Rioul92] O. RIOUL, P. DUHAMEL, *Fast Algorithms for Discrete and Continuous Wavelet Transforms*, IEEE Transaction on Information Theory, Vol. 38, No. 2, 1992.
- [Seugakkai77] N. SEUGAKKAI, *Encyclopedic Dictionary of Mathematics (Volumes 1 & 2)*, by the Mathematical Society of Japan, Edited by S. IYAGANA and Y. KAWADA, Translation reviewed by K.O. MAY, The MIT Press, 1977.
- [Shafer76] S. SHAFER, *A Mathematical Theory of Evidence*, Princeton University Press, 1976.

- [Shensa92] M.J. SHENSA, *The Discrete Wavelet Transform: Wedding the À Trous and Mallat Algorithm*, IEEE Transactions on Signal Processing, Vol. 40, No. 10, 1992.
- [Shih95] S-W. SHIH, Y-P. HUNG, W-S. LIN, *When Should we Consider Lens Distortion in Camera Calibration?*, Pattern Recognition, Vol. 28, No. 3, 1995.
- [Sid-Ahmed90] M.A. SID-AHMED, M.T. BORAIE, *Dual Camera Calibration for 3-D Machine Vision Metrology*, IEEE Transactions on Instrumentation and Measurement, Vol. 39, No. 3, 1990.
- [Simoncelli92] E.P. SIMONCELLI, W.T. FREEMAN, E.H. ADELSON, D.J. HEEGER, *Shiftable Multiscale Transforms*, IEEE Transactions on Information Theory, Vol. 38, No. 2, 1992.
- [Skea93] D. SKEA, I. BARRODALE, R. KUWAHARA, R. POECKERT, *A Control Point Matching Algorithm*, Pattern Recognition, Vol. 26, No. 2, 1993.
- [Smith86] M.J.T. SMITH, T.P. BARNWELL, *Exact Reconstruction Techniques for Tree-Structured Subband Coders*, IEEE Transactions on Acoustics, Speech and Signal Processing, Vol. 34, No. 3, 1996.
- [Smith97] S.M. SMITH, J.M. BRADY, *SUSAN - A New Approach to Low-Level Image Processing*, The International Journal of Computer Vision, Vol. 23, No. 1, 1997.
- [Starck92] J-L. STARCK, *Analyse en ondelette et imagerie à haute résolution angulaire*, Thèse de Doctorat (Université de Nice-Sophia Antipolis, France), 1992.
- [Starink95] J.P.P. STARINK, E. BACKER, *Finding Point Correspondences Using Simulated Annealing*, Pattern Recognition, Vol. 28, No. 2, 1995.
- [Strang94] G. STRANG, *Wavelets*, American Scientist, No. 82, 1994.
- [Studholme95] C. STUDHOLME, D.L.G. HILL, D.J. HAWKES, *Automated 3D Registration of Truncated MR and CT Images of the Head*, Proceedings of the British Machine Vision Conference, Editions David Pycock, 1995.
- [Sweldens93] W. SWELDENS, R. PIESSENS, *Wavelet Sampling Techniques*, Proceedings of the Joint Statistical Meetings, San Francisco, 1993.
- [Sweldens96] Wim SWELDENS, *Wavelets: What Next?*, Proceedings of the IEEE, Vol. 84, No. 4, 1996.
- [Toet89] A. TOET, *Image Fusion by a Ration of Low-Pass Pyramid*, Pattern Recognition Letter, Vol. 9, 1989.

- [Toet92] A. TOET, *Multiscale Contrast Enhancement with Applications to Image Fusion*, Optical Engineering, Vol. 31, No. 5, 1992.
- [Triebel78] H. TRIEBEL, *Interpolation Theory, Function Spaces, Differential Operators*, North Holland Publishing, 1978.
- [Ventura90] A.D. VENTURA, A. RAMPINI, R. SCHETTINI, *Image Registration by Recognition of Corresponding Structures*, IEEE Transactions on Geoscience and Remote Sensing, Vol. 28, No. 3, 1990.
- [Vetterli86] M. VETTERLI, *Filter Banks Allowing Perfect Reconstruction*, Signal Processing, Vol. 10, p. 219-244, 1986.
- [Vetterli92] M. VETTERLI, C. HERLEY, *Wavelets and Filter Banks: Theory and Design*, IEEE Transactions on Signal Processing, Vol. 40, No. 9, 1992.
- [Ville48] J. VILLE, *Théorie et applications de la notion de signal analytique*, Cables et Transmission, 2A(1), 1948.
- [Weisstein98] E.W. WEISSTEIN, *The CRC Concise Encyclopedia of Mathematics*, www.astro.virginia.edu/~eww6n/math/math0.html.
- [Weng92] J. WENG, P. COHEN, M. HERNIOU, *Camera Calibration with Distortion Model and Accuracy Evaluation*, IEEE Transactions on Pattern Analysis and Machine Intelligence, Vol. 14, No. 10, 1992.
- [Whitley] D. WHITLEY, *A Genetic Algorithm Tutorial*, available at rses.anu.edu.au/samizdat/ga_tutorial/.
- [Wilson95] T.A. WILSON, S.K. ROGERS, L.M. MYERS, *Perceptual-Based Hyperspectral Image Fusion using Multiresolution Analysis*, Optical Engineering, Vol. 34, No. 11, 1995.
- [Winter95] G. WINTER, J. PERIAUX, M. GALÁN, P. CUESTA, *Genetic Algorithm in Engineering and Computer Science*, John Wiley and Sons, 1995.
- [Yang94] M.C.K. YANG, J-S. LEE, *Object Identification from Multiple Images Based on Point Matching Under a General Transformation*, IEEE Transactions on Pattern Analysis and Machine Intelligence, Vol. 16, No. 7, 1994.
- [Zheng93] Q. ZHENG, R. CHELLAPA, *A Computational Vision Approach to Image Registration*, IEEE Transactions on Image Processing, Vol. 2, No. 3, 1993.
- [Zuniga83] O.A. ZUNIGA, R.M. HARALICK, *Corner Detection using the Facet Model*, Proceeding of the International Conference on Computer Vision and Pattern Recognition, 1983.

- [Zygmund68] A. ZYGMUND, *Trigonometric Series*, Cambridge University Press, 1968.

Appendix A

Registration: linear systems

A.1 Quadratic model: systems

The linear system, corresponding to equation (1.7), and its estimation (using the set of control points discussed in §1.6) are shown on system A.1. To obtain \tilde{f}_v , one should modify the right hand side of system A.1 and use

$$\vec{\theta}' = \left(\sum_i u_i^2 \tilde{v}'_i \quad \sum_i v_i^2 \tilde{v}'_i \quad \sum_i u_i v_i \tilde{v}'_i \quad \sum_i u_i \tilde{v}'_i \quad \sum_i v_i \tilde{v}'_i \quad \sum_i \tilde{v}'_i \right)^T$$

which gives (using the same set of control points)

$$\vec{\theta}' = (0.2593 \ 0.2492 \ 0.0543 \ -0.1747 \ 3.4322 \ 3.8765)^T$$

Solving this two systems leads to the sets of estimated parameters given in equations (1.10) and (1.11).

A.2 Third order model: systems

Systems A.2 and A.3 respectively correspond to equations (1.8) and (1.9). Solving these systems leads to the sets of estimated parameters given in equations (1.12) and (1.13).

System A.1 Linear system corresponding to equation (1.7).

$$\underbrace{\begin{pmatrix} \sum_i u_i^4 & \sum_i u_i^2 v_i^2 & 2 \sum_i u_i^3 v_i & \sum_i u_i^3 & \sum_i u_i^2 v_i & \sum_i u_i^2 \\ \sum_i u_i^2 v_i^2 & \sum_i v_i^4 & 2 \sum_i u_i v_i^3 & \sum_i u_i v_i^2 & \sum_i v_i^3 & \sum_i v_i^2 \\ \sum_i u_i^3 v_i & \sum_i u_i v_i^3 & 2 \sum_i u_i^2 v_i^2 & \sum_i u_i^2 v_i & \sum_i v_i^2 u_i & \sum_i u_i v_i \\ \sum_i u_i^3 & \sum_i u_i v_i^2 & 2 \sum_i u_i^2 v_i & \sum_i u_i^2 & \sum_i u_i v_i & \sum_i u_i \\ \sum_i u_i^2 v_i & \sum_i v_i^3 & 2 \sum_i u_i v_i^2 & \sum_i u_i v_i & \sum_i v_i^2 & \sum_i v_i \\ \sum_i u_i^2 & \sum_i v_i^2 & 2 \sum_i u_i v_i & \sum_i u_i & \sum_i v_i & n \end{pmatrix}}_Q \begin{pmatrix} a_{11} \\ a_{22} \\ a_{12} \\ b_1 \\ b_2 \\ c \end{pmatrix} = \underbrace{\begin{pmatrix} \sum_i u_i^2 \tilde{u}'_i \\ \sum_i v_i^2 \tilde{u}'_i \\ \sum_i u_i v_i \tilde{u}'_i \\ \sum_i u_i \tilde{u}'_i \\ \sum_i v_i \tilde{u}'_i \\ \sum_i \tilde{u}'_i \end{pmatrix}}_{\tilde{\theta}}$$

$$\begin{pmatrix} 0.7908 & 0.4157 & -0.0217 & 0.1019 & 0.0370 & 5.4714 \\ 0.4157 & 0.7118 & -0.0948 & 0.0714 & 0.0245 & 5.2109 \\ -0.0109 & -0.0474 & 0.8315 & 0.0370 & 0.0714 & -0.1900 \\ 0.1019 & 0.0714 & 0.0740 & 5.4714 & -0.1900 & 0.6944 \\ 0.0370 & 0.0245 & 0.1427 & -0.1900 & 5.2109 & 0.1049 \\ 5.4714 & 5.2109 & -0.3801 & 0.6944 & 0.1049 & 68.0000 \end{pmatrix} \begin{pmatrix} a_{11} \\ a_{22} \\ a_{12} \\ b_1 \\ b_2 \\ c \end{pmatrix} = \begin{pmatrix} -0.0478 \\ -0.0525 \\ 0.0352 \\ 4.2801 \\ -0.1451 \\ -1.0139 \end{pmatrix}$$

System A.2 Linear system corresponding to equation (1.8).

$$\underbrace{\begin{pmatrix} \sum_i u_i^6 & \sum_i u_i^4 v_i^2 & \sum_i u_i^5 & \sum_i u_i^3 v_i^2 & 2 \sum_i u_i^4 v_i & \sum_i u_i^4 & \sum_i u_i^3 v_i & \sum_i u_i^3 \\ \sum_i u_i^4 v_i^2 & \sum_i u_i^2 v_i^4 & \sum_i u_i^3 v_i^2 & \sum_i u_i v_i^4 & 2 \sum_i u_i^2 v_i^3 & \sum_i u_i^2 v_i^2 & \sum_i u_i v_i^3 & \sum_i u_i v_i^2 \\ \sum_i u_i^5 & \sum_i u_i^3 v_i^2 & q_{11} & q_{12} & q_{13} & q_{14} & q_{15} & q_{16} \\ \sum_i v_i^2 u_i^3 & \sum_i u_i v_i^4 & q_{21} & q_{22} & q_{23} & q_{24} & q_{25} & q_{26} \\ \sum_i u_i^4 v_i & \sum_i u_i^2 v_i^3 & q_{31} & q_{32} & q_{33} & q_{34} & q_{35} & q_{36} \\ \sum_i u_i^4 & \sum_i u_i^2 v_i^2 & q_{41} & q_{42} & q_{43} & q_{44} & q_{45} & q_{46} \\ \sum_i v_i u_i^3 & \sum_i u_i v_i^3 & q_{51} & q_{52} & q_{53} & q_{54} & q_{55} & q_{56} \\ \sum_i u_i^3 & \sum_i u_i v_i^2 & q_{61} & q_{62} & q_{63} & q_{64} & q_{65} & q_{66} \end{pmatrix}}_M \begin{pmatrix} d_1 \\ d_2 \\ a_{11} \\ a_{22} \\ a_{12} \\ b_1 \\ b_2 \\ c \end{pmatrix} = \underbrace{\begin{pmatrix} \sum_i u_i^3 \tilde{u}'_i \\ \sum_i u_i v_i^2 \tilde{u}'_i \\ \theta_1 \\ \theta_2 \\ \theta_3 \\ \theta_4 \\ \theta_5 \\ \theta_6 \end{pmatrix}}_{\tilde{v}}$$

$$\begin{pmatrix} 0.1352 & 0.0598 & 0.0162 & 0.0100 & 0.0082 & 0.7908 & -0.0109 & 0.1019 \\ 0.0598 & 0.0588 & 0.0100 & 0.0061 & 0.0070 & 0.4157 & -0.0474 & 0.0714 \\ 0.0162 & 0.0100 & 0.7908 & 0.4157 & -0.0217 & 0.1019 & 0.0370 & 5.4714 \\ 0.0100 & 0.0061 & 0.4157 & 0.7118 & -0.0948 & 0.0714 & 0.0245 & 5.2109 \\ 0.0041 & 0.0035 & -0.0109 & -0.0474 & 0.8315 & 0.0370 & 0.0714 & -0.1900 \\ 0.7908 & 0.4157 & 0.1019 & 0.0714 & 0.0740 & 5.4714 & -0.1900 & 0.6944 \\ -0.0109 & -0.0474 & 0.0370 & 0.0245 & 0.1427 & -0.1900 & 5.2109 & 0.1049 \\ 0.1019 & 0.0714 & 5.4714 & 5.2109 & -0.3801 & 0.6944 & 0.1049 & 68.0000 \end{pmatrix} \begin{pmatrix} d_1 \\ d_2 \\ a_{11} \\ a_{22} \\ a_{12} \\ b_1 \\ b_2 \\ c \end{pmatrix} = \begin{pmatrix} 0.3241 \\ 0.6155 \\ -0.0478 \\ -0.0525 \\ 0.0352 \\ 4.2801 \\ -0.1451 \\ -1.0139 \end{pmatrix}$$

System A.3 Linear system corresponding to equation (1.9).

$$\underbrace{\begin{pmatrix} \sum_i v_i^6 & \sum_i v_i^4 u_i^2 & \sum_i v_i^3 u_i^2 & \sum_i v_i^5 & 2 \sum_i u_i v_i^4 & \sum_i u_i v_i^3 & \sum_i v_i^4 & \sum_i v_i^3 \\ \sum_i v_i^4 u_i^2 & \sum_i v_i^2 u_i^4 & \sum_i v_i u_i^4 & \sum_i v_i^3 u_i^2 & 2 \sum_i v_i^2 u_i^3 & \sum_i v_i u_i^3 & \sum_i v_i^2 u_i^2 & \sum_i v_i u_i^2 \\ \hline \sum_i u_i^2 v_i^3 & \sum_i v_i u_i^4 & q_{11} & q_{12} & q_{13} & q_{14} & q_{15} & q_{16} \\ \sum_i v_i^5 & \sum_i v_i^3 u_i^2 & q_{21} & q_{22} & q_{23} & q_{24} & q_{25} & q_{26} \\ \sum_i u_i v_i^4 & \sum_i v_i^2 u_i^3 & q_{31} & q_{32} & q_{33} & q_{34} & q_{35} & q_{36} \\ \sum_i u_i v_i^3 & \sum_i v_i u_i^3 & q_{41} & q_{42} & q_{43} & q_{44} & q_{45} & q_{46} \\ \sum_i v_i^4 & \sum_i v_i^2 u_i^2 & q_{51} & q_{52} & q_{53} & q_{54} & q_{55} & q_{56} \\ \sum_i v_i^3 & \sum_i v_i u_i^2 & q_{61} & q_{62} & q_{63} & q_{64} & q_{65} & q_{66} \end{pmatrix}}_{M'} \begin{pmatrix} d'_1 \\ d'_2 \\ a'_{11} \\ a'_{22} \\ a'_{12} \\ b'_1 \\ b'_2 \\ c' \end{pmatrix} = \underbrace{\begin{pmatrix} \sum_i u_i^3 \tilde{u}'_i \\ \sum_i u_i v_i^2 \tilde{u}'_i \\ \theta'_1 \\ \theta'_2 \\ \theta'_3 \\ \theta'_4 \\ \theta'_5 \\ \theta'_6 \end{pmatrix}}_{\tilde{\theta}'}$$

$$\begin{pmatrix} 0.1141 & 0.0588 & 0.0035 & 0.0098 & 0.0122 & -0.0474 & 0.7118 & 0.0245 \\ 0.0588 & 0.0598 & 0.0041 & 0.0035 & 0.0199 & -0.0109 & 0.4157 & 0.0370 \\ 0.0035 & 0.0041 & 0.7908 & 0.4157 & -0.0217 & 0.1019 & 0.0370 & 5.4714 \\ 0.0098 & 0.0035 & 0.4157 & 0.7118 & -0.0948 & 0.0714 & 0.0245 & 5.2109 \\ 0.0061 & 0.0100 & -0.0109 & -0.0474 & 0.8315 & 0.0370 & 0.0714 & -0.1900 \\ -0.0474 & -0.0109 & 0.1019 & 0.0714 & 0.0740 & 5.4714 & -0.1900 & 0.6944 \\ 0.7118 & 0.4157 & 0.0370 & 0.0245 & 0.1427 & -0.1900 & 5.2109 & 0.1049 \\ 0.0245 & 0.0370 & 5.4714 & 5.2109 & -0.3801 & 0.6944 & 0.1049 & 68.0000 \end{pmatrix} \begin{pmatrix} d'_1 \\ d'_2 \\ a'_{11} \\ a'_{22} \\ a'_{12} \\ b'_1 \\ b'_2 \\ c' \end{pmatrix} = \begin{pmatrix} 0.2744 \\ 0.4678 \\ 0.2593 \\ 0.2492 \\ 0.0543 \\ -0.1747 \\ 3.4322 \\ 3.8765 \end{pmatrix}$$

Appendix B

Towards an automatic registration

Introduction

This chapter discusses the feasibility of designing an automatic registration procedure. Obviously, this process can be very simplified if done in a controlled environment, e.g. in presence of a calibration grid. Here, we focus on performing the registration using only the frames coming out the two cameras. Most of the time, an automatic procedure first requires to extract some control points (or salient points) within the two images. Different methods have been proposed, for example in [Zheng93] where a Gabor transform is used or in [Li96a] where a wavelet-based method is presented. However, when human-made objects are available, it may be interesting to exploit the fact that they contain corners. Moreover, a human-made object, such that a house, will (most of the time) be present in both the FIR and the NIR image. In this chapter, we focus on the pipelines of contours and corners extraction (the first one is a necessary preliminary for using direct or hybrid corner detectors) and then present briefly the problem of control points matching.

B.1 Contours extraction

This section describes the pipeline of contours extraction, based on the gradient approach, i.e. only one differentiation. In what follows, we briefly introduce the Canny [Canny86] and Deriche [Deriche87] operators, we then discuss the different steps (extraction of the local maxima and hysteresis thresholding) necessary to obtain the contours from the output of an operator.

B.1.1 Optimal edge detectors

A simple edge model

The basic idea behind optimal operators is based on a continuous edge model of the form

$$I(x) = Au_{-1}(x) + B(x)$$

where $u_{-1}(x)$ denotes the unit-step function and $B(x)$ is a centered gaussian white noise of variance equal to σ^2 . We then consider the convolution $\Theta(x)$ with an edge detector $f(x)$

$$\Theta(x) = \int_{-\infty}^{+\infty} I(y)f(x-y)dy$$

The Canny criteria

According to this model, John Canny [Canny86] has proposed to optimize the three following requirements, in order to find the form of the detector f .

Low probability of error (failing to mark or falsely marking real edge points). This criterion consists in finding an asymmetric operator which maximises the signal-to-noise ratio, i.e.

$$\Sigma = \frac{\int_{-\infty}^0 f(x)dx}{\sigma \sqrt{\int_{-\infty}^{+\infty} f^2(x)dx}}$$

Good localization. points marked as edges should be as closed as possible to the true edge. This criterion is defined as being the inverse of the standard deviation of the position of the true edge, i.e.

$$\Lambda = \frac{A|f'(0)|}{\sqrt{\int_{-\infty}^{+\infty} f'^2(x)dx}}$$

Only one response to a single edge. consists in a constraint on the average distance between two maxima (x_{\max}), i.e.

$$x_{\max} = \sqrt{\frac{\int_{-\infty}^{+\infty} f'^2(x)dx}{\int_{-\infty}^{+\infty} f''^2(x)dx}}$$

John Canny has then proposed a FIR operator which optimizes the product $\Sigma\Lambda$ under the constraint that the third criterion is fixed to a constant value k . In practice, the Canny operator is approximated by the first derivative of a Gauss function which leads to $\Sigma\Lambda = .92$ ($k = .51$).

The Deriche operator

Rachid Deriche [Deriche87] has derived an IIR operator that optimizes $\Sigma\Lambda$ and leads to $\Sigma\Lambda = 2$ ($k = .44$). The operator has the form¹

$$f(x) = Sxe^{-\alpha|x|}$$

In one dimension, this operator can be implemented using two stable second order recursive filters (an implementation using the *C*-language is given in program B.1). An interesting property of the operator comes from the α parameter which allows to adapt it to the content of the image. Roughly, for a noisy image, α has to be small (.25 to .5) which means that Σ (detection) is favoured to the detriment of Λ (localization), on the other hand, for a “clean” image, α must be relatively large (≈ 1). In two dimensions, the output of the operator is computed via two sets of two recursive filters applied separately on the rows and the columns of the image (this operation must be performed twice—with different parameters—for obtaining the partial derivatives according to x and y). More details (derivation, implementation, . . .) are notably available in [Deriche]. Figure B.1 shows the output of the Deriche operator on the “singe” image.

B.1.2 Local maxima and hysteresis thresholding

Extraction of the local maxima

Given some estimations of the partial derivatives according to x and y , one can compute the norm and the direction of the gradient, i.e.

$$|\vec{\nabla}I| = \sqrt{\left(\frac{\partial I}{\partial x}\right)^2 + \left(\frac{\partial I}{\partial y}\right)^2}$$

and

$$\phi = \tan^{-1} \frac{\partial I/\partial y}{\partial I/\partial x} \quad (\text{B.1})$$

and use this information in order to extract the local maxima of the gradient norm in the gradient direction. This is necessary for obtaining thin contours, i.e. contours whose thickness is equal to one pixel. However, the coordinates given by the gradient direction do not coincide (in general) with integer pixel coordinates: a bilinear interpolation scheme should be applied in order to get a value at this location. A given point is then marked as a local maxima if its value is greater than those of its two neighbours in the gradient direction. See figure B.2.

¹It is the limit of $f(x) = \frac{S}{\omega} e^{-\alpha|x|} \sin \omega x$ when $\omega \rightarrow 0$. This case corresponds to the largest value of $\Sigma\Lambda$.

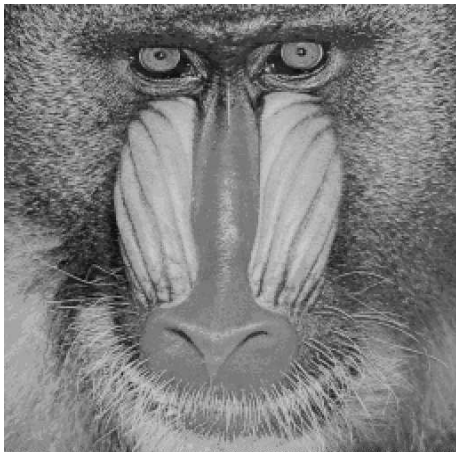
Program B.1 Implementation of the one-dimensional Deriche operator.

```

#define SQR(x) ((x)*(x))
#define ABS(x) (x<0?-1:(x>0?1:0))
void deriche1d(float *x,int n,float a)
{
    int i;
    float *y1,*y2,b,c,k;
    if(y1=(float*)malloc(n*sizeof(float)),
        y2=(float*)malloc(n*sizeof(float)),
        !y1 || !y2)
    {
        fprintf(stderr,"\nmalloc() error");
        exit(1);
    }
    b=(float)exp((double)(-a));
    c=(float)exp((double)(-2*a));
    k=SQR(1-b)/(1.+2.*a*b-c);
    for(i=0;i<n;i++)
    {
        int ii=n-i-1;
        y1[i]=(i-1<0?.0:x[i-1])+
            2*b*(i-1<0?.0:y1[i-1])-
            c*(i-2<0?.0:y1[i-2]);
        y2[ii]=(ii+1>=n?.0:x[ii+1])+
            2*b*(ii+1>=n?.0:y2[ii+1])-
            c*(ii+2>=n?.0:y2[ii+2]);
    }
    for(i=0;i<n;i++)
        x[i]=ABS(k*b*(y1[i]-y2[i]));
    free(y1);
    free(y2);
}

```

Figure B.1 Output of the Deriche operator.



(a) Original image.

(b) $\frac{\partial}{\partial x} I \otimes f$.(c) $\frac{\partial}{\partial y} I \otimes f$.

(d) Gradient norm.

Hysteresis thresholding

The last step consists in eliminating the non-significant local maxima, i.e. those which correspond to small values of the gradient norm. Most of the time, this operation is performed via a thresholding procedure. A smart way of doing it is called a hysteresis thresholding: given a high and a low level, the hysteresis thresholding keeps the local maxima with corresponding gradient norm greater than the high level or greater than the low one and connected (in a 8-connexity sense) to a local maxima whose norm is greater than the high level. The 8-connexity is defined as

Definition 8 (8-connexity) *A given point A is said to be connected to a given point B if one of its eight neighbours is the point B or if one of its eight neighbours is connected to the point B .*

This thresholding technique gives better results than a simple one-level thresholding operator, because it is able to extract some contour points below the noise level. Figure B.2 shows the contours obtained after an hysteresis thresholding.

Figure B.2 Contours extraction from figure B.1.



(a) Local maxima.

(b) Hysteresis tresh.

B.2 Corners extration

This section is devoted to corner extraction. Our entry point in this field is the recent thesis by Thierry Blaska [Blaska97]. In what follows, we first introduce the different possible ways of performing a corner extraction and then present a so-called hybrid operator.

B.2.1 Existing operators

According to [Blaska97], there are four classes of corner extractors, namely: direct, pixel-based, hybrid and model-based. A direct operator consists in extracting the local maxima of the curvature of a given contour string². However, since the contour has been discretized, a direct estimation of the curvature (using finite differences) is highly sensitive to quantization noise. Obviously, there exists different solutions for avoiding this problem [Blaska97] (an example, based on the wavelet maxima representation is available in [Lee95]). A pixel-based operator detects the corners by considering information coming only from the grey-scale values of the image, some examples are given in [Zuniga83] or (more recently) [Smith97]. Hybrid operators, such as the one presented in [Deriche90], combine some information coming from both the grey-scale values and the contours. Instead of estimating the curvature directly from the contours, they use a more robust information coming from the intensity gradient (already computed in §B.1 by means of an optimal operator). The more recent model-based approach is fully presented in [Blaska94, Blaska97].

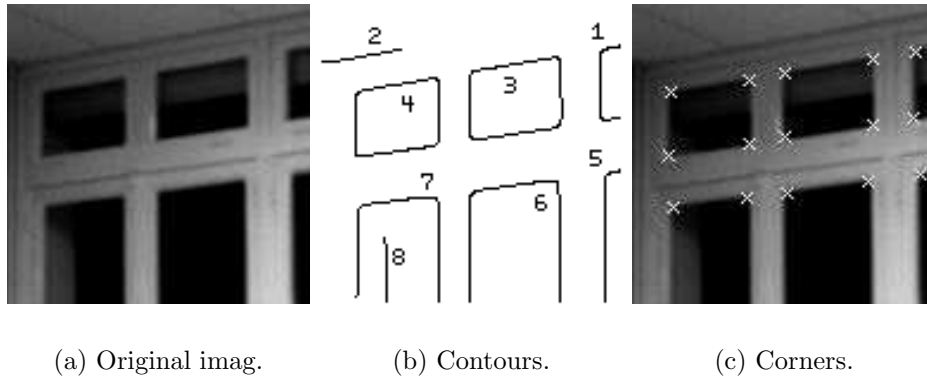
B.2.2 A hybrid operator

Here, the corners extraction is performed using a hybrid algorithm which consists in detecting the sharp variations on the orientation of a given contour. First of all, it is necessary to extract the edges by means of the pipeline discussed in §B.1. The contour strings are then memorized in a linked-list structure and their orientations (computed using equation (B.1)) provide one-dimensional signals such as the ones shown on figure B.4. The points of sharp variations are then detected by means of a one-dimensional Deriche operator (see program B.1): the locations of the local maxima of its modulus (greater than a threshold level) give the corners present on a contour string. Figure B.3 shows an example of corners detection and figure B.4 the associated orientations and responses of the one-dimensional Deriche operator.

B.3 Control points matching

Given two (or more) sets of control points, extracted automatically from two (or more) images, the point pattern matching problem consists in linking some points in the first set to some points in the second set. This problem is a tricky one and many algorithms have been proposed for solving it, e.g. [Chang97, Skea93,

²A contour is often defined as a parametric curve $C(t) = (x(t) \ y(t))^T$, $t \neq s$, whose tangent vector is given by $T(t) = (\dot{x}(t)^2 + \dot{y}(t)^2)^{\frac{1}{2}}(\dot{x}(t) \ \dot{y}(t))^T$. Its orientation is therefore given by $\tan^{-1} \phi(t) = \dot{y}(t)/\dot{x}(t)$ and its curvature is defined as $\kappa(s) = d\phi(s)/ds$, s is the curvilinear abscissa. See [Blaska97, Daintith89].

Figure B.3 Example of corners extraction.

(a) Original imag.

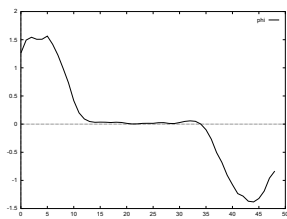
(b) Contours.

(c) Corners.

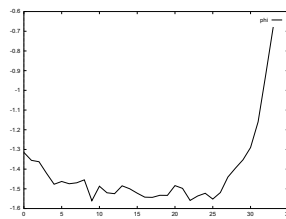
Starink95, Yang94] a survey is available in [Cox]. Due to the differences between the two images (they may have been observed with different sensors at different positions and at different wavelengths, moreover, they are—in general—not perturbed by the same noise pattern) the number of control points (say N_1) detected in the first image is, most of the time, not equal to the number of points (say N_2) detected in the second one. Moreover, a point in the first set does not necessarily have a corresponding point in the second set and vice versa. The main problem consists in the difficulty of formulating convex constraints which allow to use “classical” optimization methods, such as the gradient descent. To overcome this problem, it may be relevant to use some stochastic optimization algorithms, such as the simulated annealing method [Falkenauer98] or the genetic algorithm [Falkenauer98, Whitley, Winter95], as proposed in [Starink95, Studholme95, Hill93]. However, using these algorithms requires to design proper cost functions that take into account all the *a priori* knowledge we have about the transformation that maps one set onto the other (e.g. the parametric form of the model). A possible cost function can be based on Σ_u and Σ_v (see §1.4.2 and §1.5.2) regularized by a constraint on the minimum number of points to be matched³.

³Otherwise, the algorithm will converge to a small set of corresponding points such that $\Sigma_u = \Sigma_v = 0$.

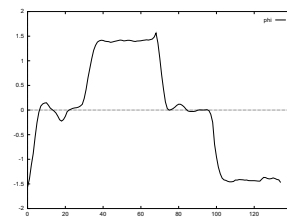
Figure B.4 Contours orientations and responses of the Deriche operator.



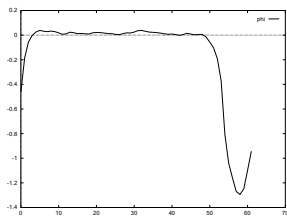
(a) Orient. (1).



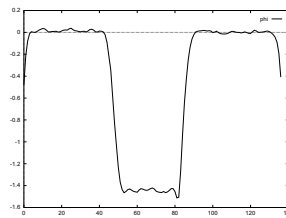
(b) Orient. (2).



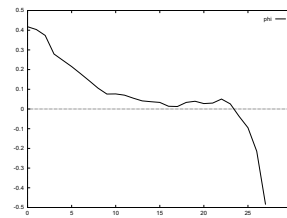
(c) Orient. (3).



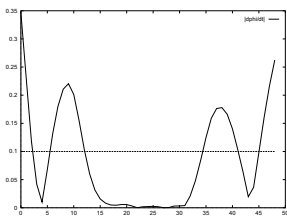
(d) Orient. (5).



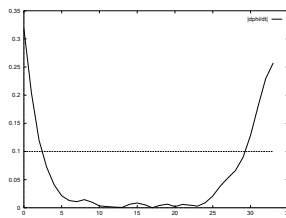
(e) Orient. (6).



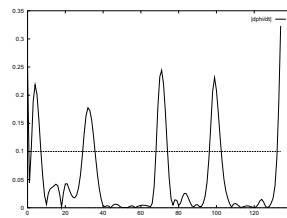
(f) Orient. (8).



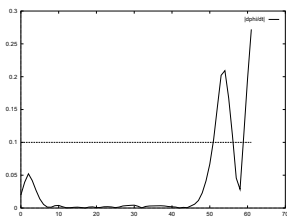
(g) Deriche (1).



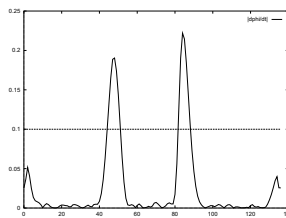
(h) Deriche (2).



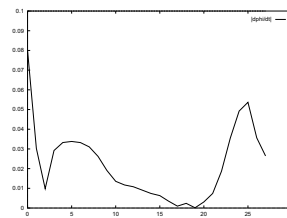
(i) Deriche (3).



(j) Deriche (5).



(k) Deriche (6).



(l) Deriche (8).

Appendix C

Wavelet transform algorithms

This chapter presents the implementation, using the *C*-language, of a few wavelet transform algorithms. Programs C.1 and C.2 propose some implementations of (respectively) the *algorithme à trous* and its inverse (see §2.3.3 and algorithm 2.1, page 34). Programs C.3 and C.4 give implementations of the fast wavelet transform and its inverse discussed in §2.6.1 (see algorithm 2.2, page 42, as well). Program C.5 gives an implementation of the P_{Γ} operator, discussed in §4.2.1, coming from cs.nyu.edu/pub/wave.

Program C.1 Implementation of the *algorithme à trous*.

```

void atrous(float *next_a,
            float *next_d, float *a, int s, int n,
            float *h, int h_begin, int h_end,
            float *g, int g_begin, int g_end)
{
    int i, j;
    for(i=0; i<n; i++)
    {
        next_a[i]=.0;
        for(j=h_begin; j<=h_end; j++)
        {
            int ii=i+(j<<s);
            ii=(ii<0?(n+ii)%n:(ii>=n?(ii%n):ii));
            next_a[i]+=a[ii]*h[j-h_begin];
        }
        next_d[i]=.0;
        for(j=g_begin; j<=g_end; j++)
        {
            int ii=i+(j<<s);
            ii=(ii<0?(n+ii)%n:(ii>=n?(ii%n):ii));
            next_d[i]+=a[ii]*g[j-g_begin];
        }
    }
}

```

Program C.2 Implementation of the inverse *algorithme à trous*.

```
void iatrous1d(float *next_a,
              float *next_d, float *a, int s, int n,
              float *h, int h_begin, int h_end,
              float *g, int g_begin, int g_end)
{
    int i, j;
    for(i=0; i<n; i++)
    {
        next_a[i]=.0;
        for(j=h_begin; j<=h_end; j++)
        {
            int ii=i+(j<<s);
            ii=(ii<0?(n+ii)%n:(ii>=n?(ii%n):ii));
            next_a[i]+=a[ii]*h[j-h_begin];
        }
        next_d[i]=.0;
        for(j=g_begin; j<=g_end; j++)
        {
            int ii=i+(j<<s);
            ii=(ii<0?(n+ii)%n:(ii>=n?(ii%n):ii));
            next_d[i]+=a[ii]*g[j-g_begin];
        }
    }
}
```

Program C.3 Implementation of the fast wavelet transform.

```

int fwt1d(float *sig,int n,
    float *h,int h_begin,int h_end,
    float *g,int g_begin,int g_end)
{
    float *tmp;
    int i,j,min_l=MAX(min_length(h_begin,h_end),
        min_length(g_begin,g_end));
    if(tmp=(float*)malloc(n*sizeof(float)),!tmp)
    {
        fprintf(stderr,"\nmalloc() error\n");
        exit(1);
    }
    while(n!=min_l)
    {
        for(i=0;i<n;i+=2)
        {
            tmp[i>>1]=.0;
            tmp[(i>>1)+(n>>1)]=.0;
            for(j=h_begin;j<=h_end;j++)
            {
                register int k=i+j;
                tmp[i>>1]+=h[j-h_begin]*(k<0?sig[n+k]:
                    (k>=n?sig[k%n]:sig[k]));
            }
            for(j=g_begin;j<=g_end;j++)
            {
                register int k=i+j;
                tmp[(i>>1)+(n>>1)]+=g[j-g_begin]*(k<0?sig[n+k]:
                    (k>=n?sig[k%n]:sig[k]));
            }
        }
        memcpy(sig,tmp,n*sizeof(float));
        n>>=1;
    }
    free(tmp);
    return(min_l);
}

```

Program C.4 Implementation of the fast inverse wavelet transform.

```

void ifwt1d(float *sig,int n,
  float *h,int h_begin,int h_end,
  float *g,int g_begin,int g_end)
{
  float *tmp;
  int i,j,l=MAX(min_length(h_begin,h_end),
                min_length(g_begin,g_end));
  if(tmp=(float*)malloc(n*sizeof(float)),!tmp)
  {
    fprintf(stderr,"\nmalloc() error\n");
    exit(1);
  }
  while(l!=n)
  {
    for(i=0;i<l<<1;i++)
    {
      tmp[i]=.0;
      for(j=-h_end;j<=-h_begin;j++)
        if( !((i+j)&0x1) )
        {
          register int k=(i+j)/2;
          tmp[i]+=h[-j-h_begin]*(k<0?sig[l+k]
            :(k>=1?sig[k%l]:sig[k]));
        }
      for(j=-g_end;j<=-g_begin;j++)
        if( !((i+j)&0x1) )
        {
          register int k=(i+j)/2;
          tmp[i]+=g[-j-g_begin]*(k<0?sig[l+k+1]:
            (k>=1?sig[k%l+1]:sig[k+1]));
        }
    }
    l<<=1;
    memcpy(sig,tmp,l*sizeof(float));
  }
  free(tmp);
}

```

Program C.5 Implementation of P_Γ .

```

interp(float u0, float un, int n,
       float *u, float r1)
{
    double r_1, r_2, r2,
           rn_1, r2n_2, r2n,
           r2n_2i, rn_i, ri, r2i, a0, an;
    int i;
    rn_1=r1;
    for(i=1;i < n-1;++i)
        rn_1*=r1;
    r2n_2=rn_1*rn_1;
    r_1=1./r1;
    r_2=r_1*r_1;
    r2=r1*r1;
    r2n=r2n_2*r2;
    a0=u0/(1.-r2n);
    an=un/(1.-r2n);
    u[0]=u0;
    r2n_2i=r2n_2;
    r2i=r2;
    ri=r1;
    rn_i=rn_1;
    for(i=1;i<n;i++)
    {
        u[i]=a0*ri*(1-r2n_2i)+an*rn_i*(1-r2i) ;
        r2n_2i*=r_2;
        r2i*=r2;
        ri*=r1;
        rn_i*=r_1;
    }
    u[n]=un;
}

```

Appendix D

Mathematical complement

D.1 Hilbert space and Riesz basis

Definition 9 (Abstract Hilbert space) *A set of abstract elements which possesses the three following properties is said to be a Hilbert space \mathcal{H} ,*

1. \mathcal{H} is a linear space i.e. the operations of addition and scalar multiplication are defined for its elements, in particular there exists an element 0 such that $0 = 0.f$ for all element of \mathcal{H} .
2. \mathcal{H} is a metric space whose metric is derived from a scalar product, denoted by $\langle f, g \rangle$, so that $\langle af, g \rangle = a \langle f, g \rangle$ for all scalar a , $\langle f + g, h \rangle = \langle f, h \rangle + \langle g, h \rangle$, $\langle f, g \rangle = \langle g, f \rangle^*$, $\langle f, f \rangle > 0$ for $f \neq 0$ and $\langle f, f \rangle = 0$ for $f = 0$. The norm of an element f is then defined by $\|f\| = \langle f, f \rangle^{\frac{1}{2}}$.
3. \mathcal{H} is a complete space i.e. if a sequence of elements $\{f_n\}$ satisfies

$$\lim_{n,m \rightarrow \infty} \|f_n - f_m\| = 0$$

then there exists an element \tilde{f} such that $\lim_{n,m \rightarrow \infty} \|f_n - \tilde{f}\| = 0$.

The properties of these spaces are notably studied in [Riesz55, Kolmogorov61].

Definition 10 (Riesz basis) *A family of element $\{e_k\}$ of an abstract Hilbert space \mathcal{H} is said to be a Riesz basis of \mathcal{H} if the following properties are (simultaneously) satisfied for all x in \mathcal{H}*

1. $\exists \{\lambda_k\} / x = \sum_k \lambda_k e_k$.
2. $\exists A, B \in \mathbb{R}^{2+} / \frac{1}{A} \|x\|^2 \leq \sum_k |\lambda_k|^2 \leq \frac{1}{B} \|x\|^2$.

D.2 Hölder (Lipschitz) regularity

D.2.1 Definition

This subsection aims at defining the concept of Hölder exponent. We use the presentation of [Mallat98]. The idea is to start from the Taylor series of f at ν (f is assumed to be N times differentiable on $[\nu - h, \nu + h]$)

$$p_\nu(x) = \sum_{k=0}^{N-1} \frac{f^{(k)}(\nu)}{k!} (x - \nu)^k + R_N$$

As shown in [Weisstein98]

$$R_N = \varepsilon(x) = f(x) - p_\nu(x) = \frac{(x - \nu)^N}{N!} f^{(N)}(x)$$

and hence

$$\forall x \in [\nu - h, \nu + h], |\varepsilon(x)| \leq \frac{|x - \nu|^N}{N!} \sup_{y \in [\nu - h, \nu + h]} |f^{(N)}(y)|$$

The notion of Hölder regularity generalizes the previous inequality to non integer exponents.

Definition 11 (Hölder regularity) *A function is pointwise Hölder- α at ν if there exists $K > 0$ and a polynomial p_ν of degree $N = \lfloor \alpha \rfloor^1$ such that*

$$\forall x \in R, |f(x) - p_\nu(x)| \leq K|x - \nu|^\alpha \quad (\text{D.1})$$

A function is uniformly Hölder- α over an interval $[a, b]$ if it satisfies the previous equation $\forall \nu \in [a, b]$ with a constant K that does not depend on ν . The Hölder regularity of f at ν over $[a, b]$ is the sup of the α such that f is Hölder- α .

D.2.2 A few remarks

If f is uniformly Hölder- α ($\alpha > N$) in the neighbourhood of ν then f is N times continuously differentiable in the neighbourhood of ν . If $0 \leq \alpha < 1$ then $p_\nu(x) = f(\nu)$ and equation (D.1) becomes

$$\forall x \in R, |f(x) - f(\nu)| \leq K|x - \nu|^\alpha$$

If $\alpha < 1$, f is not differentiable in the neighbourhood of ν and the Hölder exponent characterizes the type of singularity. For example [Daubechies92, Mallat92b] Heaviside-like singularities are Hölder-0 while Dirac-like ones are Hölder-(-1). Note that the uniform Hölder regularity of f over R is related to a condition on the decay of its Fourier transform via the following theorem (proofs in [Mallat98, Daubechies92]).

¹ $\lfloor \alpha \rfloor$ denotes the largest integer such that $N \leq \alpha$.

Theorem 10 *A function f is bounded and uniformly Hölder- α over R if*

$$\int_{-\infty}^{+\infty} |\hat{f}(\xi)|(1 + |\xi|^\alpha) d\xi < \infty$$

D.3 Spaces: W^α , $B_{p,q}^\alpha$, C^α

The purpose of this section is obviously not to provide a deep analysis of the notions of Sobolev (W^α), Besov ($B_{p,q}^\alpha$) and Hölder (C^α) spaces (the notations are taken from [Perrier, Meyer90]) spaces and their relationships with orthogonal wavelet decompositions (for that purpose the reader is directly sent to Yves Meyer's book [Meyer90]). Our goal is just to (very) briefly introduce this subject.

D.3.1 Short presentation

Besov spaces are subsets of $L^p(R)$. They are extensions of Sobolev and Hölder spaces in which the smoothness of a given function is finer characterized. Basically, the fact that a function lies in W^α or C^α gives an idea of its global smoothness, while its membership of $B_{p,q}^\alpha$ gives some information about its local smoothness, e.g. piecewise regular functions belong to Besov spaces [Mallat98]. The classical definition of Besov spaces is based on the modulus of smoothness [Zygmund68]

$$\omega_p(f; h) = \|\tau_{-h}f - f\|_{L^p(R)}$$

and on the two following semi-norms [Delyon93, Perrier, Devore92] ($1 \leq p, q < \infty$)

- $0 < \alpha < 1$:

$$N_{p,q}^\alpha(f) = \left(\int_0^{+\infty} \left(\frac{\omega_p(f; h)}{h^\alpha} \right)^q \frac{dh}{h} \right)^{\frac{1}{q}}$$

- $\alpha = 1$:

$$N_{p,q}^1(f) = \left(\int_0^{+\infty} \left(\frac{\omega_p^*(f; h)}{h} \right)^q \frac{dh}{h} \right)^{\frac{1}{q}}$$

where $\omega_p^*(f; h) = \|\tau_{-h}f - 2f + \tau_h f\|_{L^p(R)}$. If $q = \infty$, $N_{p,\infty}^\alpha(f) = \sup_{R^{+*}} \omega_p(f; h)/h^\alpha$ with the modification for $\alpha = 1$. We then need (again for $0 < \alpha \leq 1$)

$$\|f\|_{B_{p,b}^\alpha} = \|f\|_{L^p(R)} + N_{p,q}^\alpha(f)$$

for completing the definition of a Besov space.

Definition 12 (Besov space) *A function $f \in L^p(R)$ belongs to the Besov space $B_{p,q}^\alpha$ if*

- $0 < \alpha \leq 1$: $\|f\|_{B_{p,q}^\alpha} < \infty$.

- $\alpha > 1$: $\|f^{(k)}\|_{B_{p,q}^{\alpha-\lfloor\alpha\rfloor}} < \infty$, $0 \leq k \leq \lfloor\alpha\rfloor^2$

Provided $\|\cdot\|_{B_{p,q}^\alpha}$, a Besov space has a Banach space³ structure [Perrier]. Note that $B_{\infty,\infty}^\alpha = C^\alpha$ ($\{f \in L^\infty(R) / \sup_{R^{*+}} \omega_\infty(f;h)/h^\alpha < \infty\}$ [Daubechies92]) and that $B_{2,2}^\alpha = W^\alpha$ ($\{f \in L^2(R) / \|f^{(\alpha)}\|_{L^2(R)} = \frac{1}{2\pi} \|(i\xi)^\alpha \hat{f}\|_{L^2(R)} < \infty\}$, $f^{(\alpha)}$ denotes the weak or Sobolev derivative of f , α is not necessarily an integer [Mallat98]) (notably) [Perrier, Meyer90, Triebel78].

Orthogonal wavelet basis have interesting properties for analysing these classes of function. As demonstrated by Yves Meyer [Meyer90], the norm $\|\cdot\|_{B_{p,q}^\alpha}$ is equivalent to a norm on the wavelet coefficients if the multiresolution analysis generated by the scaling function/wavelet pair is r -regularly (in Meyer's sense) with $r \geq \alpha$ i.e. [Meyer90, Perrier, Delyon93, Donoho91a]

$$\|f\|_{B_{p,q}^\alpha} \asymp \|\mu_0\|_{l^p(Z)} + \left(\sum_{j=0}^{+\infty} 2^{jq(\alpha+\frac{1}{2}-\frac{1}{p})} \|\gamma_j\|_{l^p(Z)}^q \right)^{\frac{1}{q}} \quad (\text{D.2})$$

recall that $\mu_{0;k} = \langle f, \phi_{0;k} \rangle$ and that $\gamma_{j;k} = \langle f, \psi_{j;k} \rangle$, the symbol \asymp means that there exists two constants A and B such that the ratio of the two sides is bounded between them. It is therefore easier to determine if a given function $f \in L^p(R)$ belongs to $B_{p,q}^\alpha$.

A very interesting result comes from the fact that an orthogonal wavelet basis (obeying the regularity condition) provides an unconditionnal basis⁴ of $B_{p,q}^\alpha$, see (again!) [Meyer90]. This implies that orthogonal wavelet basis are “optimal” (in some sense) for analysing and processing the functions belonging to $B_{p,q}^\alpha$, e.g. simple (thresholding) operators, applied in the unconditionnal basis, work better for a whole class of problems (namely: compression, estimation and recovery) than they do in any other orthogonal basis (the mathematical details are available in [Donoho91a]). This is (roughly) a consequence of the fact that a function is characterized by a few “relevant” coefficients in the unconditionnal basis. For more details on these functionnal spaces (other definitions, extensions to n dimensions, other properties, ...) the reader is sent to [Devore88, Frazier85, Triebel78] and to almost every books about wavelet analysis since this theory uses them for an increasing number of applications (most of these works—known to the author—have already been cited in this subsection).

²The associated norm (for $\alpha > 1$) becomes $\|f\|_{B_{p,q}^\alpha} = \sum_{k=0}^{\lfloor\alpha\rfloor} \|f^{(k)}\|_{B_{p,q}^{\alpha-\lfloor\alpha\rfloor}}$.

³Banach spaces generalize the notion of Hilbert space (definition 9): the norm is not necessarily defined from a scalar product [Riesz55].

⁴As defined in [Daubechies92]: a family of elements $\{e_k\}$ of a Banach space B is a Schauder basis of B if $\forall f \in B, \exists \{\mu_k\}$ (unique) $/ f = \lim_{N \rightarrow \infty} \sum_{k=1}^N \mu_k e_k$. Moreover, if $\sum_k \mu_k e_k \in B \Rightarrow \sum_k |\mu_k| e_k \in B$ the family $\{e_k\}$ is said to be an unconditionnal basis of B . On a Hilbert space, an unconditionnal basis is a Riesz basis.

D.3.2 Example: *l'algèbre des bosses*

In order to give a more “intuitive” idea of the kind of functions that belong to Besov spaces, this subsection is devoted to a (short) presentation of $B_{1,1}^1$ also known as *l'algèbre des bosses gaussiennes* (“bump algebra” [Donoho91b]) introduced by Yves Meyer [Meyer90]. In what follows, $g_{\mu;\sigma}(x)$ denotes the Gauss function

$$e^{-\frac{(x-\mu)^2}{2\sigma^2}}$$

such that $g_{\mu;\sigma}(\mu) = 1$ instead of the usual normalization (area equal to 1). *L'algèbre des bosses* (B) is defined as the class of functions (vanishing at infinity) which admit a (non-unique) decomposition of the form

$$f(x) = \sum_{k=0}^{+\infty} \lambda_k g_{\mu_k;\sigma_k}(x) \quad (\text{D.3})$$

satisfying $\sum_k |\lambda_k| < \infty$. Provided the norm $\|f\|_B = \inf \sum_k |\lambda_k|$, such that $\{\lambda_k\}_{k \in \mathbb{N}}$ satisfies equation (D.3), B is a Banach space. In an orthogonal wavelet basis (generated by a sufficiently regular multiresolution analysis), the decomposition of a function f belonging to B must satisfy

$$\sum_{j=-\infty}^{+\infty} 2^{\frac{j}{2}} \|\gamma_j\|_{l^1(\mathbb{Z})} \quad (\text{D.4})$$

and vice versa (proof in [Meyer90]). Note that equation (D.4) corresponds to equation (D.2) with $p = q = \alpha = 1$: this illustrates the fact that the “bump algebra” is $B_{1,1}^1$. The class B contains some functions which may have considerable spatial inhomogeneity e.g. a function $f \in B$ can be extremely spiky in one part of its domain and completely flat in another location. This type of behavior could not be possible in a Hölder or Sobolev space since it is required that a function is “equally” smooth at every points on its domain [Donoho91b].

List of Figures

1.1	Radial distortion.	15
1.2	Decentering and thin-prism distortion.	17
1.3	Estimated quadratic model.	21
1.4	Estimated third-order model.	22
1.5	Example of registered image.	23
2.1	Examples of wavelets.	31
2.2	Beginning of a dyadic wavelet transform.	35
2.3	Some of the Daubechies scaling functions and wavelets.	48
3.1	Examples of multifocus data.	52
3.2	Example of multisensor data.	53
3.3	Wavelet transform of some Hölder-0 singularities (Daubechies-8).	56
3.4	Examples of signals with non-isolated singularities.	58
3.5	Organization of a two-dimensional wavelet decomposition.	61
3.6	Wavelet decompositions of some images (Daubechies-8).	62
3.7	Example of correct and failed object selection.	64
3.8	Experimental results on multifocus data.	66
3.9	Experimental results on multisensor data.	68
3.10	More experimental results on multisensor data.	69
3.11	Still more experimental results on multisensor data.	70
4.1	Quadratic spline wavelet.	79
4.2	Beginning of a two-dimensional dyadic wavelet transform.	80
4.3	Multiscale edges extracted from the “lenna” image.	82
4.4	Reconstruction via the alternate projection algorithm.	85
B.1	Output of the Deriche operator.	111
B.2	Contours extraction from figure B.1.	112
B.3	Example of corners extraction.	114
B.4	Contours orientations and responses of the Deriche operator.	115

List of algorithms, programs and systems

2.1	<i>Algorithme à trous</i>	34
2.2	Fast decimated filter bank algorithm.	42
A.1	Linear system corresponding to equation (1.7).	104
A.2	Linear system corresponding to equation (1.8).	105
A.3	Linear system corresponding to equation (1.9).	106
B.1	Implementation of the one-dimensional Deriche operator.	110
C.1	Implementation of the <i>algorithme à trous</i>	118
C.2	Implementation of the inverse <i>algorithme à trous</i>	119
C.3	Implementation of the fast wavelet transform.	120
C.4	Implementation of the fast inverse wavelet transform.	121
C.5	Implementation of P_{Γ}	122